DM

Development and Characterization of Electrochemical Sensors Based on PAMAM Dendrimers and Citrate-stabilized Gold Nanoparticles

MASTER DISSERTATION

Gina Marta Ferraz Tavares
MASTER IN NANOCHEMISTRY AND NANOMATERIALS

UNIVERSIDADE da MADEIRA
A Nossa Universidade
www.uma.pt

February | 2019

Development and Characterization of Electrochemical Sensors Based on PAMAM Dendrimers and Citrate-stabilized Gold Nanoparticles

MASTER DISSERTATION

Gina Marta Ferraz Tavares
MASTER IN NANOCHEMISTRY AND NANOMATERIALS

SUPERVISOR
José Carlos Almeida Mesquita

CO-SUPERVISOR
João Manuel Cunha Rodrigues

Development and Characterization of Electrochemical Sensors Based on PAMAM Dendrimers and Citrate-stabilized Gold Nanoparticles

Dissertation submitted to the University of Madeira in fulfillment of the requirements for the degree of Master in Nanochemistry and Nanomaterials

by Gina Marta Ferraz Tavares

Work developed under the supervision of Professor José Carlos Almeida Mesquita

and co-supervised by Professor João Manuel Cunha Rodrigues

Faculdade de Ciências Exatas e de Engenharia

Centro de Química da Madeira

Campus Universitário da Penteada

Funchal–Portugal

February 2019

Declaration

I hereby declare that this thesis is the result of my own work, is original and was written by me.

I also declare that its reproduction and publication by Madeira University will not break any third-party rights and that I have not previously (in its entirely or in part) submitted it elsewhere for obtaining any qualification or degree.

Furthermore, I certify that all sources of information used in the thesis were properly cited.

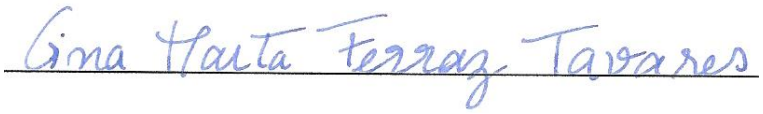

Funchal, 12th of February 2019.

Contributions

- **Oral Communication:**

1. Gina Tavares, José Carlos Mesquita, and João Rodrigues. *Development of biosensors based on PAMAM dendrimers and gold nanoparticles.* Presented at the 4th CQM Annual Meeting, 3-4 February 2017, Madeira University, Madeira Island, Portugal, organized by CQM-Centro de Química da Madeira.

- **Poster Communication:**

1. Gina Tavares, José Carlos Mesquita, and João Rodrigues. *Development and characterization of electrochemical biosensors based on PAMAM dendrimers.* Presented at MAD-NANO16: Madeira International Conference on Emerging Trends and Future of Nanomaterials for Human Health, Madeira Island, Portugal, 17-20 November 2016, organized by CQM-Centro de Química da Madeira.

Acknowledgements

I deeply thank the support and patience of my supervisors Professor José Carlos Mesquita and Professor João Rodrigues. I really appreciate the orientation, critical review and extreme patience.

I would like to acknowledge the CQM- Centro de Química da Madeira/Madeira Chemistry Research Centre (CQM) for the materials and instrumentation, and specially for the opportunity to develop this Master thesis in their laboratory facilities. The appreciation is extended to all the team members of the Molecular Materials Research Group that took the time to answer my questions and help me throughout this project, particularly, to my master colleague and friend Ivo Martins, for all the support and encouragement during the execution of this project. A great thanks is due to Dra. Carla Miguel, who crafted a special sample holder for SEM, allowing the analysis of my electrode sample.

My thanks goes also to the Fundação para a Ciência e a Tecnologia (FCT) through the CQM Strategic Project PEst-OE/QUI/UI0674/2013 and also ARDITI-Agência Regional para o Desenvolvimento da Investigação Tecnologia e Inovação through the project M1420-01-0145-FEDER-000005 - Centro de Química da Madeira - CQM^{+} (Madeira 14-20 Program).

Abstract

Electrochemical sensors are devices that allow the detection and quantification of a certain compound in a determined sample. Nanomaterials are extremely appealing for sensing purposes due their properties. Poly(amidoamine) dendrimers and gold nanoparticles are largely explored because of their small dimensions; the latter is used for its electrocatalytic properties, whilst the former is used in biosensors for its potential as an immobilization platform for biological recognition elements. This project focused on the use of PAMAM dendrimers and gold nanoparticles in electrode modification and the assessment of these modifications. Firstly, gold and glassy carbon electrodes were sequentially modified with thiols, gold layer, G5 PAMAM-NH_2 dendrimers and citrate-stabilized gold nanoparticles. The modifications were monitored by cyclic voltammetry and impedance spectroscopy in a hexacyanoferrate (II)/(III) redox couple system. All modifications were successful, with the exception of citrate-stabilized gold nanoparticle, PAMAM dendrimer and mercaptopropionic sulfonic acid-modified glassy carbon electrode. In a second part, the electrocatalytic activity of the modified electrodes towards 4-nitrophenol reduction in 0.05 M phosphate buffer solution was assessed by cyclic voltammetry. G5 PAMAM-NH_2 dendrimer assembly over vitreous carbon-based surfaces translated to electrodes with higher sensitivity, for lower limits of detection are obtained. The lowest limit of detection was calculated for PAMAM dendrimer and 3-mercaptopropionic acid-modified glassy carbon electrode, 17 μM, with 4-nitrophenol in linear range of 690 – 37 μM. Gold substrates proved to have poor electrocatalytic activity towards 4-nitrophenol reduction owing to the simultaneous reduction of 4-nitrophenol and solution on gold surface. As for vitreous carbon substrates, the use of gold, either as a layer or as citrate-stabilized nanoparticles, resulted in less sensitive electrodes, as suggested by higher detection limits.

Keywords

Sensor; PAMAM dendrimer; Gold nanoparticles; Cyclic voltammetry

Resumo

Sensores eletroquímicos são dispositivos que permitem a deteção e quantificação de um determinado composto numa dada amostra. Os nanomateriais são extremamente apelativos para fins sensitivos devido às suas propriedades. Os dendrímeros poli(amidoamina) (PAMAM) e as nanopartículas de ouro são muito explorados graças às suas pequenas dimensões. As nanopartículas de ouro são usadas pelas suas propriedades eletrocatalíticas, enquanto que o dendrímero é usado em biosensores pelo seu potencial como plataforma de imobilização de elementos de reconhecimento biológico. Este projeto é focado no uso de dendrímeros PAMAM e nanopartículas de ouro na modificação de elétrodos e na avaliação destas modificações. Numa primeira etapa, elétrodos de ouro e carbono foram sequencialmente modificados com tióis, camada de ouro, dendrímeros G5 PAMAM-NH_2 e nanopartículas de ouro estabilizadas por citrato. As modificações foram monitorizadas por voltametria cíclica e espectroscopia de impedância num sistema com o par redox hexacianoferrato (II)/(III). Todas as modificações foram bem-sucedidas, com a exceção do elétrodo de carbono vítreo modificado com ácido 3-mercapto-1-propanosulfónico, dendrímeros PAMAM e nanopartículas de ouro estabilizadas por citrato. Numa segunda etapa, a atividade eletrocatalítica dos elétrodos modificados em relação à redução de 4-nitrofenol em solução de tampão fosfato (0.05 M) foi avaliada por voltametria cíclica. A montagem de dendrímeros PAMAM sobre elétrodos baseados em carbono vítreo traduz-se em elétrodos com maior sensibilidade, já que foram obtidos limites de deteção mais baixos. O limite de deteção mais baixo foi calculado para o elétrodo de carbono vítreo modificado com ácido 3-mercaptopropiónico e dendrímero PAMAM, 17 μM, com 4-nitrofenol entre 690 – 37 μM. Os substratos de ouro provaram ter uma reduzida atividade eletrocatalítica em relação à redução de 4-nitrofenol devido à redução da solução na superfície do elétrodo de ouro que ocorria em simultâneo. Quanto aos substratos de carbono vítreo, a utilização de ouro, seja sob a forma de camada ou nanopartículas estabilizadas por citrato, resultou em elétrodos menos sensíveis, como os altos limites de deteção sugerem.

Palavras-chave

Sensor; Dendrímero PAMAM; Nanopartículas de ouro; Voltametria cíclica

Contents

List of Figures

List of Tables

List of Acronyms, Abbreviations and Symbols

A – Area
E – Electric field
$\vec{F}$ – Force
F – Faraday constant
i - Current
i^A – Anodic peak current
i^C – Cathodic peak current
R - Resistance
R_{CT} – Charge-transfer resistance
t – Time
V - Voltage
Z – Impedance

Au-ATP – ATP-modified gold electrode
Au-ATP-Au – Gold layer and ATP-modified gold electrode
Au-ATP-PAMAM – PAMAM and ATP-modified gold electrode
Au-ATP-PAMAM-AuNPs – Citrate-stabilized gold nanoparticles, PAMAM and ATP-modified gold electrode
Au-MPA – MPA-modified gold electrode
Au-MPA-Au – Gold layer and MPA-modified gold electrode
Au-MPA-PAMAM – PAMAM and MPA-modified gold electrode
Au-MPA-PAMAM-AuNPs – Citrate-stabilized gold nanoparticles, PAMAM and MPA-modified gold electrode
Au-MPS – MPS-modified gold electrode
Au-MPS-Au – Gold layer and MPS-modified gold electrode
Au-MPS-PAMAM – PAMAM and MPS-modified gold electrode
Au-MPS-PAMAM-AuNPs – Citrate-stabilized gold nanoparticles, PAMAM and MPS-modified gold electrode
AuNPs – Gold nanoparticles
Au-PAMAM – PAMAM-modified gold electrode
GC-ATP – ATP-modified glassy carbon electrode
GC-ATP-Au – Gold layer and ATP-modified glassy carbon electrode
GC-ATP-PAMAM – PAMAM and ATP-modified glassy carbon electrode
GC-ATP-PAMAM-AuNPs – Citrate-stabilized gold nanoparticles, PAMAM and ATP-modified glassy carbon electrode
GC-MPA – MPA-modified glassy carbon electrode
GC-MPA-Au – Gold layer and MPA-modified glassy carbon electrode
GC-MPA-PAMAM – PAMAM and MPA-modified glassy carbon electrode
GC-MPA-PAMAM-AuNPs – Citrate-stabilized gold nanoparticles, PAMAM and MPA-modified glassy carbon electrode
GC-MPS – MPS-modified glassy carbon electrode
GC-MPS-Au – Gold layer and MPS-modified glassy carbon electrode
GC-MPS-PAMAM – PAMAM and MPS-modified glassy carbon electrode
GC-MPS-PAMAM-AuNPs – Citrate-stabilized gold nanoparticles, PAMAM and MPS-modified glassy carbon electrode
GC-PAMAM – PAMAM-modified glassy carbon electrode

δC - Concentration difference
δx - Position difference
0D – Zero dimensional
1D – One dimensional
2D – Two dimensional
3D – Three dimensional
4-NP – 4-nitrophenol
AC – Alternate current
ATP – 4-aminothiophenol
BSD – Backscatter electron detector
C - Concentration
CV – Cyclic voltammetry
D – Diffusion coefficient
DLS – Dynamic light scattering
DNA – Deoxyribonucleic acid
DPV – Differential pulse voltammetry
e_0 – Elementary charge
$E_{1/2}$ – Half-wave potential
E^A – Anodic peak potential
E^C – Cathodic peak potential
EDA – Ethylene diamine
EDL – Electrical double layer
EDS – Energy dispersive spectroscopy
EDX – Energy-dispersive X-ray
G1 – Generation 1
G5 – Generation 5
HR-TEM – High resolution transmission electron microscope
IHP – Inner Helmholtz plan
ISE – Ion selective electrode
J – Flux of species
LOD – Limit of detection
LSV – Linear sweep voltammetry
MNPs – Metallic nanoparticles
MPA – 3-mercaptopropionic acid
MPS – 2-mercapto-1-propane sulfonic acid
MRI – Magnetic resonance imaging
n – number of electrons
OHP – Outer Helmholtz plan
PAMAM – Poly(amidoamine)

PBS – Phosphate buffer solution
pH – Potential of hydrogen
p-NP – *para*-nitrophenol
PNPs – Polymeric nanoparticles
QDs – Quantum dots
SAM – Self-assembled monolayer
SCE – Saturated calomel electrode
SD – Standard deviation
SED – Secondary electron detector
SEM – Scanning electron microscope
SMSE – Saturated mercurous sulfate electrode
SPR – Surface plasmon resonance
SWV – Square-wave voltammetry
UV-VIS – Ultraviolet and visible spectroscopy
v – Scan rate
z – Charge number

Chapter 1

1. Introduction

1.1 Electrochemical concepts

Electrochemistry is the branch of chemistry that stablishes a relation between electrical and chemical phenomena. A brief introduction to electrochemical concepts should provide the basic knowledge to understand the study of the electrochemical sensors developed and studied in this project.

1.1.1 *Electrolytes*

Solid ionic crystals, commonly known as salts, have their constituent ions strongly drawn together through Coulombic forces. This molecular interaction is especially powerful and characterized by a strong attraction between cations and anions, which allows the establishment of an equilibrium interionic distance, avoiding short-range repulsive forces. These ionic crystals have their constituents distributed in an organized three-dimensional structure, a lattice, which requires a considerable amount of energy to be destroyed (Figure 1).

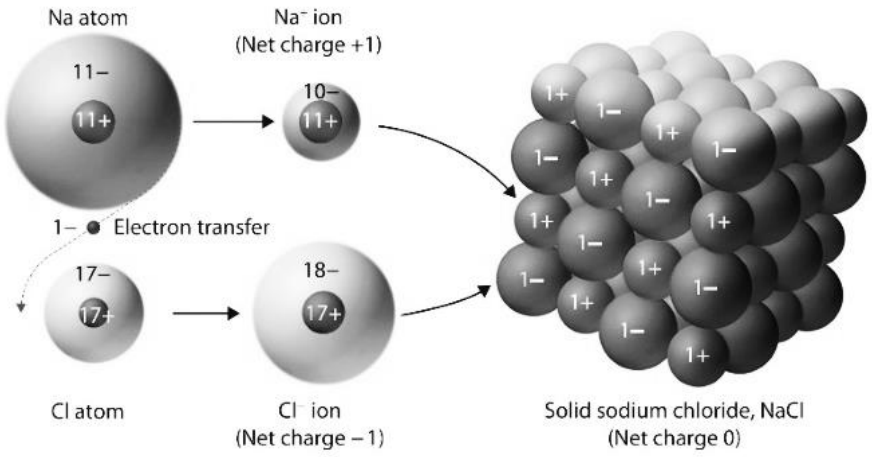

Figure 1. Representation of sodium chloride. Solid ionic crystals are formed when positively and negatively charged ions are arranged into a three-dimensional solid, the forces holding the structure are solely of attractive electrostatic nature.[1]

Due to its high dielectric constant, water can isolate the ionic components from one another, providing stabilization by positioning itself around the ions. Such process is termed solvation, and a more specific term, hydration, is used to describe the solvation by water. Any compound able to dissociate into ions when dissolved, is designated an electrolyte.[2] Electrolytes can be categorized by their strength, as they can totally or partially dissociate in a solvent. The degree of dissociation of an electrolyte is representative of the fraction of the compound that dissociates in a solvent. Electrolytes with low degree of dissociation are considered weak electrolytes whereas strong electrolytes dissociate almost completely.[3] Electrochemical measurements rely on electrolytes, as these conditionate the passage of current through a liquid medium.

1.1.2 *Mass transportation*

Mass transportation of ions between anode and cathode is relevant for the properties of an electrolyte solution.[4] Mass transport occurs through three different modes: convection, diffusion and migration, owing to the presence of density and concentration gradients and electrical fields, respectively. Movement by convection can either be a result of density gradients or physical stimulus (*e.g.* stirring the solution or vibrating the electrode), commonly termed natural and forced convection.[5] The introduction of an electric field into an electrolyte solution induces ion motion by migration. Migration is exclusive of charged species and even neutral species, due to the existence of dipoles and induced dipoles, respectively.[4] Diffusion occurs when at least one of the components of a solution is unevenly distributed.[3] Fick's first law (Eq. I) describes diffusion as the flux (*J*) of species dependent on concentration gradient ($\delta c/\delta x$) and diffusion coefficient (D):

$$\textbf{Eq. I} \qquad J = D\frac{\delta c}{\delta x}$$

Fick's law is applicable to low ion concentrations, as the proportionality between diffusion flux and concentration gradient is neglectable at high concentrations, conditions at which the diffusion coefficient will no longer be constant.[3,4]

1.1.3 *Electric current*

When an electric field (*E*) is applied to an electrolyte solution, its constituent ions will experience a force ($\vec{F}$) responsible for their motion, accordingly to the sign of the charge (z).

$$\textbf{Eq. II} \qquad \vec{F} = Ze_0E$$

Negatively or positively-charged ions will move against or in the direction of the applied electric field. This displacement leads to charge transport, originating an electrical current, which flows through the solution.[2] The velocity at which ions move is dependent on their charge and size; the latter limits the motion of the solvated ion along the solution whilst the former dictates the interactions with the surrounding species as well as the direction of migration.[4] Electric fields provoke the motion of charged species, thus inducing motion by migration and subsequent concentration differences. Although non-charged species are not influenced by these fields, diffusion occurs due the formation of concentration gradients. The mobility of the solvated ions under the influence of an electric field limits the ability of a solution to withstand the flow of electrical current. Viscosity, electric field strength and resulting frictional force charged-species experience play an important role regarding the electrical conductivity of the solution.

The introduction of an electric field into an electrolyte solution requires the placement of at least two electronic conductors and the application of a voltage. Electronic conductors, commonly termed as electrodes, allow the passage of electric current.[6] These conductors can be built from free electron-containing liquids or solids such as metals, carbon, semiconductors and others.[4] Charge transport through an electrolyte solution or an electronic conductor is quite different owing to the migrating species and the effects of migration itself. Once an electrolyte solution is disturbed by an electric field, ions migrate accordingly to their charge (supporting this migration of charge makes an electrolyte solution an ionic conductor). Inherently, ion migration will change the electrolyte distribution, by creating concentration differences due to ion motion towards different electrodes. On the other hand, electronic conductors conduct electrons and these charged species migrate without changing the conductor.[2]

Theoretical treatment of electrochemical systems is simplified if the mass transport in solution is made by a single process, like diffusion. Thus, migration of electroactive species caused by the electric field is undesirable and can be diminished by the presence of an inert electrolyte at high concentrations. Commonly termed supporting electrolytes, inert electrolytes are the major source of electrically conducting ionic species. Whilst supporting electrolytes can be employed at up to 1 M, electroactive species are present at much lower concentrations (≤ 5 mM).[4] These concentration differences allow current flow through the electrochemical cell without modifying the distribution of electroactive species throughout the cell.

1.1.4 *Electrode-solution interface*

As current flows in the cell, ions move towards electrodes of contrary nature, negatively and positively-charged ions move towards the positive and negative electrodes, correspondingly. Anions are attracted to the anode whilst cations are attracted to the cathode. Non-ionic electrolytes can also move towards electrodes through diffusion, and once electrolytes reach the electrode surface, only electroactive species are able to suffer transformation, namely oxidation or reduction. An electrode acts as an anode or cathode when electrons are drained or provided by the potential meter, respectively. Electroactive species suffer oxidation at the anode, and reduction at the cathode (Figure 2).

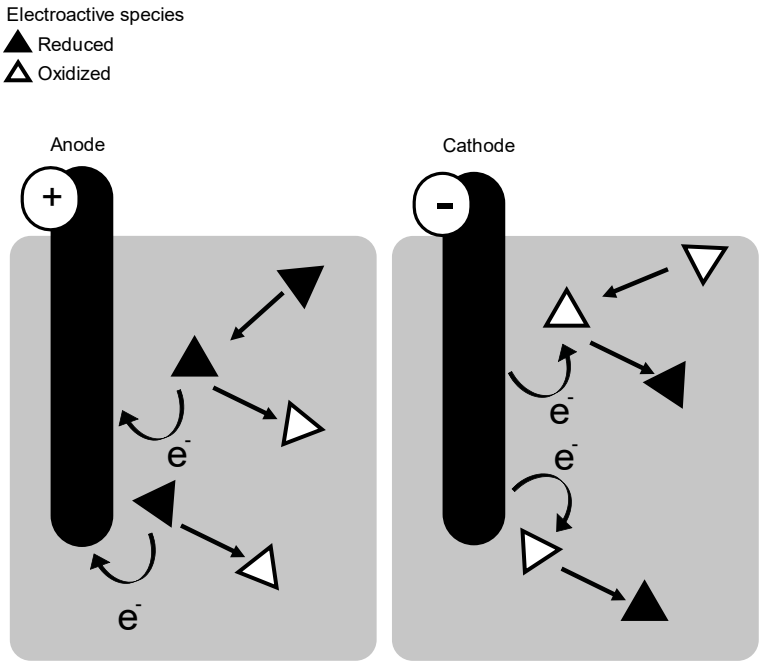

Figure 2. Representation of electrode reactions.

1.1.4.1 Electrical double layer

Near the electrode surface, charged species are rearranged to compensate for the excess of charge on the electrode.[6] Positively-charged electrodes attract a predominant layer of negative ions, which will then attract a layer of positive ions. Negatively-charged electrodes attract a predominant layer of positive ions followed by a layer of negative ions. Both cases generate the architecture termed electrical double layer (EDL).

The first electrical double layer model was described by Helmholtz back in 1879 and consisted in two layers of rigidly arranged anions and cations at the electrode-solution interface, moreover, the effect was considered to be confined to that specific region.[5] Even though the model explained the behaviour of a certain number of systems, it could not explain more complex systems, therefore, the double layer model suffered modifications throughout the years in order to fit experimental data (Figure 3). It wasn't until 1947 that the specific adsorption of ions was taken into consideration by Grahame, whose model considered that once an ion is specifically adsorbed onto the electrode surface, it loses its solvation layer and can be of equal or opposite charge as that of the electrode surface. In 1963, Bocknis, Devanathan and Müller developed a model in which both solute and solvent molecules are adsorbed on the electrode surface, differing from the previous models by taking in consideration that the orientation of solvent dipoles is controlled by the electrode charge.[4] Solvated ions and solvent molecules are adsorbed at the surface of the electrode, displayed along an imaginary plane termed inner Helmholtz plane (IHP). Long-range coulombic forces are responsible for the attachment of these species to the

electrode surface. An additional array of ions will form at the periphery of the IHP and create a second layer of ions along a plane termed outer Helmholtz plane (OHP).

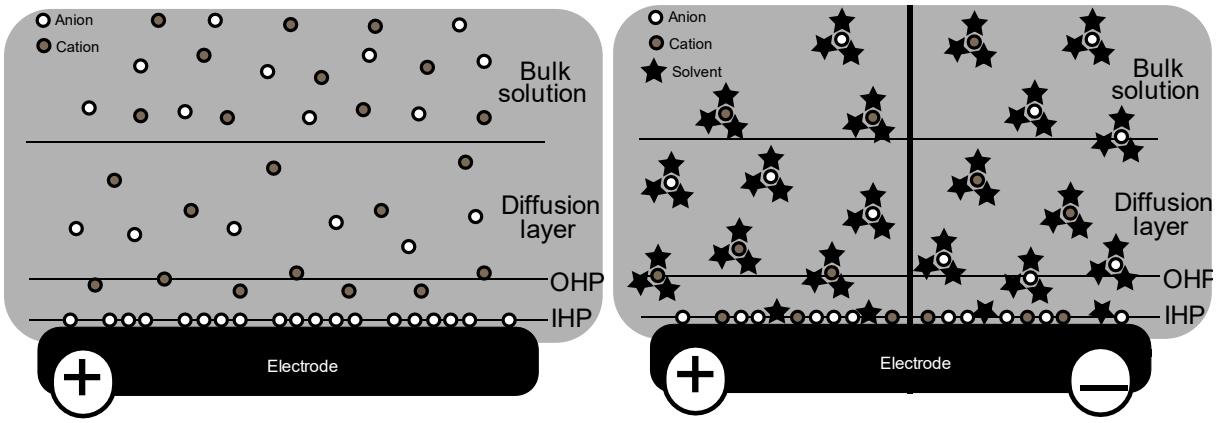

Figure 3. Electrical double layer representation, [left] based on the Helmholtz model and [right] based on a Bocknis, Devanathan and Müller's concept. IHP, inner Helmholtz plane and OHP, outer Helmholtz plane.

The double-layer acts as a capacitor, meaning it stores energy in an electric field. Double layer capacitance is proportional to the surface area of the double layer and is determined by the electrode potential, except for a broad potential window in which it is constant. Electrical double layer formation occurs at the electrode surface once subjected to voltage, therefore, adsorption of substances onto the electrode surface affects the double layer capacitance, as it directly affects the formation of the EDL.[5,6] Additional factors play a role in double layer capacitance, such as temperature, ionic concentration, electrode surface morphology, impurities, and others.

1.1.5 *Faraday's laws*

Michael Faraday formulated two laws in the 19th century, correlating the number of reactants spent in reaction with the charge flowing through the circuit. Faraday's first law stablishes a stoichiometric relation between both reactants and produced electricity. In practical terms, the quantity of reactants involved in a chemical change is proportional to the number of electrons flowing through the system. An electrochemical reaction produces a mass of products proportional to its chemical equivalents, as described by Faraday's second law.[3] Hence, for an equal quantity of charge, the mass ratio of material converted at the two electrodes is equal to the ratio of molar masses of the ion equivalents (M/z).[2] The amount of charge correspondent to the conversion of one chemical equivalent of a certain substance is represented by the Faraday constant (C mol^{-1}), a magnitude of electric charge for a mole of electrons. Steady currents follow rigorously the laws formulated by Faraday, as opposed to transient currents; thus, steady and transient currents are known as faradaic and non-faradaic

currents. Exception to the rule are those currents whose charge accumulates in certain parts of the circuit (*e.g.* near interfaces), aside from being involved in the electrode reactions.[3]

1.2 Electrochemical techniques

Electrode characterization throughout this project will be mainly made by cyclic voltammetry and impedance spectroscopy, briefly introduced in this section, along with chronoamperometry, a technique used in this work to determine the electrode surface area. Electrode modification of any nature, implies the alteration of its surface, thus changing the manner in which the electrode responds to the external environment. Therefore, cyclic voltammetry and impedance spectroscopy will be useful to determine if the alterations to the electrodes made in this project were successful.

1.2.1 *Chronoamperometry*

Chronoamperometry is a useful technique in the determination of diffusion coefficients, rates of electrode processes, adsorption parameters and rates of coupled chemical reactions.[6] Chronoamperometric experiments are either conducted in a single or double-potential step. Single potential step measurements consist in the direct variation of the working electrode potential in one step. Initially, the working electrode is at a potential value at which no reaction occurs, being instantaneously changed to a value at which a reaction takes place. Double potential step measurements provide additional information regarding the species generated in the first potential step. The currents formed by the potential modification are recorded with respect to time. Regarding chronoamperometric studies, the reaction rate depends on the signal input and electronic transfer rate. If the input signal is enough to produce a potential at which the reaction occurs with a significant electronic transfer rate, the reaction is controlled by both diffusion and electronic transfer rate. On the other hand, without the influence of electronic transfer rate, the reaction is controlled by diffusion. Initial and final potentials to be applied are chosen so that the electrode reaction occurs solely by diffusion. When mass transport is strictly made through diffusion, the current decays with time and can be related with other properties such as concentration and diffusion coefficient of electroactive species as well as the electrode's effective area; as given by the Cottrell equation (Eq. III).

$$\textbf{Eq. III} \qquad i = \frac{nFAC\sqrt{D}}{\sqrt{\pi}\sqrt{t}}$$

Where *n* is the number of electrons per molecule; *F* is the Faraday constant (96485 C mol^{-1}); A is the area of the electrode (cm^2); C is the concentration of the active species (mol cm^{-3}); D is the diffusion coefficient of the active species (cm^2 s^{-1}).[5] Electrode surface area or the diffusion coefficient of the electroactive species under

study can be determined if one of them is known. Cottrell's equation is exclusive of electrode processes controlled by diffusion. At short time intervals, besides faradaic contribution, currents are also a product of double-layer charging and at longer time intervals, influenced by natural convection. Therefore, to determine parameters from the Cottrell equation, measurements should be made under no stirring or heating and preferably not at long time intervals in order to eliminate the contribution of natural convection, condition in which the Cottrell equation is not applicable.

1.2.2 *Cyclic voltammetry*

Cyclic voltammetry is a widely used electroanalytical technique in which the potential of a stationary working electrode is linearly scanned through a triangular potential wave-form and resulting currents are registered. Cyclic voltammograms elucidate the type of reaction occurring at the electrode surface.[4] Additionally, cyclic voltammetry is known for its simplicity and low cost. Reactions taking place at the electrode surface determine the electrode behaviour, so that a cyclic voltammogram provides information regarding the thermodynamics of redox processes, kinetics of heterogeneous electron-transfer reactions, coupled chemical reactions or adsorption processes.[5] Reversible, quasi-reversible and irreversible electron transfer reactions will give rise to different cyclic voltammograms (Figure 4). Reversible reactions originate cyclic voltammograms of symmetric anodic and cathodic peaks because the product of the forward potential scan, be it positively or negatively directed, will suffer reduction or oxidation at the reverse potential scan, respectively. On the other hand, irreversible electrode reactions translate differently into cyclic voltammograms, as generally the peaks are different; the reverse scan originates a peak significantly smaller or even inexistent, in comparison to the peak previously formed in the forward scan. Quasi-reversible reactions are characterized by less intense peaks, with higher peak-to-peak separation. Regarding peak shape, reversible reactions are characterized by sharp peaks, whilst broader peaks are characteristic of quasi reversible and irreversible reactions.

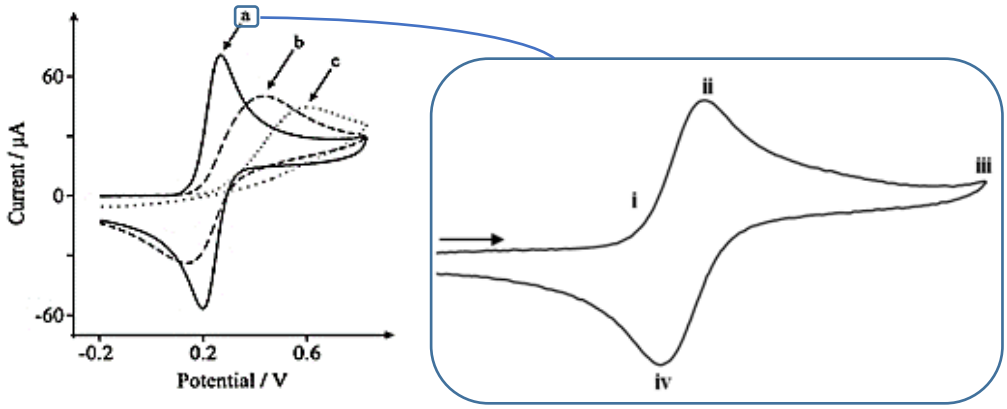

Figure 4. Cyclic voltammogram of reversible (a), quasi-reversible (b), and irreversible (c) electron transfer.[7]

Considering a reversible single electron transfer reaction:

$$O + e^{-} \rightleftharpoons R$$

And a system consisting of R species, if the potential scan begins at a potential at which no electrode reactions take place, as the potential increases, a small amount of R is oxidized at the electrode surface and a small layer of O is formed (i), until the maximum oxidation current is achieved (ii) (Figure 4). Past the maximum anodic current, the current decreases as the concentration of R at the electrode surface is close to zero (iii). The response is controlled by electrode kinetics until the maximum current is achieved, past this point, it is controlled by diffusion. The scan is reversed (iii) and the O species previously formed in the forward scan are reduced to R until a maximum cathodic current is achieved (iv). At the cathodic peak, all O species near the electrode surface are converted to R. Beyond the cathodic peak, remaining O species diffuse towards the electrode and are converted to R, until the concentration of R species are regenerated.

1.2.3 *Impedance Spectroscopy*

Electrical resistance (*R*) represents the capacity of a circuit element to resist the flow of electrical current, Ohm's law (Eq. II) states that resistance is the proportion between input voltage (*V*) and output current (*I*).

$$\textbf{Eq. II} \qquad R = \frac{V}{I}$$

Ohm's law is only applicable to a particular circuit element, namely an ideal resistor, whose resistance is independent of AC frequency, AC current and voltage. Impedance (*Z*) is a complex electrical resistance, and similar to resistance, impedance represents the opposition of an element to a current when a voltage is applied. Unlike resistance, impedance takes in consideration the phase differences between the applied voltage and output

current. Impedance comprises both resistance to the flow of electrical current and ability to store electrical energy, respectively represented as real and imaginary impedance terms.[8]

Impedance studies are based on the measurement of an electrochemical cell response when exposed to a small-amplitude alternating potential. Typically, the cell is exposed to a range of frequencies and the phase shift of the resulting current is monitored. Processes such as mass transport, adsorption and chemical steps, electron transfer, and other electrochemical phenomena contribute to the total potential drop across the electrochemical cell. Distinction between ohmic resistances (from the solution) and non-ohmic, complex and frequency-dependent resistances (impedances) is essential when an AC current flows through the cell. Applying an AC potential to an electrochemical cell induces the oscillation of the processes at the electrode surface, in accordance to the applied frequency. If a reversible couple is at the vicinity of the electrode surface, the concentrations of both reduced and oxidized species will also oscillate, from the electrode surface throughout the solution; the oscillation progressively reduces as the distance from the electrode increases. Although the contributions to the overall electrochemical process can be discerned, the results are complex and are commonly presented as equivalent model circuits. Model circuits are meant to represent an intricate system, for instance, the Randles circuit (Figure 5).

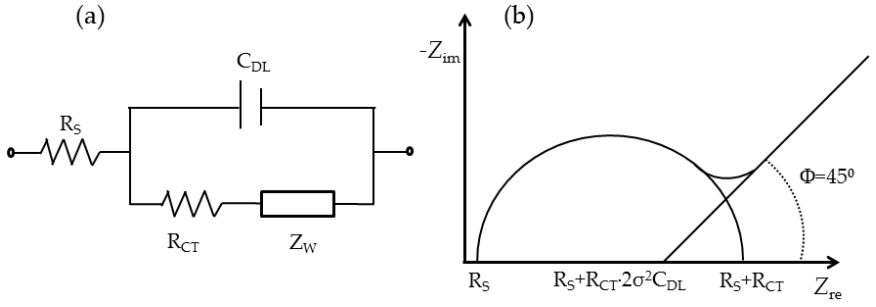

Figure 5. Randles circuit (a) and complex impedance plot (b).[9]

A Randles circuit is an equivalent circuit composed of a solution resistance (R_S) in series with a double-layer capacitance (C_{DL}), which is in parallel with the reaction impedance. The reaction impedance is composed of a charge-transfer impedance (R_{CT}) and a Warburg impedance (Z_W). Warburg impedance is one of the components of the Randles circuit, this impedance is strictly associated with mass transport. At higher frequencies, the magnitude of Warburg impedance decreases; and due to fast reversals of the reaction direction, oxidized and reduced species concentrations are no longer propagated into the solution; therefore, high frequencies allow the exploration of electron-transfer kinetics.[2]

A typical complex impedance plot for a Randles circuit is characterized by a semicircle and a 45° line. The semicircle, as the electrode response to higher frequencies, is related to charge-transfer processes; it is electrically represented by a resistance in parallel with a capacitor ($C_{DL} \parallel R_{CT}$). The 45° line defines a Warburg region of semi-infinite diffusion of species to the electrode, resultant of low frequencies.[10]

1.2.4 *Practical considerations*

The most common circuit in electrochemical measurements is the three-electrode arrangement, in which three electrodes, reference, working and auxiliary, are connected to a potentiostat (Figure 6). Reference electrodes, as suggested by the designation, are electrodes of constant and known potential to which other potentials can be referred to, as potentials are strictly presented as potential differences. The electrode at which the reactions of interest will take place throughout the measurements is termed working electrode, and its potential is manipulated to reach a determined potential. Working electrode potential is controlled in relation to the reference electrode. Counter or auxiliary electrode is an inert electrode whose main purpose is to complete the circuit, as it receives the current formed during the experiments. Electrode placement is crucial in electrochemical techniques. Although the position of the counter electrode is unimportant, the distance from the reference electrode relative to the working electrode is very important. Short distances are aimed to minimize the potential drop between the two electrodes.

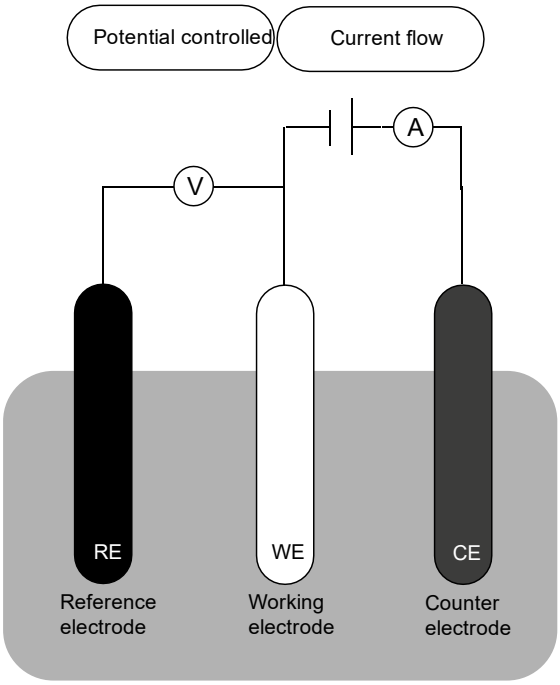

Figure 6. Three-electrode cell. (RE) reference, (WE) working, and (CE) counter electrodes.

1.3 Sensors

Sensors are designed to retrieve information regarding a specific target; when that target is of a specific chemical nature, the devices are termed chemical sensors. Depending on the property being explored, these can be divided into categories like electrical, optical, mass or thermal chemical sensors, among others. Electrochemical sensors are advantageous, due to their great detectability (sensitivity), low-cost and simplicity experimentally-wise.[11,12] Electrochemical sensors comprise a recognition element that will interact with the target chemical species, thus generating a signal, connected to a transducer, responsible for the conversion of the response into a measurable signal. The chemical changes resultant from the interaction between the target species and recognition element are converted by the transducer into electrical signals; which are correlated to the concentration of target chemical species. Authors divide electrochemical sensors into several groups, potentiometric, amperometric, voltammetric, and conductometric sensors (Figure 7).[13]

Potentiometric sensors are used to detect a target species by measuring the potential response with a two-electrode system. Potential measurements are made when the electrode interface is at equilibrium and no current is formed. A potential meter measures the potential amid two electrodes, indicating and reference electrodes, which will depend on the analyte concentration.[11] Ion-selective electrodes (ISEs) are the most common potentiometric sensors, having been extensively used for the determination of inorganic and organic ions in environmental, industrial and medical samples. Out of the parameters a sensor is judged upon, limit of detection (LOD) is quite important, as it is literally the minimum concentration of analyte that can be detected. ISEs have low limit of detection and additional interesting features such as small size, which translates into device portability, ease of operation and low cost. According to Yin *et al.*, nanomaterials are of great importance to apply as solid contacts, biosensing transducers and substrates for ionophore immobilization. Properties such as conductivity, electrocatalytic activity, mechanical strength and large surface area to volume ratio, make nanomaterials appealing for sensing purposes.[14]

Amperometric sensors work by applying a potential between two electrodes, which will cause the oxidation or reduction of an electroactive species and thus lead to the formation of a current that is measured afterwards. The relation between the produced current and electroactive species concentration is expected to be proportional. Amperometric experiments expose the electrochemical cell to a single potential. Voltammetric experiments are performed through the scanning of potential, and the current is recorded with relation to the applied potential.

Gopalan *et al.* built a voltammetric sensor used for the simultaneous determination of ascorbic acid and dopamine, by depositing a β-cyclodextrin and 4-aminothiophenol complex on a glassy carbon surface, which was further modified with electrochemically reduced gold nanoparticles.[15] Cheng *et al.* constructed a voltammetric sensor consisting of electrochemically reduced silver nanoparticles over a MPS monolayer assembled over glassy carbon electrode, which had a great electrocatalytic activity towards oxygen reduction.[16] Arévalo *et al.* assembled an amperometric sensor for the detection of glycerol in biodiesel samples by applying a dispersion of multi-walled carbon nanotubes and pectin over glassy carbon electrode.[17]

Less explored than the types of electrochemical sensors mentioned above, conductometric sensors are devices that rely on electric conductivity changes of a film or a bulk material [11], meaning that reactions which involve changes of a medium regarding charged species are easily detected by these devices.

Selectivity is a parameter of great importance, as sensors are seldom built to be used in pure environments. Most samples are complex, containing a panoply of molecules of both similar and different chemical nature/function, which might interfere with the detection of a certain compound. Interferences are immensely unwanted, and a way to deviate this phenomenon that gives rise to false positives and/or may induce errors in the target-analyte quantification, is to have entities that are highly specific towards the target-analyte. Biological materials like enzymes, proteins that mediate specific reactions, are known for their remarkably high specificity; sensors that incorporate biological entities are termed biosensors.

Biosensors are devices constituted by a biological entity linked to a transducer, capable of detecting and/or quantifying biological target molecules, thus being of great importance and value. Its sensing capability is based on the recognition of a chemical or biological analyte, by the biological entity, commonly termed bioreceptor. Once the target analyte is detected by the bioreceptor, a reaction takes place, thus inducing changes that will be detected. Both specificity and biocompatibility are issues of enormous importance for biosensors, having in mind that the device is expected to be in contact with biological samples. Specific targeting and compatibility with samples of biological nature are desired attributes of biosensors and rather limiting regarding sensor composition. Enzymatic reactions comprise either the consumption or production of charged species, therefore modifying the ionic composition of the sample, which makes conductometric biosensors based on the immobilization of enzymes in thin films, a doable and simple approach. Such interesting devices come with peculiar advantages, like suitability for miniaturization and large-scale production, light sensibility and unrequired reference electrode.[18,19]

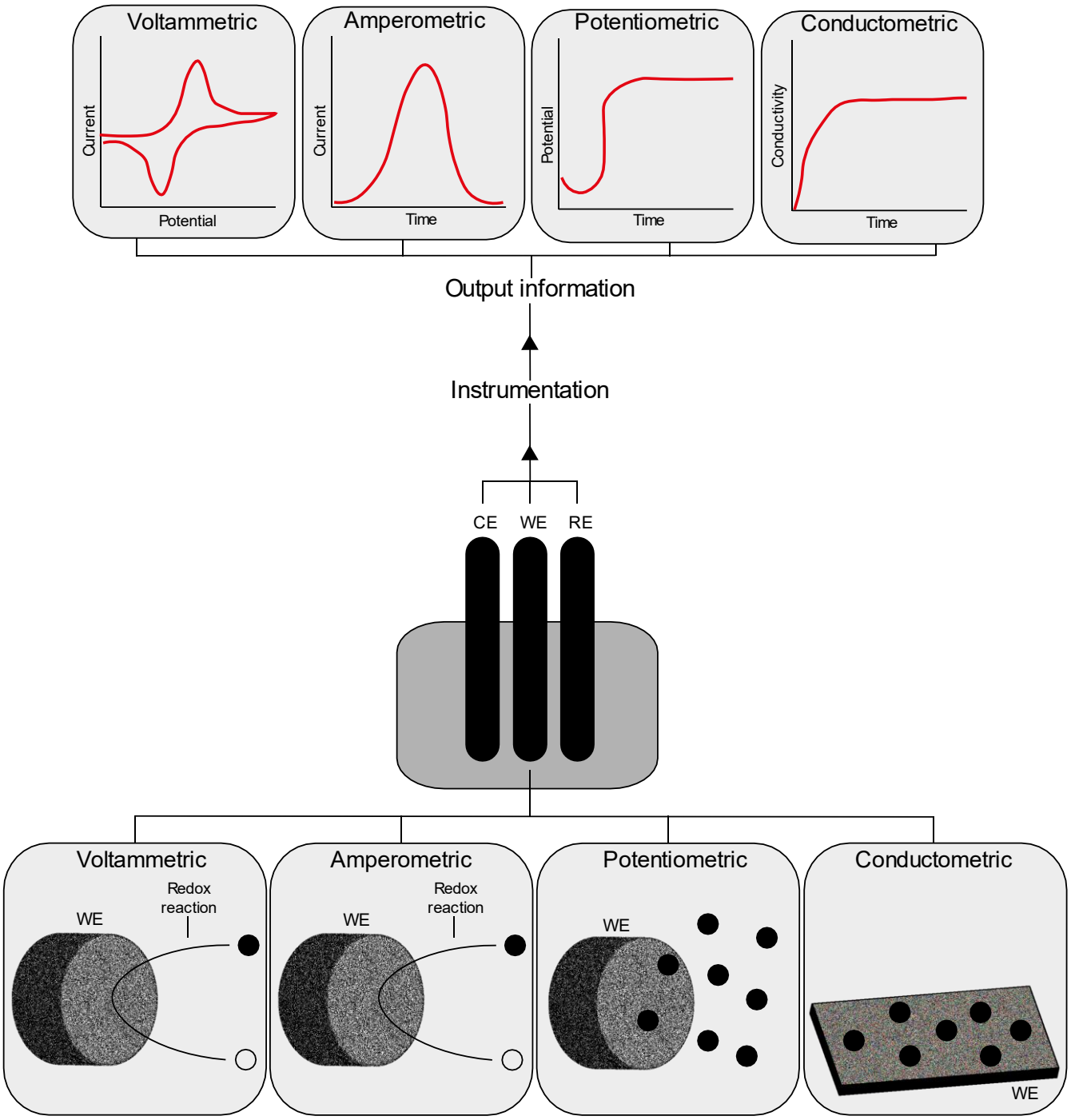

Figure 7. Electrochemical sensors representation.

1.4 Nanomaterials

Nanochemistry is the field of chemistry responsible for the study of materials designated as nanomaterials; whilst nanotechnology consists on the manipulation, characterization and engineering of nanomaterials. This relatively novel field of science has drawn attention due to the promising properties nanomaterials exhibit and consequently, the multiple applications they can have. Nanochemistry is not a secluded field, it englobes knowledge from fields other than chemistry, such as physics, biology, material sciences and engineering; making it a multidisciplinary area of study. The applications are equally multiple, from electronics to textile. Nanotechnology has had a considerable impact, allowing the improvement of our life-style. Its development is the target of great interest and investment.

To define a nanomaterial, many authors focus on a specific definition: a material with 1-100 nm in at least one dimension.[20] European Commission defines a nanomaterial as a natural, accidental or manufactured material where 1-50% of the particles in the number size distribution have one or more external dimensions is in the size range of 1-100 nm. The particles can either be aggregated, agglomerated or unbound.[21] Nano-sized particles display different properties from the bulk material [22], such as higher surface to mass ratio, enhanced surface reactivity, ion release [23], electrical, optical, catalytic and magnetic properties.[24] Application-wise, nanomaterials are extremely versatile, as concrete and specific use can be given to these materials taking advantage of their specific properties. Nanomaterials are employed in medicine, namely in drug and gene delivery, tissue engineering, detection of pathogens, proteins and other biological components, as well as fluorescent biological labels and contrast enhancer in magnetic resonance imaging (MRI).[25,26] As for food industry, nanomaterials are employed in agricultural production, food development, processing and preservation.[23] From batteries to wastewater treatment, a smaller but equally important part of nanomaterial-related research is directed towards nowadays issues, such as clean and renewable energy and drinkable water.[24]

Nanomaterials are an extensive group and their categorization is crucial. These materials can be distributed along four categories: zero, one, two or three-dimensional nanomaterials. Nanomaterials are inserted into a category according to the number of dimensions it exhibits within the nanoscale range (1-100 nm). Zero, one and two-dimensional nanomaterials have all three, two and one dimensions at the nanoscale range, respectively. Three-dimensional nanomaterials are not at the nanoscale, but have zero, one or two-dimensional nanomaterials in their composition.

Nanoparticles are zero-dimensional materials, as all their dimensions (length, width and height) fall into the nanoscale range of 1-100 nm.[20] Nanoparticles are obtained through one of two approaches: bottom-up or

top-down. Top-down synthesis implies a bulk reagent which, through a disruptive process, will originate nanoparticles of the same material (*e.g.* etching**)**. Bottom-up synthesis revolves around the fabrication of nanoparticles using starting-materials comprised in their composition (*e.g.* seed mediated method).[27] Nanoparticles can be discriminated into a wide number of groups (like quantum dots, metallic and polymeric nanoparticles) and some of them have applications in the field of electrochemistry.

Luminescent semiconducting nanocrystals, commonly termed quantum dots (QDs), are mainly used for imaging purposes due to their size-dependent bright coloration and photoluminescent properties. CdSe and CdTe nanoparticles are the most known quantum dots, although their biological applications are limited as a result of their toxic composition. Nevertheless, toxic effects associated to QDs can be prevented by functionalization.[28] Their synthesis and characterization methods are broadly accessible and relatively simple. Owing to their optoelectronic properties, quantum dots are broadly employed as electronic transistors and photodetectors, as well as in circuitry and photovoltaic devices.[29] Polymers are molecules built by small building blocks (monomers). Polymeric nanoparticles (PNPs) are versatile; the size, shape, and monomer nature conditionate PNPs properties and applications. Polymeric nanoparticles have applications in medicine (*e.g.* as components in drug delivery systems), in nanocomposites and optoelectronics.[30]

Metallic nanoparticles (MNPs) are nano-sized particles composed of metallic elements. The main focus has been nanoparticles of noble metals such as Pd, Pt, Ru, Rh, Au and Ag; and expanded towards other metals for instance Cu, Fe, and Zn.[26] MNPs assume morphologies other than spherical, such as conical, triangular, oval, cylindrical, amongst others. Nanoparticle morphology and composition dictate their physical and chemical properties, *e.g.* spherical silver and gold nanoparticles are yellow and red, correspondingly.[22] Recently, metallic nanoparticles have been widely applied in biomedical sciences and engineering owing to their modifiability. Synthesis and modification of nanoparticles is a junction of infinite options, as nowadays a nanomaterial is tailored accordingly to its purpose. Diagnostic imaging is an important area of application for metallic nanoparticles such as silver, gold and magnetic nanoparticles of iron oxide (Fe_3O_4), which have been extensively employed in the fabrication of novel contrast agents for MRI.[26,31]

One-dimensional nanomaterials display two out of three dimensions at the nanoscale, and have been the focus regarding electronics, devices and systems at the nanoscale.[32] Top-down (electric arc discharge, laser ablation, ball milling-annealing) and bottom-up (chemical vapor deposition) approaches can be used to fabricate one-dimensional nanomaterials such as nanotubes, nanorods and nanowires. Size and structure of 1D nanomaterials can be controlled by the processes applied in their synthesis and treatment.[33,34] Two-dimensional nanomaterials have one dimension at the nanoscale range, and are materials that differ from the bulk material as

they have size and shape-dependent characteristics that have proved to be interesting when employed in sensors, photocatalysts, templates and nanodevices. Nanosheets, nanodisks, nanoplates, self-assembled monolayers and nanocoatings are examples of 2D nanomaterials.[32]

1.4.1 *Self-Assembled Monolayers*

Self-assembled monolayers are a result of the spontaneous adsorption of organic molecules from solution or gas phase onto solid surfaces, forming crystalline or semi crystalline structures (Figure 8). Organic molecules are easily adsorbed into metal and metal oxide surfaces, thus decreasing the free energy of the surface-ambient environment boundary. Randomly coated surfaces exhibit non-specific chemical and physical properties (*e.g.* conductivity and resistance to corrosion). Therefore, once optimized, self-assembled monolayers grant a simple system that provides reproducibility.[35] Organic monolayers have applications on wetting control, corrosion inhibition, molecular and bioelectronic devices.[36]

The organic molecule is sectioned into three parts: head-group or ligand, body and end-group; each of them important for the SAM formation (Figure 8). The head-group is responsible for the adsorption of the molecule to the substrate surface and exhibits a specific substrate affinity. High affinities towards a surface results in the displacement of adventitious organic materials previously adsorbed at the surface (impurities). Ligand absorption modifies electronic states and stabilizes surface atoms. Considering that the end-group will be exposed to the external environment of the covered surface upon formation of the monolayer, it can be termed functional group, once it determines surface properties of the modified material. The body acts as a physical barrier of a precise thickness and modifies electronic conductivity and local optical properties.[35] SAMs are stable enough to resist removal by solvent rinsing, owing to ligand-substrate bonds and lateral Van der Waals interactions amid the molecules.[37]

Alkanethiols and related molecules naturally adsorb onto noble metals, consequentially forming a well-defined monolayer with mutable chemical functionalities displayed at the exposed boundary. Sulphur has a great affinity towards gold and S-Au bonds are predominantly of covalent nature with a polar component.[35,37] Self-assembled monolayers of alkanethiols are naturally formed and the spontaneous assembly process is characterized by two kinetically different phases, adsorption and reorganization. Whilst adsorption happens swiftly, molecular reorganization occurs slowly over larger periods, even for several hours.

Molecular adsorption and desorption can be electrochemically activated, as alkanethiol SAM formation kinetics is increased at positive potentials and the opposite phenomenon, alkanethiol monolayer desorption, takes place in alkaline solutions at negative potentials.[36,37]

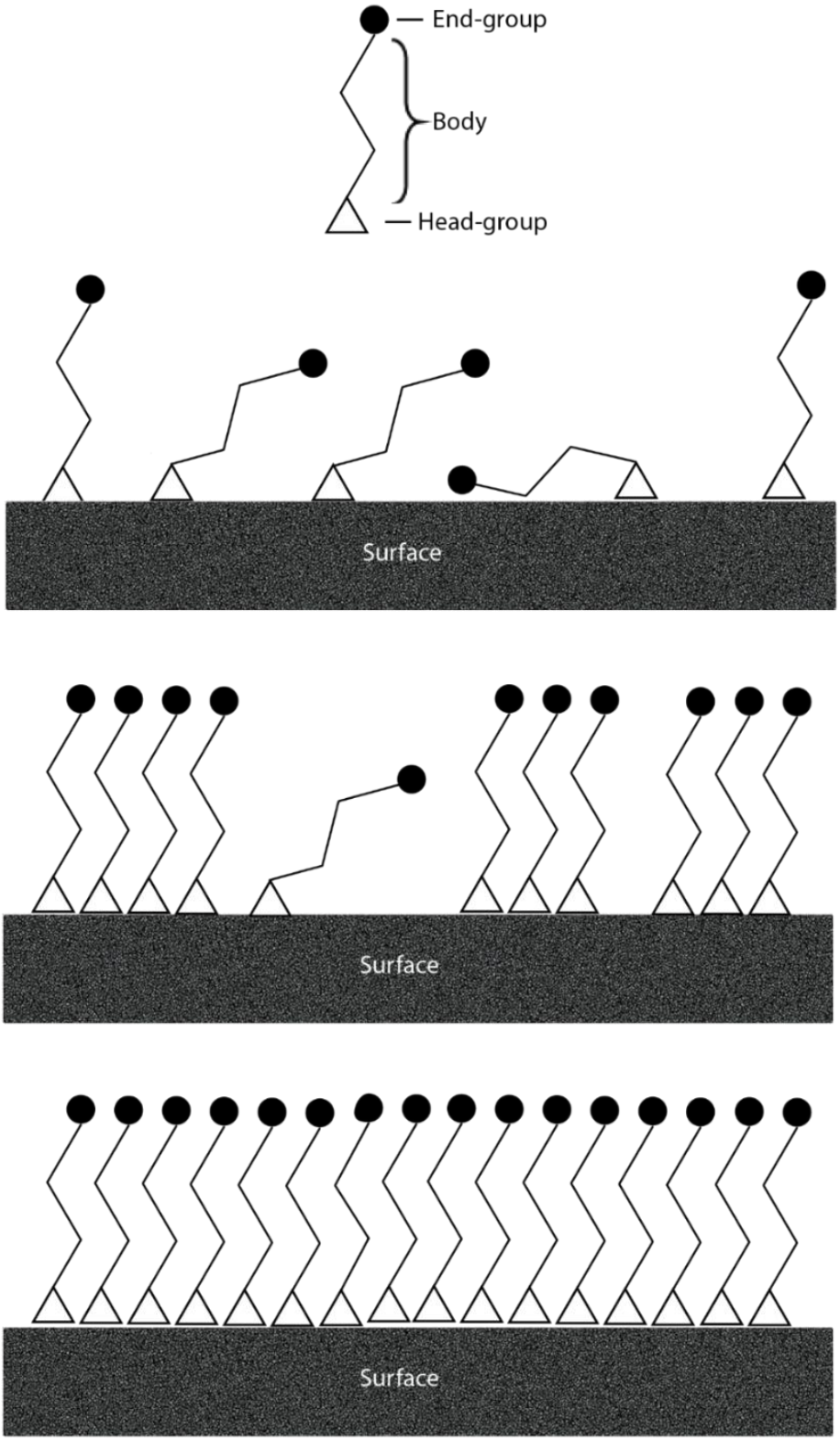

Figure 8. Assembly of a self-assembled monolayer (SAM).

1.4.2 *PAMAM Dendrimers*

Dendrimers are highly symmetrical branched polymeric nanoparticles, typically divided into three parts: a core, branched units and surface groups. The branched units are repeated in layers, termed generations. These synthetic molecules are applied in biosensor technology owing to properties such as monodispersity, tuneable size and structure, surface modifiability, multivalency, hydrophilicity and high stability, both mechanical and chemical.[38-42] Dendrimer synthesis is divided into two major approaches, divergent and convergent. Divergent synthesis consists in the successive monomer addition to the molecules resulting from previous addition of monomer branching units to the core, thus growing uniformly; as for convergent synthesis, dendrons are created separately until the desired generation is reached and linked to form the final product. Hindrance effects are accentuated as dendrimer generation increases, owing to a growing number of end-groups, which are concentrated in a limited space. Therefore, hindrance effects limit the number of generations a dendrimer can be grown into. Morphologically, dendrimers are flat at lower generations, becoming more globular as the generation increases.[43]

Noticeable for being the first commercially available dendrimers, poly(amidoamine) (PAMAM) dendrimers have well-defined structures, and are composed by an ethylene diamine (EDA) core and an amidoamine repeating monomer unit (Figure 9). The surface functionalization can be changed from primary amine (NH_2) to carboxylate ($-COO^-$), hydrophobic chains, and others. This dendrimer family has generation-dependent size and number of end-groups; and whilst diameter increases linearly, surface groups increase exponentially (Table 1).

Although PAMAM dendrimers are mainly associated to the field of medicine due the amount of research groups studying it as drug carriers and delivery agents as well as other finalities with therapeutic effects[41], other applications have been explored (*e.g.* sensing).[38] Lately, a growing tendency to develop biosensors based on PAMAM dendrimers is noticeable. Whilst enzymes, DNA (deoxyribonucleic acid), and other biomolecules dictate the specificity of a biosensor, PAMAM dendrimers constitute a good platform for the attachment of biomolecules to the transducer without altering the functionality of both bioreceptor and sensor as a whole. Also, its multivalency allows the conjugation of one dendrimer with multiple biomolecules. The purpose of PAMAM dendrimers inclusion in the construction of a sensor is the increase of surface area, which could lead to signal amplification. While the considerable low conductivity of PAMAM dendrimers is not very enticing for electrochemical purposes, it can be increased by the addition of conductive nanomaterials, like metallic nanoparticles, therefore improving electron transfer. Bahadir *et al.* report biosensor stability and sensitivity were improved by the presence of PAMAM dendrimers.

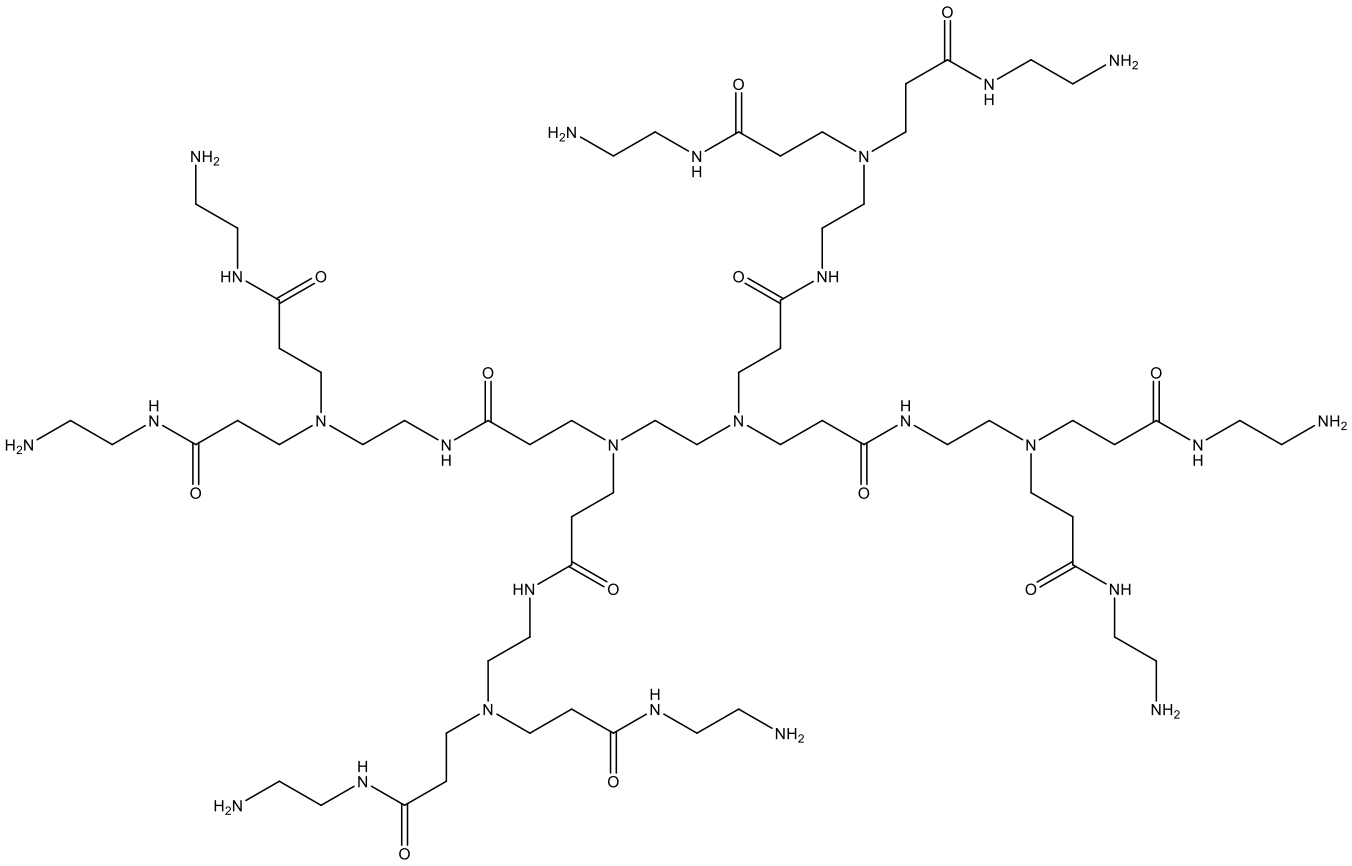

Figure 9. G1 Polyamidoamine dendrimer.

Table 1. Amine-terminated PAMAM dendrimer properties, molecular weight, size and number of end-groups.[44]

Generation	***0***	***1***	***2***	***3***	***4***	***5***	***6***
Molecular weight (g/mol)	517	1430	3256	6909	14215	28826	58048
Size (nm)	1.5	2.2	2.9	3.6	4.5	5.4	6.7
End-groups	4	8	16	32	64	128	256

1.4.3 *Gold Nanoparticles*

Scientific interest in gold nanoparticles can be dated back to the 1850s, when Michael Faraday reported that colloidal gold solutions displayed different colorations from the bulk material.[45,46] At the time, it was known that the characteristic golden coloration resulted from interaction between the bulk material and light. Therefore, different coloration attributed to colloidal gold should be a result of different interaction of the colloidal particles with light. Thus, spherical colloidal gold exhibits a red/pink colour as opposed to the golden yellow found in jewellery (Figure 10).

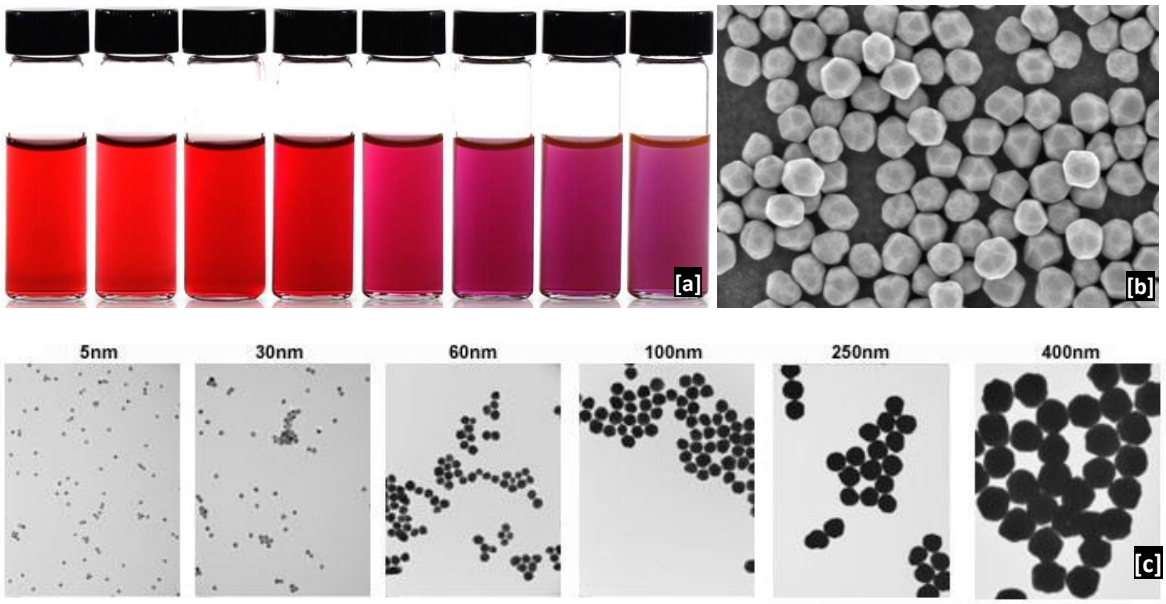

Figure 10. (a) Colloidal gold solutions;[47] (b) SEM image of gold nanoparticles;[48] and (c) HR-TEM image of gold nanoparticles[49].

Gold nanoparticle formation is made with a gold precursor (any compound that dissociates into gold ions) and a reducing agent, furthermore, it occurs through two phases: nucleation and growth (Figure 11). Nucleation entails the process by which gold ions are reduced to gold atoms (Au^0), forming small nuclei. The agent-mediated reduction is extended, and further gold ions in solution are reduced at the surface of the previously formed nuclei, which will grow in size. Physichochemical properties such as size and shape, are dictated by the type of reducing agent, particularly its reducing strength and concentration. The employment of strong reducing agents results in smaller particles, while larger particles are formed when weaker reducing agents are used. Also, high concentrations of reducing agents will generate smaller particles, for the amount of nuclei formed will be higher, resulting in smaller particles. Low concentrations generate fewer nuclei, leading to less particles with greater size. In addition to reducing agent strenght, pH plays an important role in the kinetic of gold nanoparticle synthesis with acidic media favouring the formation of smaller particles.[50] Some compounds can influence particle growth,

allowing nanoparticle tailoring. Also, stabilizers addition is common as such compounds avoid nanoparticle agglomeration and further precipitation.

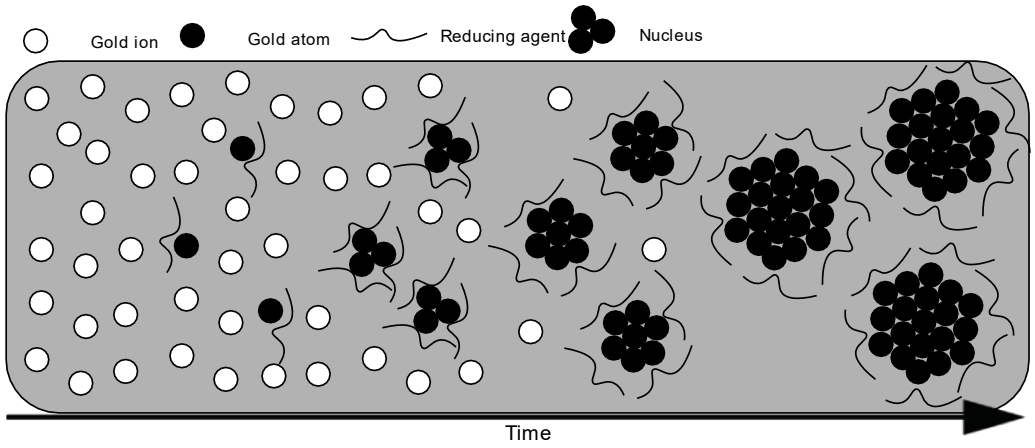

Figure 11. Representation of gold nanoparticle synthesis.

When exposed to an oscillating electromagnetic field (light) the free electrons of the metal nanoparticles oscillate with respect to the metal lattice; at a particular frequency, such oscillation is resonant and is termed surface plasmon resonance (SPR) (Figure 12). The adsorbed energy is radiatively and non-radiatively expelled as scattered light or heat.[31] SPR effect is dependent of the nanoparticle polarizability, which is determined by properties such as shape, size, composition, solvent and surface coating. SPR wavelength for spherical nanoparticles takes place between 520 nm and 800 nm, and is determined by its radius, composition, and refractive index of the solvent.[51] Morphological dependence of SPR is shown by the red shift observed in spherical nanoparticles as radius increases and multiple SPR modes attributed to non-symmetrical nanoparticles, *e.g.* gold nanorods exhibit transverse and longitudinal SPR. Adsorption and desorption of molecules from the nanoparticle surface changes the refractive index of the surrounding medium, translating into different SPR wavelengths, which makes plasmonic nanoparticles great candidates in molecular sensing.[52]

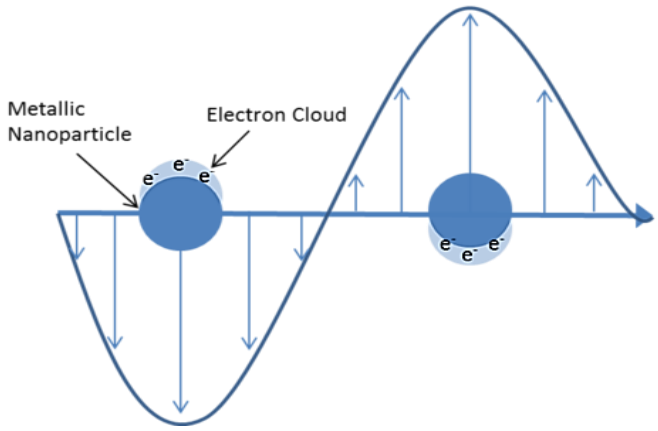

Figure 12. Surface plasmon resonance (SPR) for a spherical gold nanoparticle.[52]

Due to its biocompatibility, gold nanoparticles are widely employed in biosensors, such as enzymatic sensors.[53,54] Besides increasing conductivity, gold nanoparticles are suitable to connect biological entities responsible for analyte detection to electrodes, with the biomolecules maintaining their functional conformation. Appealing characteristics of gold nanoparticle employment on electrode architecture include enhanced sensitivity as electron transfer is enhanced, and larger surface area, in comparison to bare electrodes.[55-57]

Akella *et al.* built a voltammetric biosensor based on glucose oxidase, whose immobilization onto the electrode was made by glutathione-coated gold nanoparticles.[58] An amperometric biosensor was constructed by Karadag *et al.*, glucose oxidase was immobilized onto glutaraldehyde, PAMAM dendrimer, cysteamine, and 6-ferrocenyl-1-hexanethiol- modified gold electrode, which was further modified with gold nanoparticles. Glucose detection and determination were heightened by the application of gold nanoparticles.[53] A different approach was pursued by Crespilho *et al.* in the use of both PAMAM dendrimers and gold nanoparticles in a glucose oxidase-based electrode. Multilayers of poly(vinylsulfonic acid) and PAMAM-gold nanoparticles were successively deposited onto an electrode substrate, and followed by a final layer of glucose oxidase. Their approach was different due the use of PAMAM-encapsulated gold nanoparticles, where gold ions are reduced by formic acid inside the dendrimer.[59] Liu *et al.* modified glassy carbon electrodes with 4-aminothiophenol and 4-phenylenediamine before modifying with gold nanoparticles, according to this author, a stable surface was obtained.[60]

1.5 Objectives

The objective of this project is the development and characterization of electrochemical sensors based on PAMAM dendrimers and gold nanoparticles. Therefore, this project was carried out in two parts, synthesis and characterization of modified electrodes and application of the modified electrodes in the reduction of 4-nitrophenol. The first part entails the successive modification of gold and vitreous carbon electrodes with the desired compounds and subsequent modification assessment with cyclic voltammetry and impedance spectroscopy. The modified electrodes characterization was made in hexacyanoferrate (II)/(III) redox couple in potassium chloride. Once the modifications were determined, PAMAM and gold-modified electrodes were tested for the reduction of 4-nitrophenol. In this second part, 4-nitrophenol reduction was evaluated in deoxygenated phosphate buffer solutions containing 4-nitrophenol.

Chapter 2

2. Materials and Methods

2.1 Reagents

Potassium chloride was purchased from Panreac; nitric acid (65%) and analytical grade potassium hexacyanoferrate (III) were obtained from Riedel-deHaën; potassium hexacyanoferrate (II) trihydrate (99%) from Absolve; hexacyanoferrate (II) trihydrate (99%) from José Manuel Gomes dos Santos; sulfuric acid (95%) from AnalaR NORMAPUR; analytical reagent grade ethanol from Fisher Chemicals; 3-mercaptopropionic acid from Fluka Analytical; technical grade 3-mercapto-1-propane sulfonic acid, sodium salt (90%) from Aldrich; 4-aminothiophenol (96%) from ACROS Organics; gold(III) chloride trihydrate and 4-nitrophenol (spectrophotometric grade) from Sigma-Aldrich; G5 NH_2-PAMAM dendrimer from Dendritech; trisodium citrate dihydrate (99%) from Merck; potassium dihydrogen phosphate from Pronalab; di-potassium hydrogen phosphate trihydrate from Merck.

2.2 Electrode modification

2.2.1 *Self-assembled monolayers of thiols*

Prior to any modification, the working electrodes were polished with alumina slurry of 0.3 μm, rinsed with distilled water, polished with alumina slurry of 0.05 μm, rinsed with distilled water, briefly sonicated in distilled water, and then dipped in a thiol-containing solution for two hours. Three thiols were tested, 3-mercaptopropionic acid, 2-mercapto-1-propane sulfonic acid and 4-aminothiophenol. Modification with 3-mercaptopropionic acid (MPA) was made at room temperature at a concentration of 1 M[61]. Modification with 2-mercapto-1-propane sulfonic acid (MPS) was made at a concentration of 0.1 M[16]. Modification with 4-aminothiophenol (ATP) was performed at a concentration of 10 mM[62]. The modified electrodes were rinsed with an ethanolic solution and distilled water, before cyclic voltammetry and impedance spectroscopy characterization.

2.2.2 *Gold layer*

A gold layer was formed over thiol-modified electrodes, through the direct reduction of gold ions. Previously MPA, MPS and ATP-modified electrodes were dipped in a 0.25 mM $HAuCl_4$ solution and a potential of -0.832 V was applied for 60 seconds. Afterwards, the electrodes were briefly rinsed with distilled water and characterized by cyclic voltammetry and impedance spectroscopy.[63,64]

2.2.3 *PAMAM dendrimers*

A 200 μL aliquot of NH_2-PAMAM dendrimer (G5) in methanol (19.81 % (w/w)) was purified through dialysis for an extent of 28 hours, followed by the removal of water by freeze-drying. The isolated PAMAM was dissolved in deionized water. Thiol-modified electrodes were additionally modified with G5-NH_2 PAMAM dendrimers. MPA, MPS and ATP-modified gold and glassy carbon electrodes were dipped in a 1 mg/mL aqueous solution of G5-NH_2 PAMAM dendrimer for two hours.[61] The modified electrodes were rinsed with distilled water. Every modification was assessed through cyclic voltammetry and impedance spectroscopy.

2.2.4 *Gold nanoparticles*

PAMAM-modified electrodes were further modified with gold nanoparticles. Gold nanoparticles, herein colloidal gold, were obtained by the reduction of gold ions by citrate; 2.9 mL of 39 mM trisodium citrate was added to 29 mL of boiling 1 mM solution of chloroauric acid under stirring.[65] As the solution turned a deep red coloration, both heating and stirring were removed. The resulting gold colloid was characterized by ultraviolet and visible spectroscopy (UV-VIS) and dynamic light scattering (DLS). PAMAM-modified electrodes were dipped in a (1:3) gold nanoparticle solution for 2 hours, followed by a brief rinse with distilled water before characterization by cyclic voltammetry and impedance spectroscopy.

2.3 4-Nitrophenol reduction

The detection of 4-nitrophenol was made in 0.05 M PBS (pH 7.4) at a concentration of 0.5 mM. Further cyclic voltammetry measurements were made in 0.05 M PBS (pH 5.3), with p-nitrophenol concentration ranging from 1200 to 12 μM. All solutions were purged with nitrogen (N_2) prior to any measurements.[66]

2.4 Labware cleaning

Electrochemical techniques are highly sensitive to the presence of impurities, specially charged ones, which can affect the currents created during the experiments. Therefore, it is crucial to use impurity-free labware. Thus, prior to any use, all glass labware was sequentially rinsed with water, acetone, water and submerged in Panreac's Derquim detergent (5%) for 15 minutes and then abundantly rinsed with water and distilled water.

2.5 Electrodes and electrochemical equipment

Electrochemical measurements, like cyclic voltammetry, double potential step, and impedance studies were performed using PARSAT 2263 from Princeton Applied Research, controlled by Electrochemistry Power Suite software. Glassy carbon (ϕ = 2.54 mm) was glued to a copper wire with silver glue and immobilized at the

extremity of a glass tube using epoxy glue (Araldite, Ceys). Gold electrode was composed of a gold wire (ϕ = 1 mm) equally immobilized by epoxy glue to the end of a glass tube. The reference electrode used in cyclic voltammetry and double potential step experiments was a saturated calomel electrode (SCE, Radiometer analytical), whilst a platinum sheet electrode was used in the impedance studies. Hence, all potentials related to each technique are referred to its respective reference electrode. Cyclic voltammetry studies were carried in a 5 mM hexacyanoferrate (II) and 0.2 M potassium chloride aqueous solution; impedance studies were performed in an equimolar solution of hexacyanoferrate (II) and hexacyanoferrate (III) (2.5 mM each) and 0.2 M potassium chloride, and double potential step measurements were made in a 5 mM hexacyanoferrate (II) and 0.1 M potassium chloride solution. Every solution was prepared with Millipore water and degasified for 15 minutes with nitrogen gas prior to any measurements, whose conditions are resumed below (Table 2).

Table 2. Conditions used in cyclic voltammetry, double potential step and impedance measurements.

<table>
<tr><td colspan="4">Cyclic voltammetry</td></tr>
<tr><td>Probe</td><td>Hexacyanoferrate</td><td>4-nitrophenol</td><td rowspan="5"> 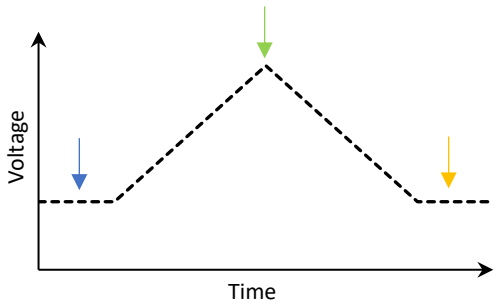
</td></tr>
<tr><td>Initial potential (V)</td><td>-0.2</td><td>-0.2</td></tr>
<tr><td>Vertex potential (V)</td><td>0.7</td><td>-1.2</td></tr>
<tr><td>Final potential (V)</td><td>-0.2</td><td>-0.2</td></tr>
<tr><td>Scan rate (mV s^{-1})</td><td>50</td><td>50</td></tr>
<tr><td colspan="4">Double potential step</td></tr>
<tr><td>Stabilization time (s)</td><td>0.1</td><td rowspan="6"> 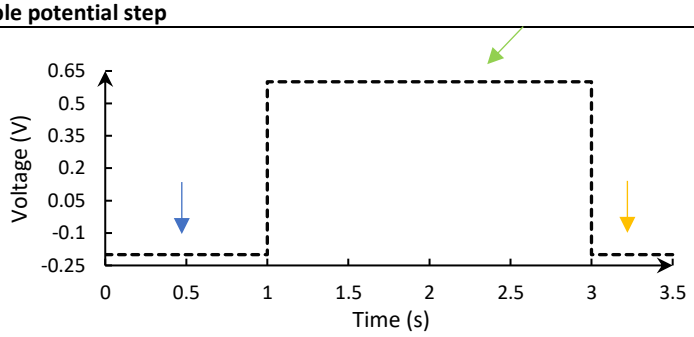
</td></tr>
<tr><td>t_1 (s)</td><td>1</td></tr>
<tr><td>t_2 (s)</td><td>2</td></tr>
<tr><td>E_0 (V)</td><td>-0.2</td></tr>
<tr><td>E_1 (V)</td><td>0.6</td></tr>
<tr><td>E_2 (V)</td><td>-0.2</td></tr>
<tr><td colspan="4">Impedance spectroscopy</td></tr>
<tr><td colspan="2">Start frequency</td><td>200 kHz</td><td rowspan="6">Frequencies applied:
200 kHz, 125 kHz, 78.4 kHz, 49.1 kHz, 30.8 kHz, 19.3 kHz, 12.1 kHz, 7.55 kHz, 4.73 kHz, 2.96 kHz, 1.86 kHz, 1.16 kHz, 728 Hz, 456 Hz, 285 Hz, 179 Hz, 112 Hz, 70.1 Hz, 43.9 Hz, 27.5 Hz, 17.2 Hz, 10.8 Hz, 6.75 Hz, 4.23 Hz, 2.65 Hz, 1.66 Hz, 1.04 Hz, 650 mHz, 407 mHz, 255 mHz, 160 mHz, 100 mHz</td></tr>
<tr><td colspan="2">End frequency</td><td>100 mHz</td></tr>
<tr><td colspan="2">Number of points</td><td>32</td></tr>
<tr><td colspan="3">Logarithmic point spacing</td></tr>
<tr><td colspan="2">AC Amplitude (mV rms)</td><td>10</td></tr>
</table>

2.5.1 *Supporting equipment*

For gold nanoparticle characterization, absorption spectra were obtained from an UV-Vis Spectrophotometer (Lambda 25) from Perkin-Elmer, refraction indexes were measured with ATAGO RX-100 digital refractometer, hydrodynamic sizes and zeta-potential measurements were made with a Zetasizer Nano ZS from Malvern Instruments, and SEM images were obtained with SEM Phenom ProX equipped with BSD, SED, and EDS.

SEM images of bare and modified vitreous carbon surface were obtained with SEM Phenom ProX equipped with BSD, SED, and EDS. Phosphate buffer solutions were prepared and pH measurements were made with a 744 pH meter from Metrohm.

Chapter 3

3. Results and Discussion

3.1 Bare electrodes

Bare electrodes were mainly characterized by cyclic voltammetry and impedance spectroscopy. Apart from this set of techniques, chronoamperometry was used for surface area determination. Prior to any measurement, clean gold and vitreous carbon electrodes were obtained by successive polishment in 0.3 and 0.05 μm alumina slurries and brief sonication in distilled water, followed by rinse with distilled water.

The behaviour of the working electrodes in the supporting electrolyte solution, 0.2 M potassium chloride, was assessed by sweeping the applied potential between 0 and 0.9 V and -0.2 and 1.2 V, for gold and glassy carbon respectively (Figure 13). Anodic currents formation around 0.8 V and 1 V, correspondingly, indicate gold and glassy carbon electrode oxidation. Henceforth, concerning cyclic voltammetry measurements, both gold and glassy carbon electrodes were used in a -0.2 V to 0.7 V potential window, thus excluding the contributions of electrode oxidation.

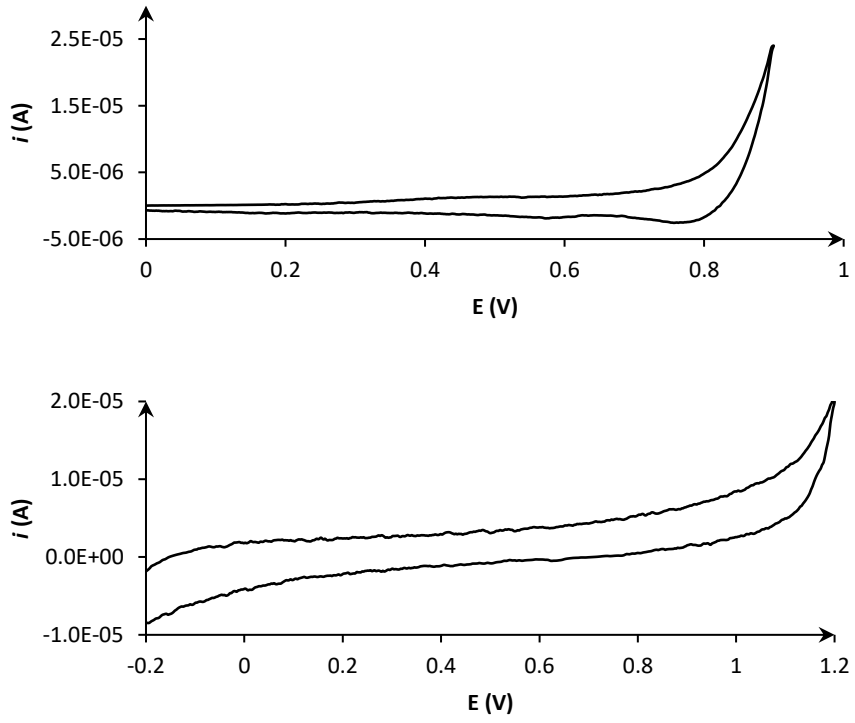

Figure 13. Cyclic voltammogram of gold and glassy carbon electrodes in 0.2 M potassium chloride aqueous solution (vs. SCE). Potential scan between 0 V and 0.9 V and -0.2 and 1.2 V for gold [top] and glassy carbon [bottom] electrodes, respectively; v: 50 mV s^{-1}.

Once a suitable potential window was determined, the characterization of the electrodes in the presence of the electroactive species, hexacyanoferrate (II) was made. Cyclic voltammetry was performed in a solution of 5 mM hexacyanoferrate (II) in 0.2 M potassium chloride (Figure 14). Anodic and cathodic peaks of the hexacyanoferrate (II)/(III) redox couple are respectively placed at 232 mV and 156 mV for gold electrode and 263 mV and 144 mV for the vitreous carbon electrode, at a scan rate of 50 mV s^{-1}. Half-wave potential of the hexacyanoferrate (II)/(III) redox couple in 0.2 M potassium chloride was determined to be 199 ± 5 mV.

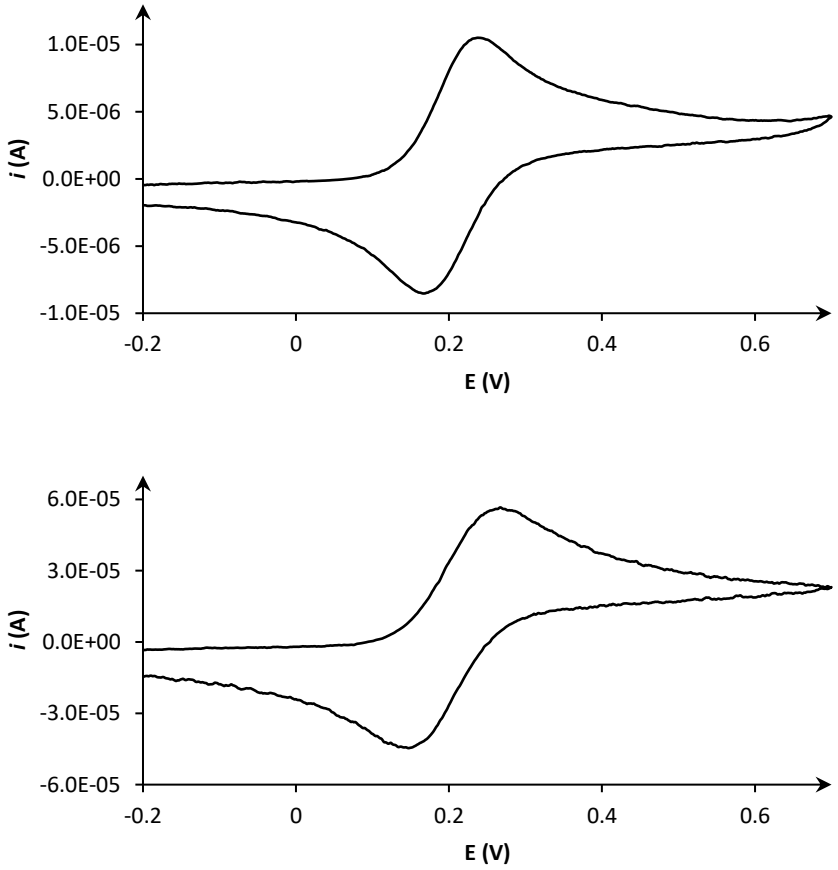

Figure 14. Cyclic voltammogram of bare gold [top] and glassy carbon [bottom] electrodes in 5 mM hexacyanoferrate (II) and 0.2 M potassium chloride aqueous solution (*vs*. SCE). Potential scan between -0.2 V and 0.7 V; v: 50 mV s^{-1}.

Impedance studies were performed on bare gold and vitreous carbon electrodes, which exhibited charge-transfer resistances of 557 Ω and 378 Ω, respectively (Figure 15). Impedance measurements were made in a solution of 2.5 mM hexacyanoferrate (II) and 2.5 mM hexacyanoferrate (III) in 0.2 M potassium chloride. Logarithmically-spaced frequencies were applied from 200 kHz to 100 mHz, with an AC amplitude of 10 mV rms.

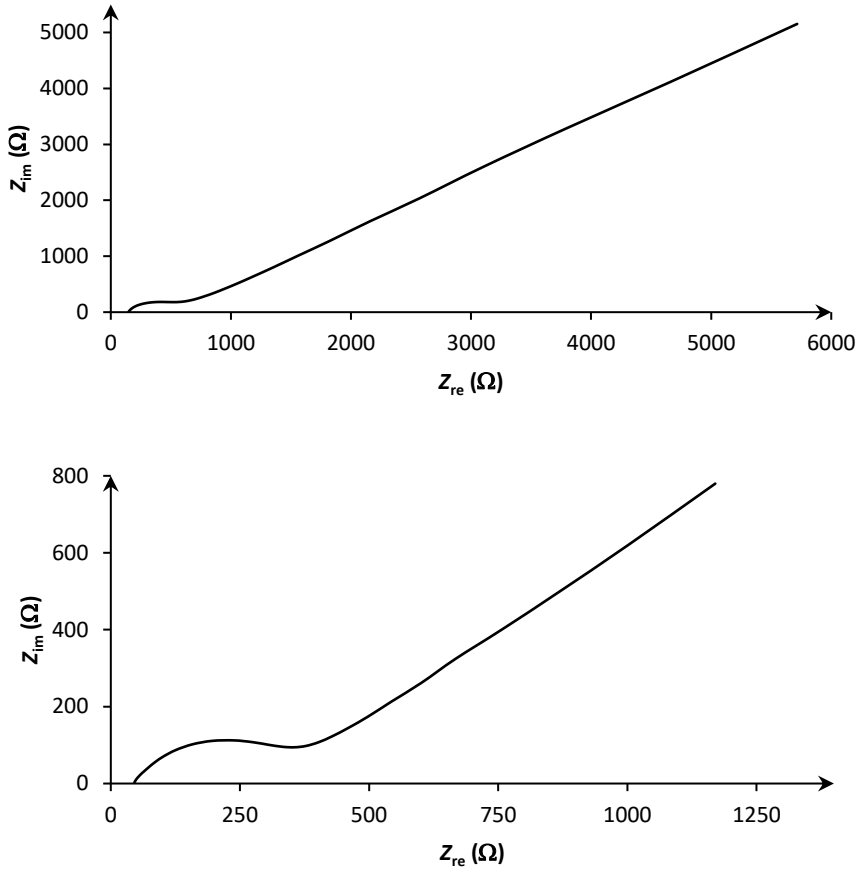

Figure 15. Complex impedance plot of the bare gold [top] and glassy carbon [bottom] electrodes in equimolar 2.5 mM solution of hexacyanoferrate (II) and (III) in 0.2 M potassium chloride (*vs*. Pt). The frequency range is 2×10^5 – 0.1 Hz, AC amplitude of 10 mV rms.

3.1.1 *Mechanistic studies*

Cyclic voltammetry is a technique from which information regarding the thermodynamics of redox processes as well as the kinetics of heterogeneous electron-transfer reactions can be obtained. Several parameters given by the technique are indicators of the type of mechanism taking place. The mechanism of hexacyanoferrate (II) and (III) redox pair is well-known, a quasi-reversible electron-transfer reaction.

$$[Fe(CN_6)]^{4-} \leftrightharpoons [Fe(CN_6)]^{3-} + e^-$$

Five different scan rates were chosen to trace the cyclic voltammograms: 10, 20, 50, 100 and 200 mV s^{-1}. The assays were carried out in a 5 mM hexacyanoferrate (II) and 0.2 M potassium chloride solution (Figure 16). The collected information: anodic and cathodic current peak (i^A and i^C), anodic and cathodic potential peak (E^A and E^C) and half-wave potential ($E_{1/2}$), regarding the employment of hexacyanoferrate (II) as a probe, is condensed in Table 3**.**

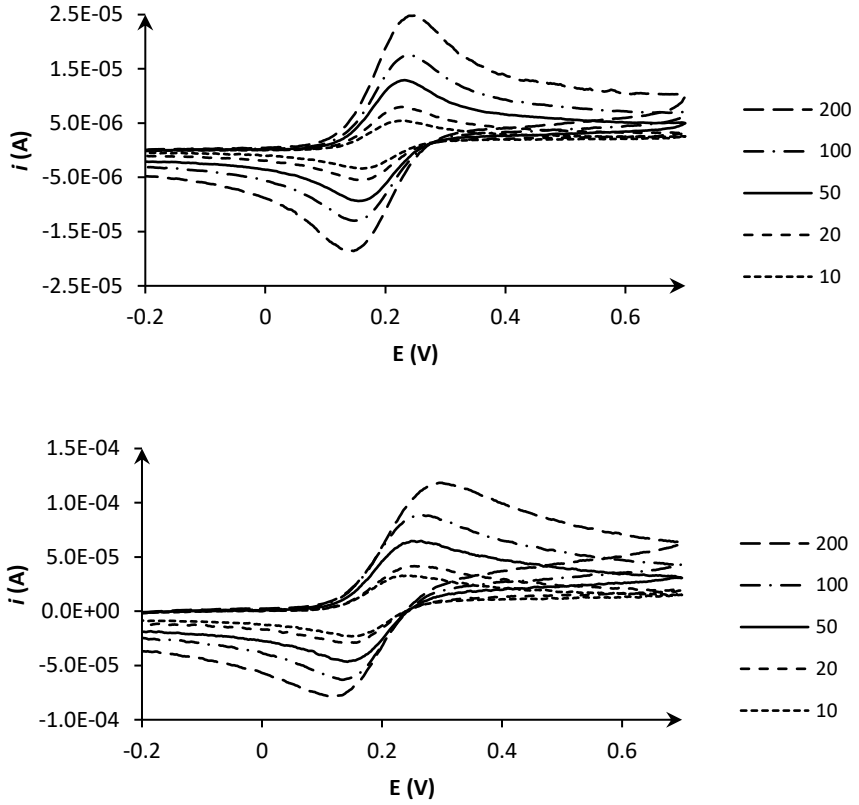

Figure 16. Cyclic voltammograms of gold [top] and glassy carbon [bottom] electrodes in the aqueous solution of 5 mM hexacyanoferrate (II) and 0.2 M potassium chloride (*vs*. SCE). Potential scan between –0.2 V and 0.7 V; at different v: 10, 20, 50, 100 and 200 mV s^{-1}.

As the scan rate increases, anodic and cathodic currents were higher; anodic peaks were shifted towards higher potential values, whereas cathodic peaks were deviated to lower potentials (Table 3). As predicted by the Randles-Sevcik equation, the peak currents are proportional to the scan rate. High scan rates translate to large concentration gradients, therefore, the conversion of hexacyanoferrate (II) to hexacyanoferrate (III) increases, giving rise to currents higher than those fabricated at lower scan rates.

Reversible charge-transfer reactions are characterized by several parameters, such as symmetrical peaks ($|i^C/i^A| = 1$), peak current directly proportional to the scan rate square root ($i_p \propto \sqrt{v}$), and a defined potential difference ($\Delta E = E^A - E^C = 59/n$ mV, where n is the number of electrons involved in the reaction). Mechanistic studies revealed a quasi-reversible charge-transfer reaction taking place, as potential difference is larger than 59 mV and peaks are almost symmetric ($0.81 < |i^C/i^A| < 0.98$). Regarding quasi-reversible systems, both reduction and oxidation kinetics are to be taken in consideration simultaneously. Irreversibility is greater as the scan rate increases, in addition to a bigger separation of peaks and a decreased peak current in comparison to the reversible counterpart.[4]

Table 3. Values of current and potentials of anodic and cathodic peaks and half-wave potentials (mean ± standard deviation). Gold (Au) and glassy carbon (GC) electrodes at different v. Solution: 5 mM hexacyanoferrate (II) and 0.2 M potassium chloride. Values are mean ± SD.

Gold Electrode					
v (mV s^{-1})	**E^A (mV)**	**i^A (μA)**	**E^C (mV)**	**i^C (μA)**	**$E_{1/2}$ (mV)**
200	248.2 ± 1.8	24.0 ± 0.1	147.4 ± 0.0	-20.7 ± 0.2	197.8 ± 0.9
100	240.1 ± 0.9	17.6 ± 0.6	151.0 ± 1.8	-15.3 ± 0.6	195.6 ± 0.5
50	232.0 ± 0.0	12.4 ± 0.2	156.4 ± 1.5	-10.7 ± 0.1	194.2 ± 0.7
20	227.5 ± 0.9	7.7 ± 0.2	160.0 ± 1.8	-7.0 ± 0.1	193.8 ± 0.5
10	229.3 ± 2.7	5.4 ± 0.1	160.9 ± 0.9	-5.3 ± 0.1	195.1 ± 0.9
Glassy Carbon Electrode					
v (mV s^{-1})	**E^A (mV)**	**i^A (μA)**	**E^C (mV)**	**i^C (μA)**	**$E_{1/2}$ (mV)**
200	292.3 ± 4.5	112.3 ± 0.4	123.2 ± 0.9	-99.0 ± 1.5	207.7 ± 1.8
100	264.4 ± 3.6	82.8 ± 1.0	139.4 ± 2.7	-77.2 ± 0.8	201.9 ± 3.2
50	262.6 ± 1.5	62.6 ± 2.0	144.4 ± 1.7	-58.5 ± 4.0	203.5 ± 0.4
20	257.2 ± 3.6	41.0 ± 1.3	144.3 ± 2.3	-33.2 ± 4.3	200.8 ± 0.7
10	241.9 ± 2.7	32.2 ± 1.6	151.0 ± 1.8	-28.0 ± 4.8	196.5 ± 0.5

3.1.2 *Effective surface area*

Chronoamperometric studies were performed on solutions of 5 mM hexacyanoferrate (II) in 0.1 M potassium chloride (Figure 17). Effective surface areas of 0.10 cm^2 and 0.02 cm^2 were estimated through the Cottrell equation, for the vitreous carbon and gold electrodes, correspondingly. Hexacyanoferrate (II) diffusion coefficient was taken to be 6.4 x 10^{-6} cm^2s^{-1}.[67] Despite its geometric area of 0.05 and 0.01 cm^2, vitreous carbon and gold electrodes exhibit a greater effective surface area, as imperfections contribute to an uneven surface at the nanoscale. Identical geometric and effective surface area would translate to a perfect planar surface, which is experimentally difficult to achieve. Even though electrode polishing is made to diminish the roughness, the result is hardly a perfectly flat surface.

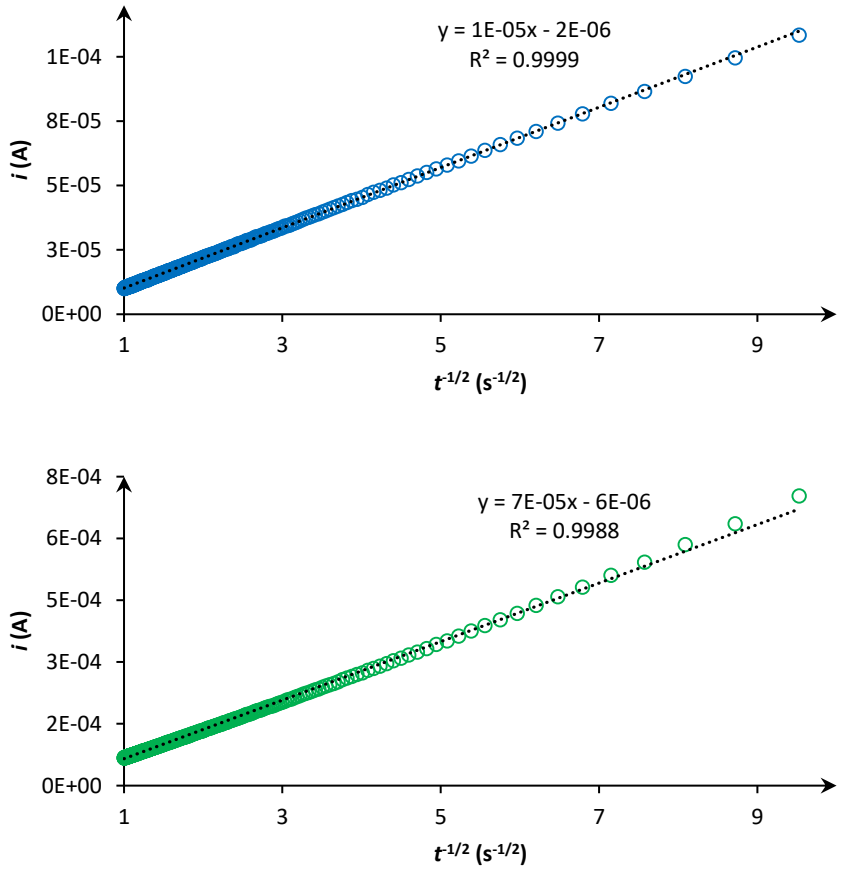

Figure 17. Current *vs.* inverse of square root of time plot of gold [top] and glassy carbon [bottom] electrodes in aqueous solution of 0.1 M potassium chloride and 5 mM hexacyanoferrate (II). The slope is 1.114 x 10^{-5} and 6.562 x 10^{-5}, for gold and vitreous carbon electrodes, respectively.

3.2 **Thiol-modified electrodes**

Sulphur-containing molecules are easily adsorbed onto heavy metal surfaces (*e.g.* gold), owing to a high affinity of thiolates towards these substrates and the formation of a covalent bond.[68] The composition of the alkanethiol determines its ability to form a monolayer, as well as its stability and functionalization. Large carbon skeleton alkanethiols can form long monolayers. Heavily packed monolayers are highly impeditive, as they restrict the access to the electrode surface. Sulphur-heavy metal affinity is not applicable in the vitreous carbon-alkanethiol interface, however, several authors demonstrated that alkanethiols form monolayers onto glassy carbon surfaces. Electrochemical cleaning of the glassy carbon electrode is commonly employed, thus generating a different surface from the simply polished electrode, which will be the surface used in this work. Electrochemical adsorption of alkanethiol onto gold surfaces can be made through an anodic process (I)[37], while desorption can be electrochemically promoted through a cathodic process of one electron reduction process (II) in alkaline environments[36] (Figure 18).

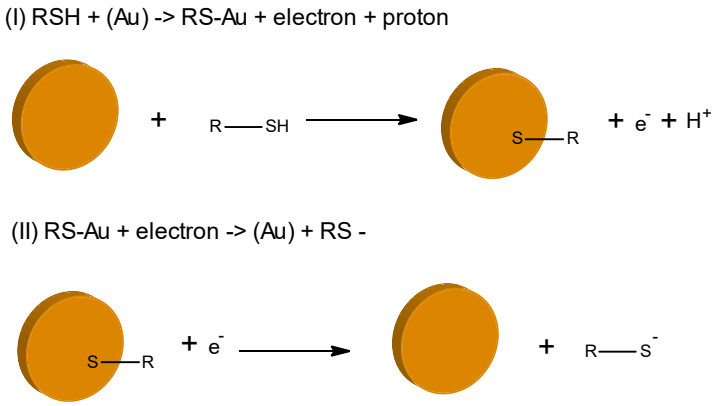

Figure 18. Anodic adsorption and cathodic desorption of alkanethiols from a gold substrate.

Self-assembled monolayers are essentially a functionalization of the substrate surface. In addition to having a protective role, these monolayers conditionate the interaction between the surface and the external medium, therefore justifying the great volume of research made in this area. Once monolayers act as electron and ion barriers, redox reactions that may take place have to occur by diffusion of electroactive species through pinholes to free sites on the electrode, where electron transfer is made.[69] In this project, gold and vitreous carbon electrodes were modified with three different thiols: mercaptopropionic acid (MPA), mercaptopropionic sulfonic acid (MPS), and 4-aminothiophenol (ATP). Both electrodes were exposed to thiol solutions for equal extent of time, at room temperature, and received the same post-modification treatment. Electrode performance was assessed by cyclic voltammetry and impedance spectroscopy (Figures 19-20). In these figures and throughout this project, presented electrode representations are not to scale and are for illustrative purposes only.

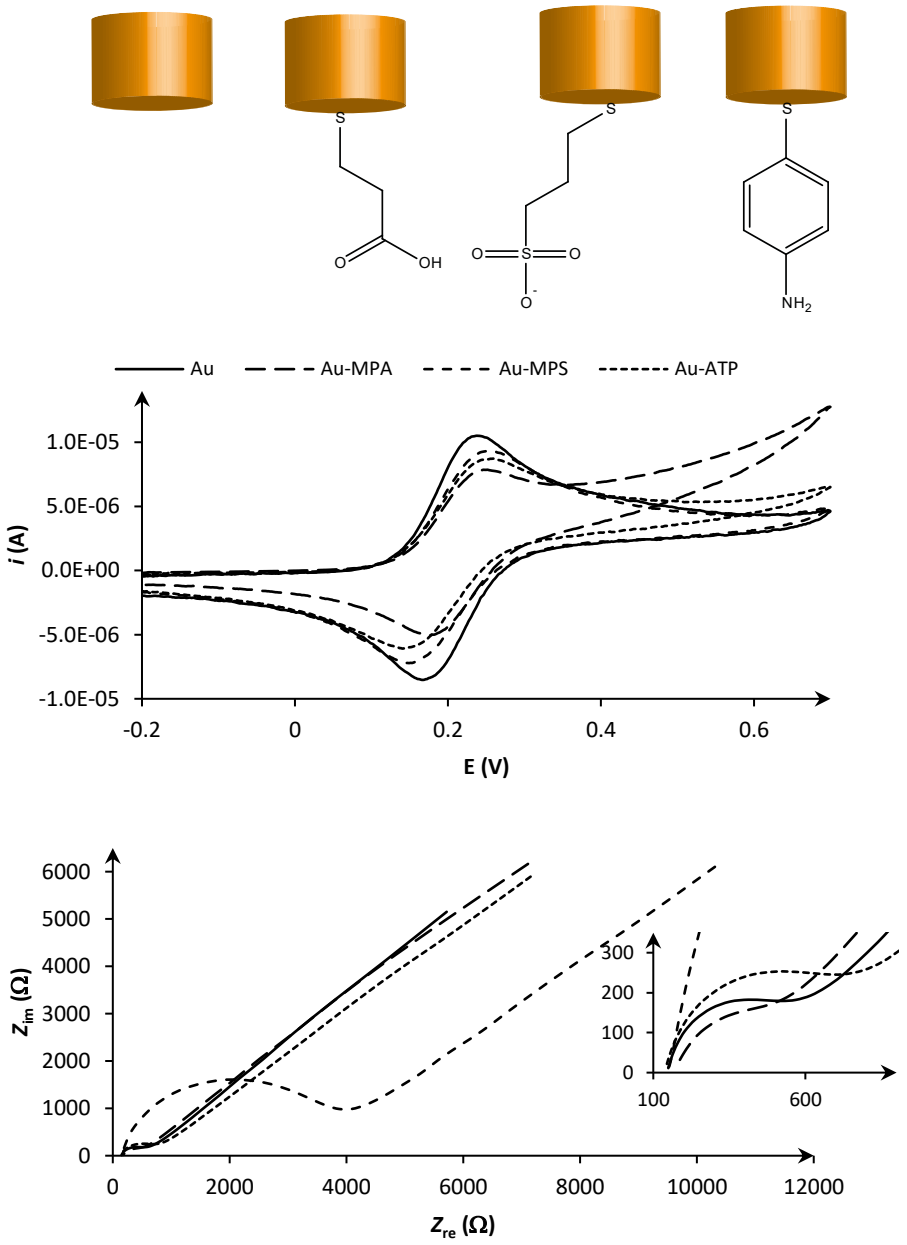

Figure 19. Cyclic voltammogram of gold electrode in 5 mM hexacyanoferrate (II) and 0.2 M potassium chloride aqueous solution (*vs*. SCE), v: 50 mV s^{-1}. Complex impedance plot of the gold electrode in equimolar 2.5 mM solution of hexacyanoferrate (II) and (III) in 0.2 M potassium chloride (*vs*. Pt). The frequency range is 2×10^5 – 0.1 Hz, AC amplitude of 10 mV rms. (Au) bare, (Au-MPA) 3-mercaptopropionic acid-modified; (Au-MPS) mercaptopropionic sulfonic acid-modified and (Au-ATP) 4-aminothiophenol-modified gold electrode.

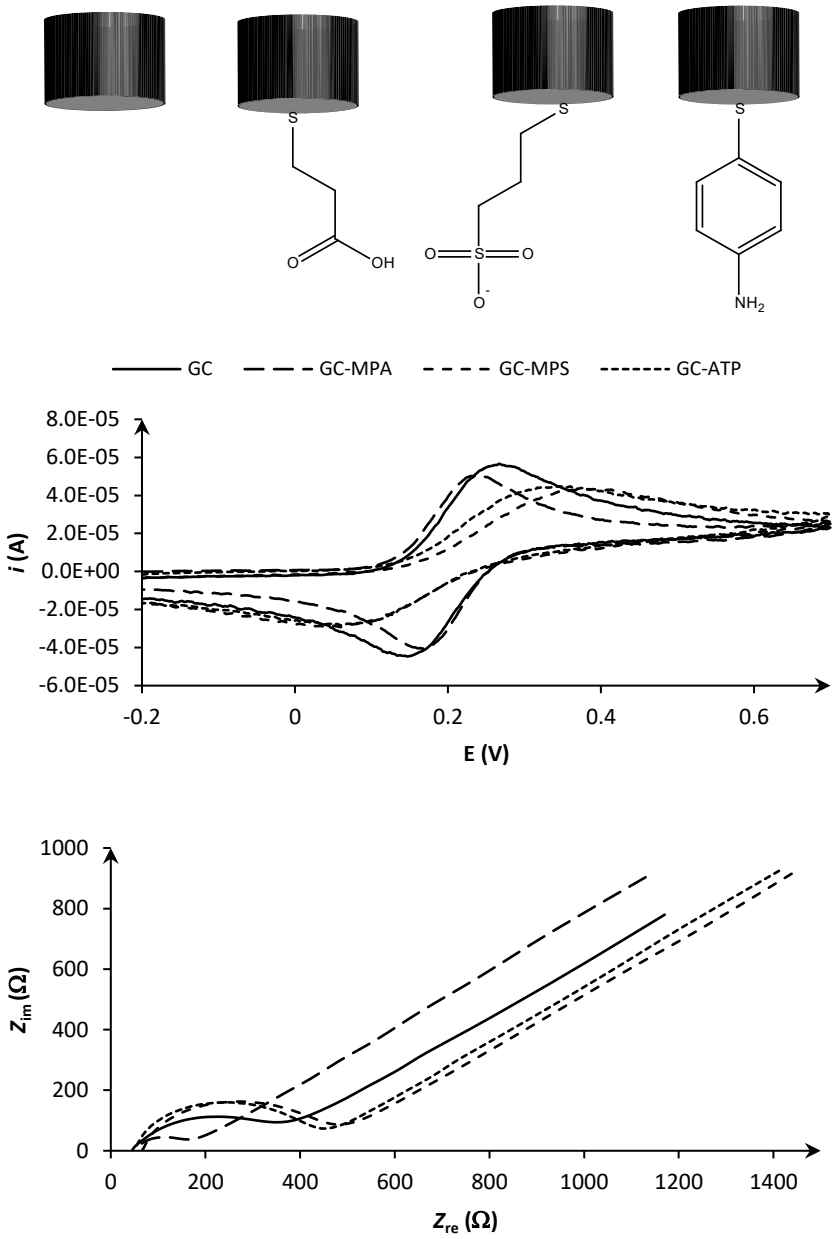

Figure 20. Cyclic voltammogram of glassy carbon electrode in 5 mM hexacyanoferrate (II) and 0.2 M potassium chloride aqueous solution (*vs*. SCE), v: 50 mV s^{-1}. Complex impedance plot of the glassy carbon electrode in equimolar 2.5 mM solution of hexacyanoferrate (II) and (III) in 0.2 M potassium chloride (*vs*. Pt). The frequency range is 2×10^5 – 0.1 Hz, AC amplitude of 10 mV rms. (GC) bare; (GC-MPA) 3-mercaptopropionic acid-modified; (GC-MPS) mercaptopropionic sulfonic acid-modified, and (GC-ATP) 4-aminothiophenol-modified glassy carbon electrode.

Assembly of the selected thiols onto gold and glassy carbon electrodes was successful and characterized by decreased peak currents, suggesting a decreased accessibility of hexacyanoferrate (II) to the electrode surface. Mercaptopropionic sulfonic acid and 4-aminothiophenol-modified vitreous carbon and gold electrodes exhibited a higher charge-transfer resistance than their bare counterpart, however, charge-transfer resistance attributed to 3-mercaptopropionic acid-modified electrodes was lower (Tables 4-5). Higher charge-transfer resistances are expected as the assembly of these molecules over the electrode surface constitutes a barrier between the electrode surface and the solution, barrier through which electrons need to be exchanged in order to oxidize and reduce hexacyanoferrate (II) and hexacyanoferrate (III). Monolayer charge dictates its interaction with the solution; in this particular case, negatively charged monolayers such as MPS repel hexacyanoferrate (II) and interfere with the electron-transfer, as MPS-modified electrodes required a higher amount of energy to oxidize hexacyanoferrate (II).[61]

Table 4. Current and potentials of anodic and cathodic peaks, half-wave potentials and charge-transfer resistance. (Au) bare, (Au-MPA) 3-mercaptopropionic acid-modified; (Au-MPS) mercaptopropionic sulfonic acid-modified and (Au-ATP) 4-aminothiophenol-modified gold electrode. v: 50 mV s^{-1}. Values are mean ± SD.

	Electrode			
	Au	**Au-MPA**	**Au-MPS**	**Au-ATP**
E^A (mV)	239.2 ± 2.6	252.5 ± 1.4	252.4 ± 1.7	250.7 ± 4.2
i^A (μA)	10.3 ± 0.1	7.9 ± 0.2	9.3 ± 0.0	8.9 ± 0.3
E^C (mV)	170.2 ± 2.2	176.6 ± 0.7	154.6 ± 1.5	147.8 ± 4.2
i^C (μA)	-9.4 ± 0.1	-4.9 ± 0.1	-8.4 ± 0.1	-7.7 ± 0.2
$E_{1/2}$ (mV)	204.7 ± 2.2	214.5 ± 0.7	203.5 ± 1.1	199.3 ± 1.9
R_{CT} (ohms)	557.1 ± 48.2	507.6 ± 39.3	3856.5 ± 36.6	696.6 ± 42.0

Table 5. Current and potentials of anodic and cathodic peaks, half-wave potentials and charge-transfer resistance. (GC) bare; (GC-MPA) 3-mercaptopropionic acid-modified; (GC-MPS) mercaptopropionic sulfonic acid-modified, and (GC-ATP) 4-aminothiophenol-modified glassy carbon electrode. v: 50 mV s^{-1}. Values are mean ± SD.

	Electrode			
	GC	**GC-MPA**	**GC-MPS**	**GC-ATP**
E^A (mV)	260.8 ± 3.9	240.6 ± 1.5	377.8 ± 3.6	273.4 ± 8.3
i^A (μA)	57.5 ± 0.5	56.0 ± 4.7	41.8 ± 0.1	47.1 ± 3.3
E^C (mV)	148.0 ± 0.8	166.3 ± 2.7	56.6 ± 2.7	122.2 ± 5.2
i^C (μA)	-53.0 ± 1.1	-54.8 ± 3.3	-27.1 ± 0.2	-41.8 ± 4.0
$E_{1/2}$ (mV)	204.4 ± 1.9	203.4 ± 1.7	217.2 ± 0.4	196.9 ± 4.9
R_{CT} (ohms)	378.2 ± 1.2	120.1 ± 5.7	399.3 ± 24.8	408.7 ± 37.1

3.2.1 *3-Mercaptopropionic acid-modified electrodes*

As expected, the gold electrode was successfully modified with 3-mercaptopropionic acid (Figure 19). MPA-modified gold electrode exhibited a different electrochemical behaviour, namely decreased currents and shifted peak potentials. Past the anodic peak attributed to the oxidation of hexacyanoferrate (II) at 0.25 V, an increment in anodic current is observed. Taking in consideration that this current is inexistent on the bare electrode cyclic voltammogram, it is easily assumed that this current is the product of MPA oxidation. Repeatability challenges arise in the modification of vitreous carbon electrode with MPA. A quasi-identical behaviour to the bare electrode is exhibited in the first cycle, with smaller peak currents and similar charge-transfer resistance (Figure 20). However, peak currents gradually increase as the number of scan increase, suggesting an ever-changing electrode-solution interface. As a result of a weak affinity between the carbon surface and MPA, the electrode is progressively stripped of MPA. After a few scans, an identical behaviour to the bare electrode is exhibited, suggesting that a bare surface is obtained.

3.2.2 *Mercaptopropionic sulfonic acid-modified electrodes*

Mercaptopropionic sulfonic acid has been explored for multiple purposes, *e.g.* electrodeposition of copper, with emphasis on copper-MPS interaction and influence over growth patterns. In terms of sensing, MPS self-assembly has been explored in the building of biosensors through multilayer assembly architectures with enzymes. This charged thiol is also employed in the development of conducting polymer films.[16] Electrochemical characterization of the MPS-modified gold and glassy carbon electrodes suggested a successful modification of the electrodes surface with the thiol (Figures 19-20). Cyclic voltammetry of MPS-modified gold and vitreous carbon electrodes showed decreased anodic and cathodic peak current, as well as increased peak-to-peak separation.

3.2.3 *4-Aminothiophenol-modified electrodes*

The adsorption of 4-aminothiophenol onto the electrodes was successful (Figures 19 – 20). However, the vitreous carbon electrode proved to be a poor substrate for the assembly and stabilization of 4-aminothiophenol; as substantiated by the different electrochemical behaviour of the modified electrode at every subsequent assay. Concerning vitreous carbon, a major difference is observable in 3-mercaptopropionic acid and 4-aminothiophenol-modified electrodes. As mentioned above, despite 3-mercaptopropionic acid adsorbed onto the glassy carbon surface, repeatedly cycled GC-MPA exhibited an electrochemical behaviour similar to that of the bare electrode, hinting the desorption of MPA from the electrode surface. 4-aminothiophenol also adsorbs onto the GC surface during the modification period, as substantiated by the first cycle of GC-ATP. However, subjecting

GC-ATP to multiple cycles induces modifications at the electrode surface, namely increased peak-to-peak separation and decreased current peaks. According to Jiang *et al.*, bare and ATP-modified gold electrodes exhibit the same cyclic voltammetry behaviour regarding the use of ferricyanide redox pair, however, the electroreduction of oxygen was reduced.[70] Although 4-aminothiophenol monolayers allow electron-transfer process to take place at the substrate surface, further studies showed that ATP monolayers were unstable to frequent electrochemical cycling. Electrochemical reduction and oxidation induce the conversion of ATP into a different compound. Reproducibility is compromised, owing to the high molecular disorder within the monolayer as a result of the steric effect of the ring structure, as aromatic molecules arrange themselves into poorly defined monolayers.

3.2.4 *Thiol monolayer removal*

The successful removal of the thiol monolayers determines the degree of repeatability of the modifications made to the electrodes. Vitreous carbon surfaces are easily regenerated by polishing the thiol-modified electrodes in alumina slurries of 0.3 and 0.05 μm, however, the polishing proved unfruitful to the regeneration of gold surfaces. The use of a coarser alumina, 1 μm, to clean the gold surface was unsuccessful. Electrochemical desorption of the thiols (namely MPA and MPS) was attempted, by cycling the electrode in 1 M sulfuric acid between -0.2 and 1.4 V (vs. SCE) at 100 mV/s. A clean surface is achieved at the fifth cycle, remaining unchangeable throughout the additional cycles.

3.3 PAMAM-NH_2 dendrimer-modified electrodes

G5 PAMAM-NH_2 dendrimer was allowed to assemble onto the bare and thiol-modified electrodes for two hours at room temperature (Figures 21-22). PAMAM-modified bare electrodes exhibited similar behaviour to PAMAM and MPA, MPS and ATP-modified electrodes. However, a characteristic anodic current at the potential window of 0.4 - 0.7 V of Au-MPA-PAMAM indicated that mercaptopropionic acid was present at the electrode surface along the dendrimer. These results suggest that once PAMAM is present, and regarding hexacyanoferrate (II)/(III) redox, its effect is specific, independently of the monolayer it was assembled over. Differences that may allow the discernment of the thiol are not detectable by cyclic voltammetry, except for Au-MPA-PAMAM. Overall, PAMAM dendrimer assembly over thiol-modified electrodes is characterized by smaller peak-to-peak separation, and higher and lower peak currents, for vitreous carbon and gold substrates, correspondingly, in comparison to their bare counterparts.

Contrary to vitreous carbon electrodes modified with thiols such as 3-mercaptopropionic acid and 4-aminothiophenol, where the surface suffered alterations throughout consecutive cyclic voltammetry

measurements, further modification with PAMAM dendrimers resulted in highly stable surfaces, which were subjected to the same conditions without experiencing changes.

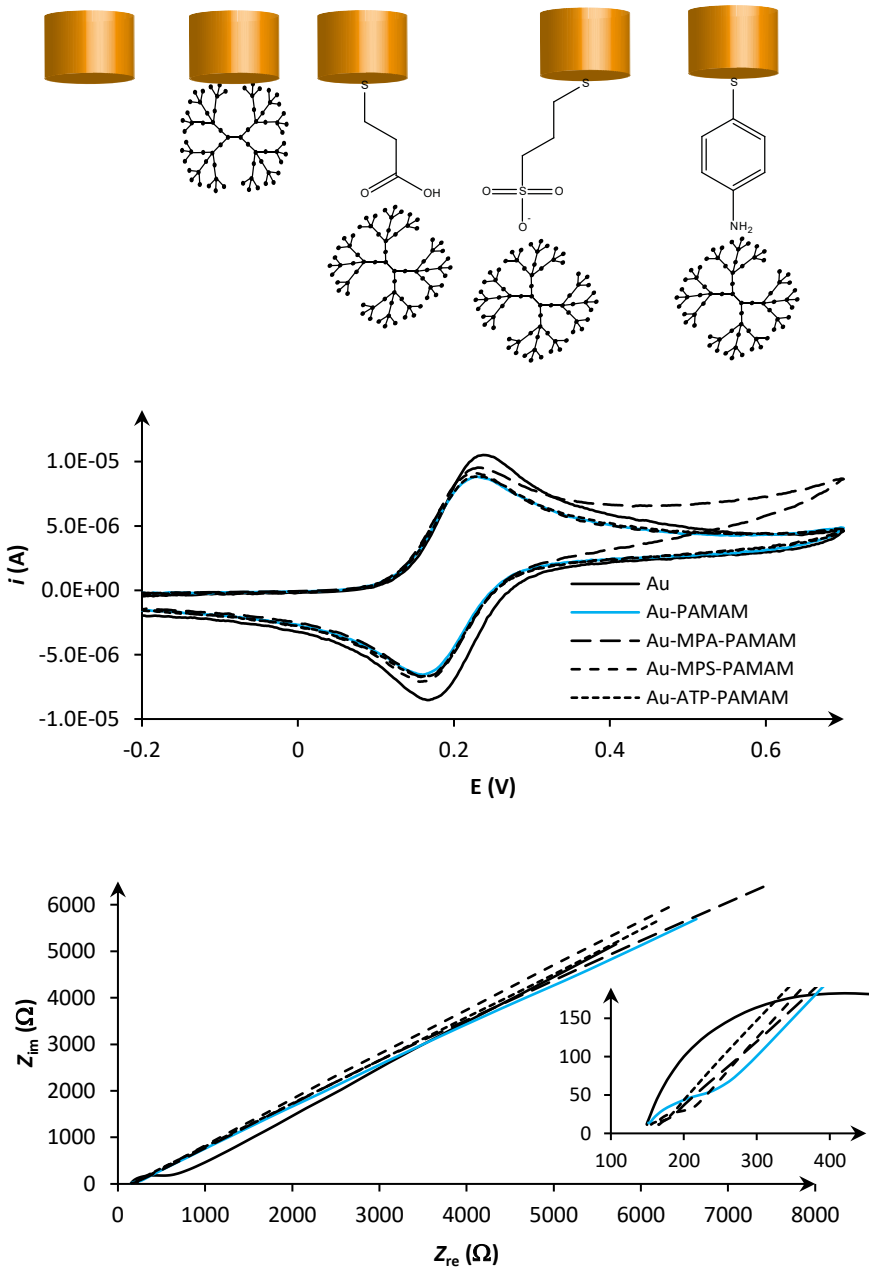

Figure 21. Cyclic voltammogram of gold electrode in 5 mM hexacyanoferrate (II) and 0.2 M potassium chloride aqueous solution (*vs*. SCE), v: 50 mV s^{-1}. Complex impedance plot of the gold electrode in equimolar 2.5 mM solution of hexacyanoferrate (II) and (III) in 0.2 M potassium chloride (*vs*. Pt). The frequency range is 2×10^5 – 0.1 Hz, AC amplitude of 10 mV rms. (Au) bare, (Au-PAMAM) PAMAM-modified, (Au-MPA-PAMAM) PAMAM and MPA-modified, (Au-MPS-PAMAM) PAMAM and MPS-modified, and (Au-ATP-PAMAM) PAMAM and ATP-modified gold electrode.

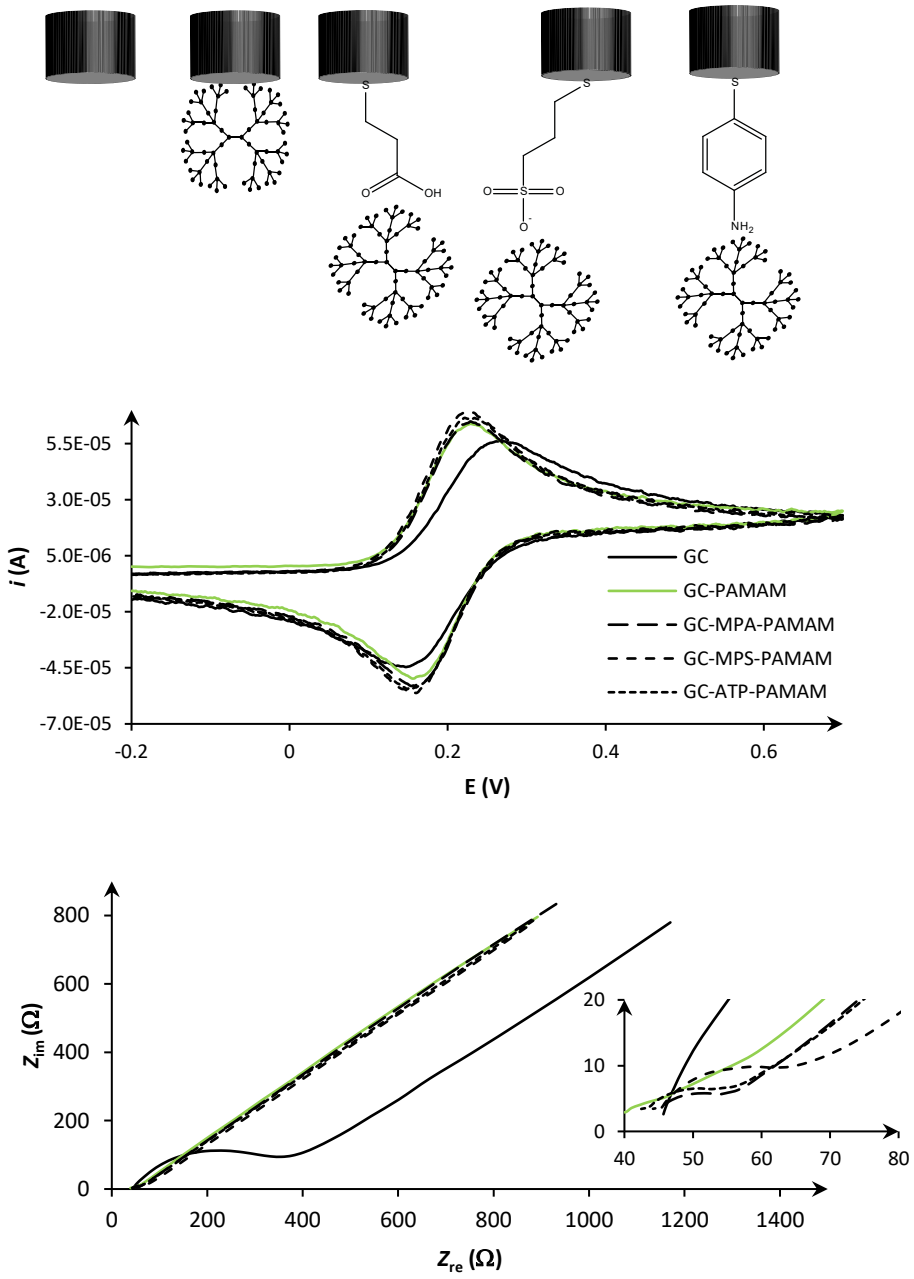

Figure 22. Cyclic voltammogram of glassy carbon electrode in 5 mM hexacyanoferrate (II) and 0.2 M potassium chloride aqueous solution (*vs*. SCE), v: 50 mV s^{-1}. Complex impedance plot of the glassy carbon electrode in equimolar 2.5 mM solution of hexacyanoferrate (II) and (III) in 0.2 M potassium chloride (*vs*. Pt). The frequency range is 2×10^5 – 0.1 Hz, AC amplitude of 10 mV rms. (GC) bare glassy carbon electrode; (GC-PAMAM) PAMAM-modified vitreous carbon electrode; (GC-MPA-PAMAM) PAMAM-modified GC-MPA; (GC-MPS-PAMAM) PAMAM-modified GC-MPS; and (GC-ATP-PAMAM) PAMAM-modified GC-ATP.

PAMAM-modified electrodes are characterized by lower charge-transfer resistances than both their bare and thiol monolayer-modified counterparts (Tables 6-7). Even though PAMAM dendrimer assembly represents an additional layer, the charge-transfer resistance is diminished, which could be justifiable by assuming that somehow PAMAM dendrimers enable the exchange of electrons between the electroactive probes and the electrode surface. In comparison to MPA, MPS and ATP-modified electrodes, hexacyanoferrate (II) is oxidized at lower potentials at PAMAM-modified electrodes; whereas hexacyanoferrate (III) is reduced at higher potentials at PAMAM dendrimer and MPS and ATP-based electrodes, independently of the electrode material. PAMAM dendrimer assembly translates to a greater electrocatalytic activity towards hexacyanoferrate (II) oxidation and hexacyanoferrate (III) reduction on MPS and ATP-modified electrodes.

Table 6. Current and potentials of anodic and cathodic peaks, half-wave potentials and charge-transfer resistance. (Au) bare, (Au-PAMAM) PAMAM-modified, (Au-MPA-PAMAM) PAMAM and MPA-modified, (Au-MPS-PAMAM) PAMAM and MPS-modified, and (Au-ATP-PAMAM) PAMAM and ATP-modified gold electrode. v: 50 mV s^{-1}. Values are mean ± SD.

	Electrode				
	Au	**Au-PAMAM**	**Au-MPA-PAMAM**	**Au-MPS-PAMAM**	**Au-ATP-PAMAM**
E^A (mV)	239.2 ± 2.6	230.7 ± 2.7	231.6 ± 1.8	226.6 ± 1.3	229.1 ± 2.7
i^A (μA)	10.3 ± 0.1	8.7 ± 0.0	9.6 ± 0.3	9.0 ± 0.1	8.9 ± 0.2
E^C (mV)	170.2 ± 2.2	157.8 ± 2.0	166.5 ± 2.2	160.9 ± 2.0	161.5 ± 2.6
i^C (μA)	-9.4 ± 0.1	-8.0 ± 0.0	-7.5 ± 0.2	-8.3 ± 0.1	-7.8 ± 0.2
$E_{1/2}$ (mV)	204.7 ± 2.2	195.7 ± 3.4	199.1 ± 1.1	193.8 ± 1.0	195.3 ± 1.3
R_{CT} (ohms)	557.1 ± 48.2	202.7 ± 11.1	82.1 ± 6.3	86.3 ± 8.0	58.2 ± 2.3

Table 7. Current and potentials of anodic and cathodic peaks, half-wave potentials and charge-transfer resistance. (GC) bare glassy carbon electrode; (GC-PAMAM) PAMAM-modified vitreous carbon electrode; (GC-MPA-PAMAM) PAMAM-modified GC-MPA; (GC-MPS-PAMAM) PAMAM-modified GC-MPS; and (GC-ATP-PAMAM) PAMAM-modified GC-ATP. v: 50 mV s^{-1}. Values are mean ± SD.

	Electrode				
	GC	**GC-PAMAM**	**GC-MPA-PAMAM**	**GC-MPS-PAMAM**	**GC-ATP-PAMAM**
E^A (mV)	260.8 ± 3.9	228.4 ± 1.3	230.2 ± 2.2	224.8 ± 3.9	227.0 ± 3.5
i^A (μA)	57.5 ± 0.5	65.8 ± 2.0	65.2 ± 0.8	70.0 ± 0.2	68.1 ± 0.7
E^C (mV)	148.0 ± 0.8	156.9 ± 1.5	158.7 ± 3.2	154.6 ± 2.5	153.9 ± 3.7
i^C (μA)	-53.0 ± 1.1	-63.0 ± 1.9	-62.6 ± 1.0	-64.9 ± 1.9	-63.8 ± 0.5
$E_{1/2}$ (mV)	204.4 ± 1.9	192.6 ± 1.3	194.4 ± 2.3	189.7 ± 2.6	190.4 ± 3.3
R_{CT} (ohms)	378.2 ± 1.2	16.3 ± 0.7	17.7 ± 1.0	20.4 ± 2.1	18.3 ± 0.8

3.4 Gold-modified electrodes

Gold was employed on the electrode fabrication through two approaches, gold layer and self-assembly of citrate-stabilized gold nanoparticles. The gold layer comprised the direct reduction of gold ions (Au^{3+}) onto the thiol-modified electrodes. Gold nanoparticles synthesized through chemical reduction, namely the Turkevich method, were allowed to assemble onto PAMAM-modified electrodes. Herein, gold layer formation is the reduction of gold ions over the thiol monolayer. This gold architecture is different from the colloidal gold, not only synthesis-wise, but structurally. Colloidal gold is characterized by the presence of some compound responsible for the stabilization of the nanoparticle surface, this stabilizer is crucial to prevent nanoparticle aggregation and subsequent precipitation, also, gold reduction experiments are not performed in the presence of such compound.

3.4.1 *Modification with gold layer*

Gold reduction was performed in a 0.25 mM chloroauric acid solution, where 3-mercaptopropionic acid, mercaptopropionic sulfonic acid and 4-aminothiophenol-modified electrodes were subjected for a minute to a potential of -0.832 V (*vs.* SCE). Gold electroreduction over 3-mercaptopropionic acid, mercaptopropionic sulfonic acid and 4-aminothiophenol-modified electrodes translates to distinct electrochemical profiles, suggesting that thiol-modified electrodes were further modified (Figures 23-24).

Gold layer-modified gold electrodes are characterized by decreased peak currents and greater peak-to-peak separation in comparison to the bare gold electrode. As for the glassy carbon-based electrodes, gold electroreduction over mercaptopropionic sulfonic acid and 4-aminothiophenol-modified vitreous carbon electrode is characterized by lower peak currents and higher peak-to-peak separation in comparison to the bare glassy carbon electrode, contrary to 3-mercaptopropionic acid-modified electrode, which exhibits a smaller peak-to-peak separation.

In relation to the previous monolayer, the further modification of thiol-modified glassy carbon electrodes with reduced gold translated to electrodes with higher cathodic and anodic peak currents. Thiol-modified gold electrodes were characterized by lower cathodic and anodic peak currents. Less energy was required to oxidize hexacyanoferrate (II) in gold layer-modified electrodes. Specifically, the electrodes resultant from the electroreduction of gold over previously modified electrodes like 3-mercaptopropionic acid-modified gold electrode, mercaptopropionic sulfonic acid-modified glassy carbon electrode, and 4-aminothiophenol-modified gold and glassy carbon electrodes.

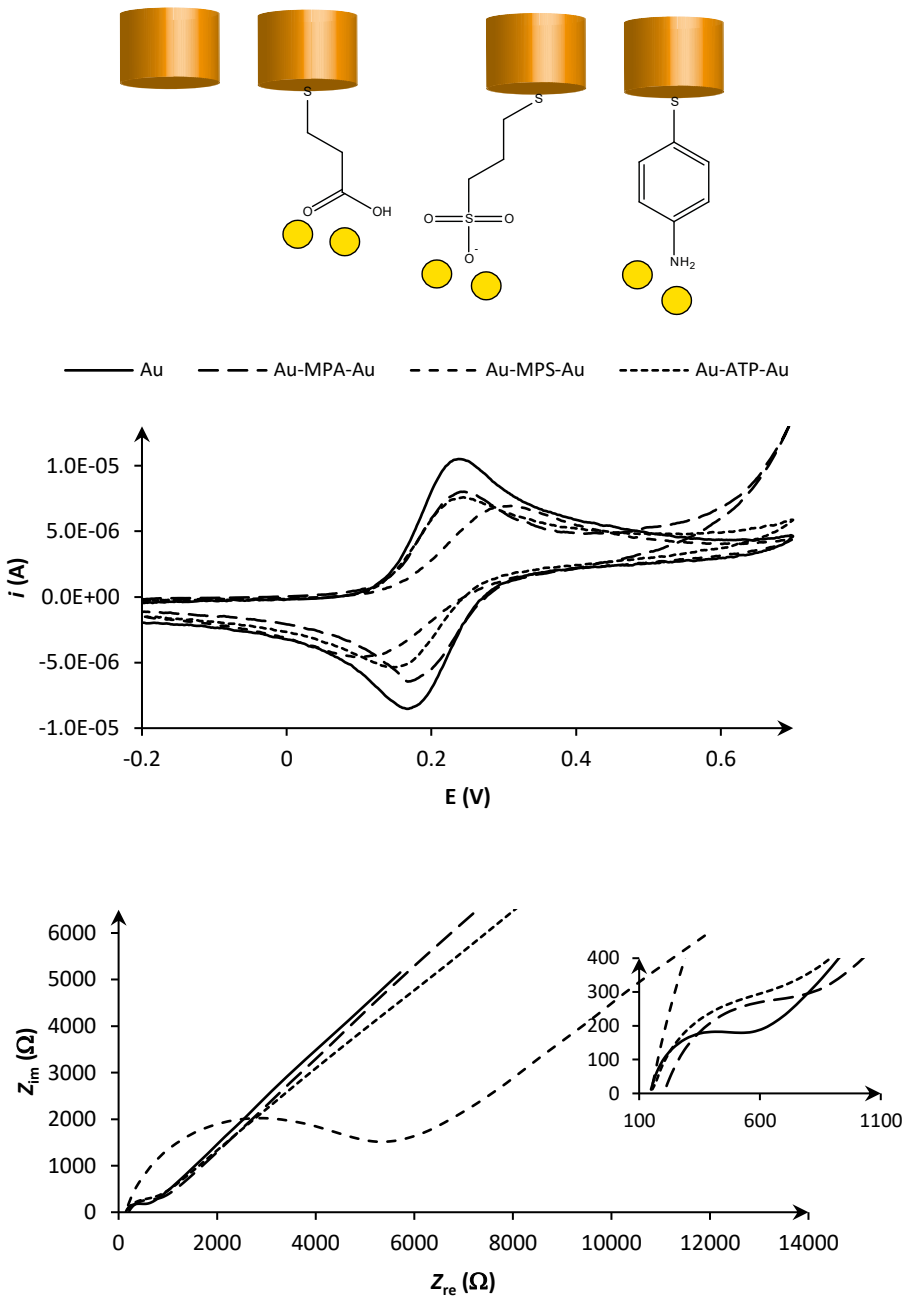

Figure 23. Cyclic voltammogram of the gold electrode in 5 mM hexacyanoferrate (II) and 0.2 M potassium chloride aqueous solution (*vs*. SCE), v: 50 mV s^{-1}. Complex impedance plot of the gold electrode in equimolar 2.5 mM solution of hexacyanoferrate (II) and (III) in 0.2 M potassium chloride (*vs*. Pt). The frequency range is 2×10^5 – 0.1 Hz, AC amplitude of 10 mV rms. (Au) bare, (Au-MPA-Au) gold layer and MPA-modified, (Au-MPS-Au) gold layer and MPS-modified, (Au-ATP-Au) gold layer and ATP-modified gold electrode. Modification of MPA, MPS and ATP-modified electrodes with gold layer was made by electroreduction of gold ions over the thiol monolayer.

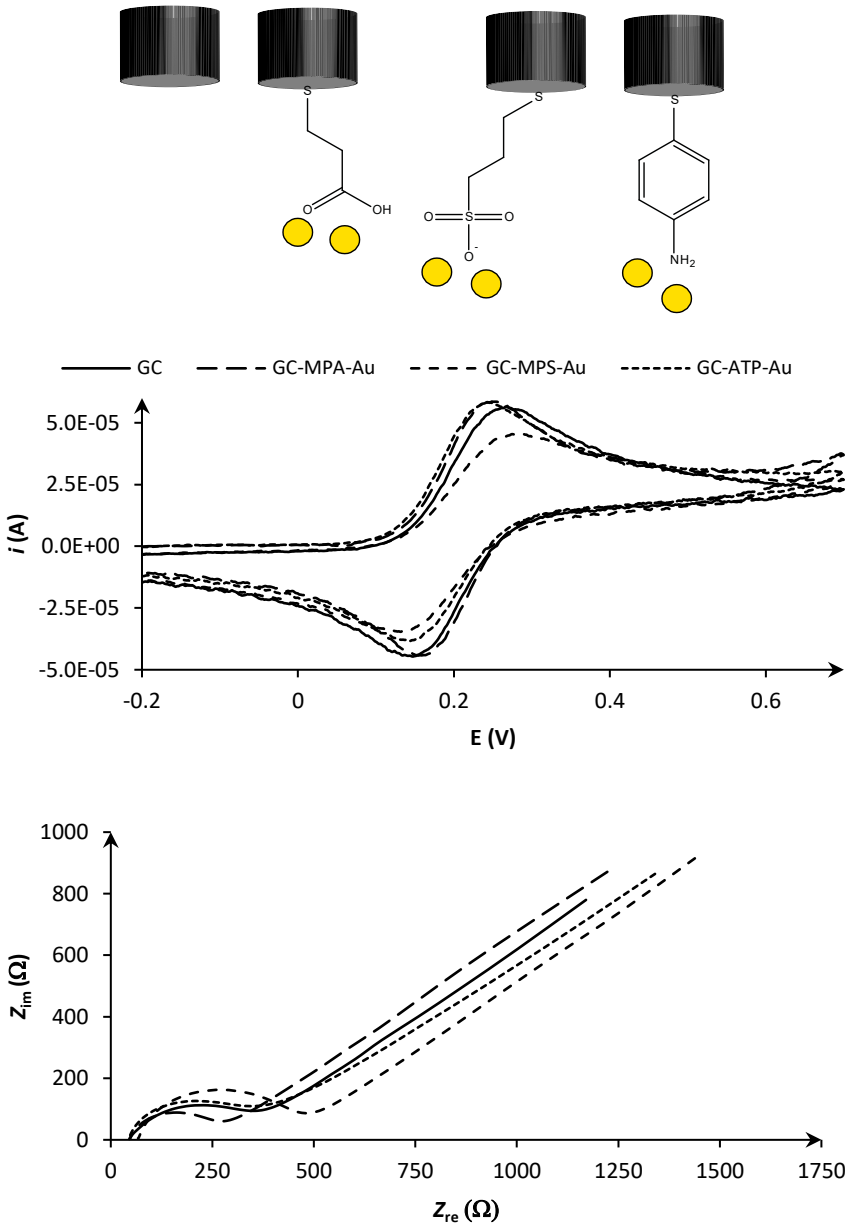

Figure 24. Cyclic voltammogram of vitreous carbon electrode in 5 mM hexacyanoferrate (II) and 0.2 M potassium chloride aqueous solution (*vs*. SCE), v: 50 mV s^{-1}. Complex impedance plot of the glassy carbon electrode in equimolar 2.5 mM solution of hexacyanoferrate (II) and (III) in 0.2 M potassium chloride (*vs*. Pt). The frequency range is 2×10^5 – 0.1 Hz, AC amplitude of 10 mV rms. (GC) bare, (GC-MPA-Au) gold layer and MPA-modified, (GC-MPS-Au) gold layer and MPS-modified, (GC-ATP-Au) gold layer and ATP-modified vitreous carbon electrode. Modification of MPA, MPS and ATP-modified electrodes with gold layer was made by electroreduction of gold ions over the thiol monolayer.

Gold reduction over the previously assembled thiol monolayer translates to a greater electrocatalytic activity towards hexacyanoferrate (II) oxidation and hexacyanoferrate (III) reduction on 4-aminothiophenol-modified gold and vitreous carbon electrodes. Gold layer and mercaptopropionic sulfonic acid-modified gold and glassy carbon electrodes exhibited higher charge-transfer resistance than their bare and mercaptopropionic acid and 4-aminothiophenol-modified complements (Tables 8-9). Charge-transfer resistance of reduced gold-modified electrodes is greater than their thiol-modified counterparts. Gold presence and morphology should be assessed by a microscopic technique (*e.g.* SEM). The nature of the modification needs further characterization in order to determine if a gold layer is formed over the thiol monolayer, if the thiol monolayer remained intact or suffered alterations, and if the resulting architecture is homogeneous.

Table 8. Current and potentials of anodic and cathodic peaks, half-wave potentials and charge-transfer resistance. (Au) bare, (Au-MPA-Au) gold layer and MPA-modified, (Au-MPS-Au) gold layer and MPS-modified, (Au-ATP-Au) gold layer and ATP-modified gold electrode. Modification of MPA, MPS and ATP-modified electrodes with gold layer was made by electroreduction of gold ions over the thiol monolayer. v: 50 mV s^{-1}. Values are mean ± SD.

	Electrode			
	Au	**Au-MPA-Au**	**Au-MPS-Au**	**Au-ATP-Au**
E^A (mV)	239.2 ± 2.6	245.8 ± 3.1	308.0 ± 5.6	237.0 ± 6.6
i^A (μA)	10.3 ± 0.1	7.7 ± 0.1	6.7 ± 0.1	7.9 ± 0.4
E^C (mV)	170.2 ± 2.2	168.4 ± 0.8	106.5 ± 2.0	153.2 ± 4.3
i^C (μA)	-9.4 ± 0.1	-6.1 ± 0.3	-4.7 ± 0.1	-6.6 ± 0.2
$E_{1/2}$ (mV)	204.7 ± 2.2	207.1 ± 1.1	207.3 ± 2.0	195.1 ± 3.6
R_{CT} (ohms)	557.1 ± 48.2	836.2 ± 52.9	5313.3 ± 371.5	982.8 ± 27.1

Table 9. Current and potentials of anodic and cathodic peaks, half-wave potentials and charge-transfer resistance. (GC) bare, (GC-MPA-Au) gold layer and MPA-modified, (GC-MPS-Au) gold layer and MPS-modified, (GC-ATP-Au) gold layer and ATP-modified vitreous carbon electrode. Modification of MPA, MPS and ATP-modified electrodes with gold layer was made by electroreduction of gold ions over the thiol monolayer. v: 50 mV s^{-1}. Values are mean ± SD.

	Electrode			
	GC	**GC-MPA-Au**	**GC-MPS-Au**	**GC-ATP-Au**
E^A (mV)	260.8 ± 3.9	248.2 ± 1.3	282.8 ± 4.1	257.6 ± 8.6
i^A (μA)	57.5 ± 0.5	58.0 ± 2.4	44.5 ± 0.8	53.8 ± 1.8
E^C (mV)	148.0 ± 0.8	158.2 ± 3.4	132.6 ± 3.5	129.4 ± 9.4
i^C (μA)	-53.0 ± 1.1	-54.5 ± 1.7	-36.0 ± 0.9	-44.2 ± 2.3
$E_{1/2}$ (mV)	204.4 ± 1.9	203.2 ± 1.6	207.7 ± 3.2	193.5 ± 3.4
R_{CT} (ohms)	378.2 ± 1.2	259.7 ± 15.7	753.9 ± 9.3	434.6 ± 51.8

3.4.2 *Modification with citrate-stabilized gold nanoparticles*

Citrate-stabilized gold nanoparticles were synthesized and characterized (Figure 25). A reddish pink solution was obtained, characterized by an absorption band centred at 522 nm (λ_{max} = 522 nm), as shown in the absorption spectrum. The particles' hydrodynamic size was determined by a Dynamic Light Scattering analysis, out of the three peaks, the band centred at 31 nm is the most intense (90.8%). The remaining peaks at 3915 nm (≈ 4 μm) and 1.7 nm correspond to particle agglomerates and small nuclei, respectively. The size distribution indicates a non-homogenic solution. The colloidal gold had a negative zeta-potential, which could be due to the presence of citrate ions, characteristically negative.

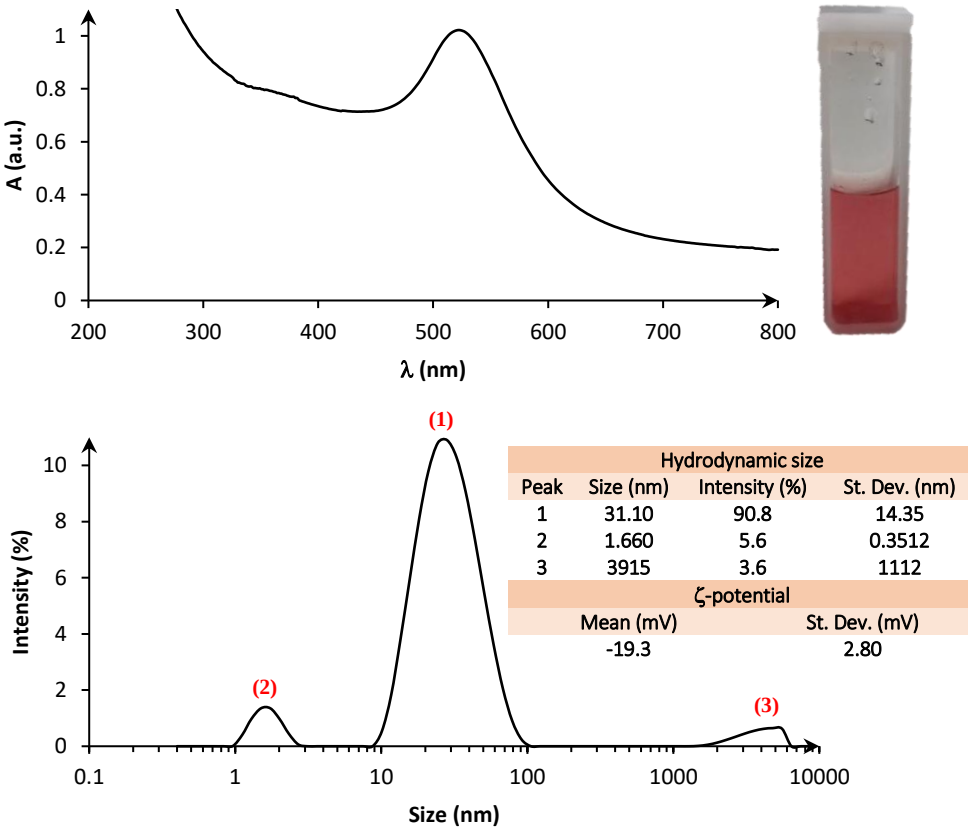

Figure 25. Absorption spectrum of obtained colloidal gold (top). Hydrodynamic size distribution by intensity plot (bottom).

Scanning electron microscopy was employed to observe the synthesized gold nanoparticles (Figure 26). Microscopic agglomerates are observable on the SEM image of freeze-dried gold nanoparticles, due to the conditions imposed, these agglomerates are originated by low temperature exposure followed by solvent removal by sublimation. The elemental composition of the agglomerate was obtained through an energy-dispersive X-ray (EDX) analysis; elements such as Au, O, C, Na, and Si were detected, being gold the most abundant (88.7%); oxygen and carbon follow with 5 and 3%, for these elements compose the reducing and stabilizing agent, citrate. Trace amounts of silicon were detected, owing to the synthesis being carried on a glass round-bottom flask.

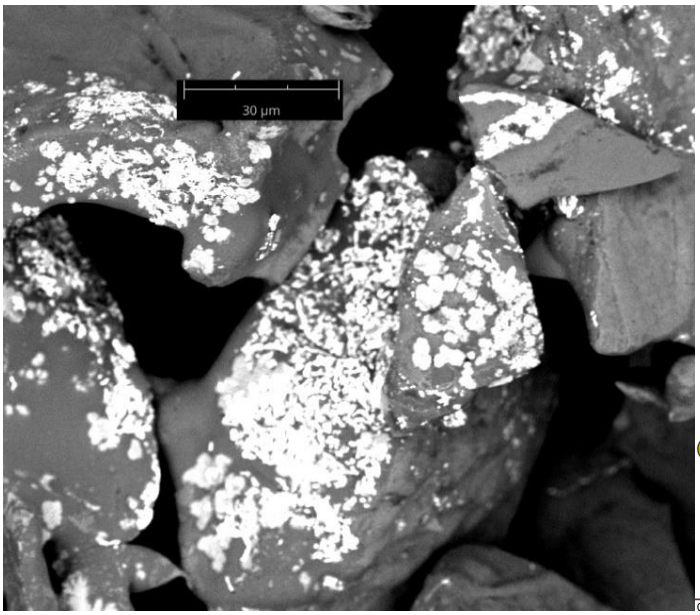

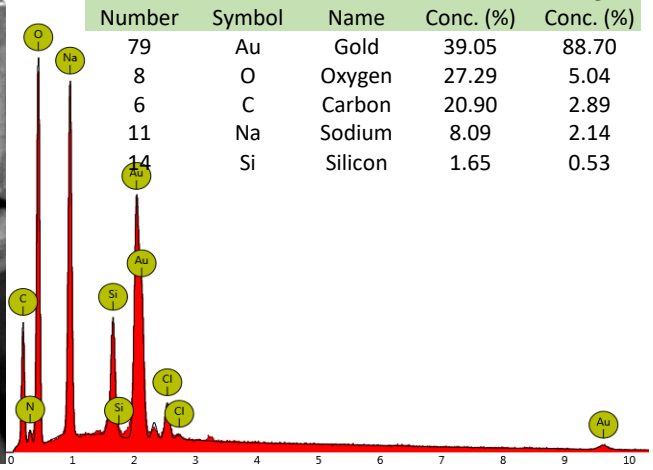

Element Number	Element Symbol	Element Name	Atomic Conc. (%)	Weight Conc. (%)
79	Au	Gold	39.05	88.70
8	O	Oxygen	27.29	5.04
6	C	Carbon	20.90	2.89
11	Na	Sodium	8.09	2.14
14	Si	Silicon	1.65	0.53

Figure 26. SEM image of freeze-dried gold nanoparticles (left), scale bar indicates 30 µm. EDX spectrum and elemental composition (right).

PAMAM-modified electrodes were dipped in a diluted solution of gold nanoparticles for two hours, after which cyclic voltammetry studies were performed (Figures 27-28). Concerning the previous modification, the assembly of citrate-stabilized gold nanoparticles resulted in similar electrochemical response as that of PAMAM-modified electrodes, even though an overall slight peak current decrease was observable. Citrate-stabilized gold nanoparticle-modified gold and glassy carbon electrodes exhibited a greater electrocatalytic activity towards hexacyanoferrate (II) oxidation and hexacyanoferrate (III) reduction, in comparison to their bare counterparts; although the conversion of hexacyanoferrate (III) to its reduced form required more negative potentials for gold-based electrodes.

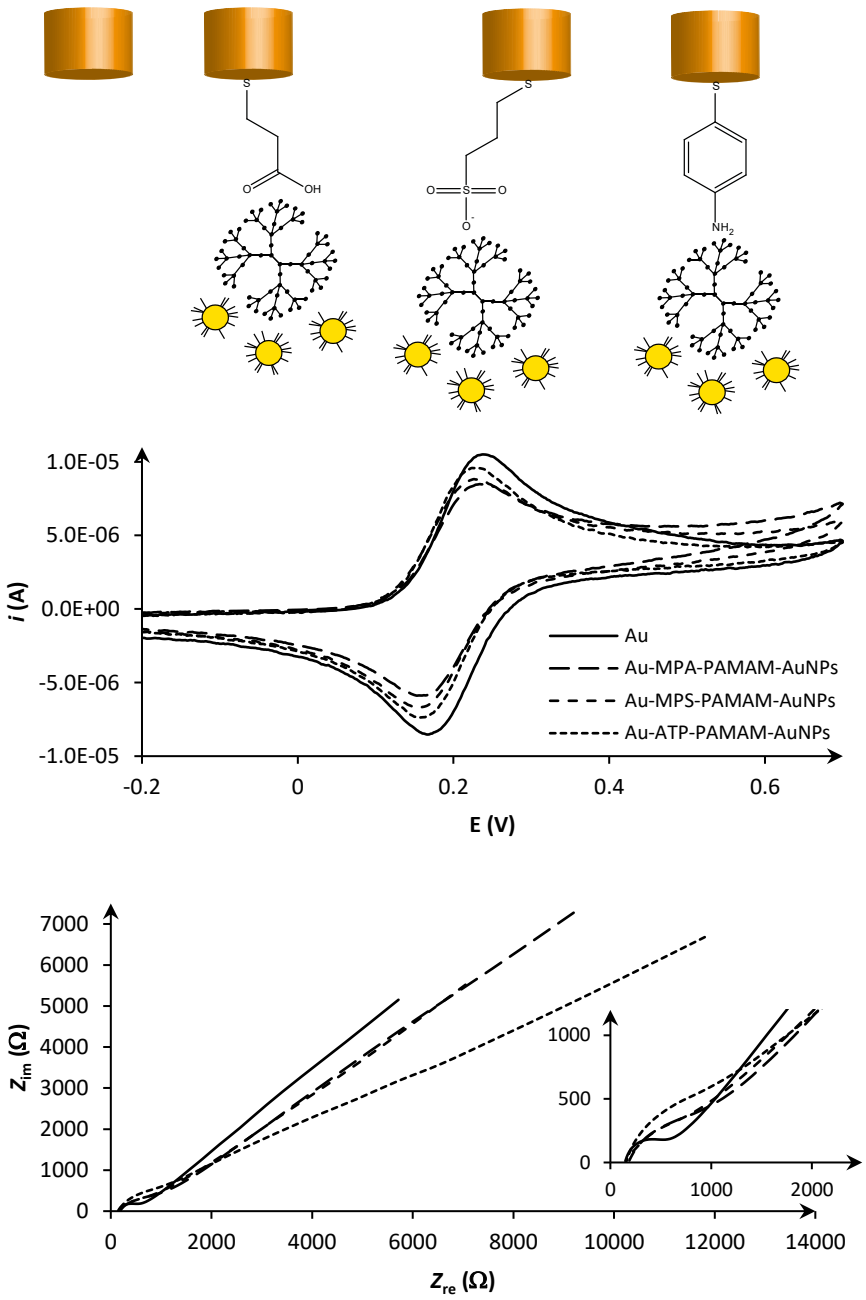

Figure 27. Cyclic voltammogram of the gold electrode in 5 mM hexacyanoferrate (II) and 0.2 M potassium chloride aqueous solution (*vs*. SCE), v: 50 mV s^{-1}. Complex impedance plot of the gold electrode in equimolar 2.5 mM solution of hexacyanoferrate (II) and (III) in 0.2 M potassium chloride (*vs*. Pt). The frequency range is 2×10^5 – 0.1 Hz, AC amplitude of 10 mV rms. (Au) bare, (Au-MPA-PAMAM-AuNPs) gold and PAMAM-MPA-modified, (Au-MPS-PAMAM-AuNPs) gold and PAMAM-MPS-modified, (Au-ATP-PAMAM-AuNPs) gold and PAMAM-ATP-modified gold electrode. Modification of PAMAM and MPA, MPS and ATP-modified electrodes with gold nanoparticles was made with citrate-stabilized gold nanoparticles.

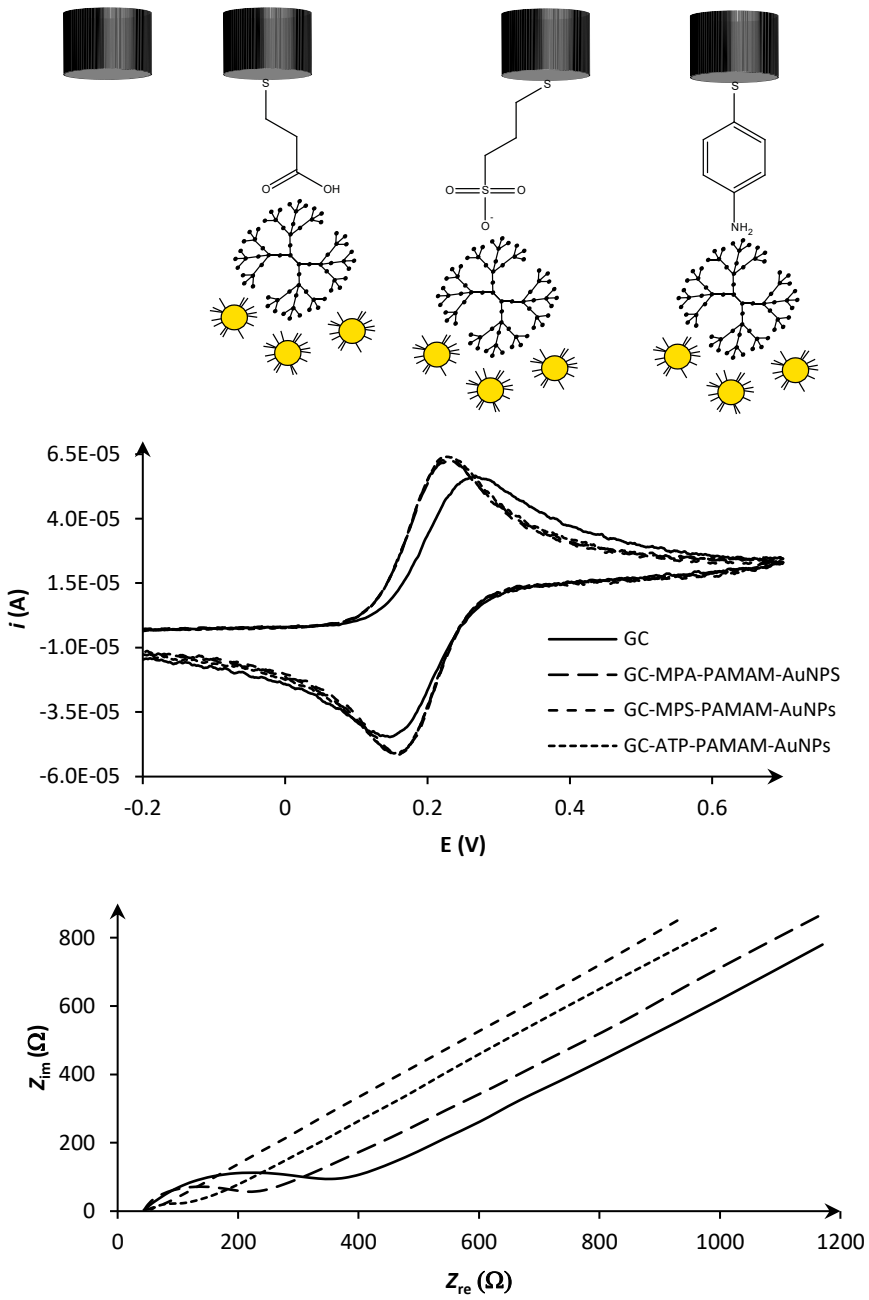

Figure 28. Cyclic voltammogram of the glassy carbon electrode in 5 mM hexacyanoferrate (II) and 0.2 M potassium chloride aqueous solution (*vs*. SCE), v: 50 mV s^{-1}. Complex impedance plot of the glassy carbon electrode in equimolar 2.5 mM solution of hexacyanoferrate (II) and (III) in 0.2 M potassium chloride (*vs*. Pt). The frequency range is 2×10^5 – 0.1 Hz, AC amplitude of 10 mV rms. (GC) bare, (GC-MPA-PAMAM-AuNPs) gold and PAMAM-MPA-modified, (GC-MPS-PAMAM-AuNPs) gold and PAMAM-MPS-modified, (GC-ATP-PAMAM-AuNPs) gold and PAMAM-ATP-modified glassy carbon electrode. Modification of PAMAM and MPA, MPS and ATP-modified electrodes with gold nanoparticles was made with citrate-stabilized gold nanoparticles.

Impedance studies suggest a change in the surface constitution as a result of the interaction between gold nanoparticles and PAMAM-modified gold electrode, for the charge-transfer resistance is greater when the electrodes are further dipped in a colloidal gold solution (Tables 10-11). Amidst all three variations, gold-based electrodes display similar charge-transfer resistance, independently of the thiol monolayer present. Glassy carbon-based electrodes display different charge-transfer resistances; 3-mercaptopropionic acid and 4-aminothiophenol-based electrodes have higher charge-transfer resistance than their PAMAM-modified counterparts, still lower than the bare electrode. Gold nanoparticles, PAMAM and mercaptopropionic sulfonic acid-modified vitreous carbon electrode exhibits an identical charge-transfer resistance to that of its PAMAM-modified counterpart, which in addition to a similar cyclic voltammetry behaviour, implies that gold nanoparticles are absent, and its assembly onto the surface of GC-MPS-PAMAM did not occur.

Table 10. Current and potentials of anodic and cathodic peaks, half-wave potentials and charge-transfer resistance. (Au) bare, (Au-MPA-PAMAM-AuNPs) gold and PAMAM-MPA-modified, (Au-MPS-PAMAM-AuNPs) gold and PAMAM-MPS-modified, (Au-ATP-PAMAM-AuNPs) gold and PAMAM-ATP-modified gold electrode. Modification of PAMAM and MPA, MPS and ATP-modified electrodes with gold nanoparticles was made with citrate-stabilized gold nanoparticles. v: 50 mV s^{-1}. Values are mean ± SD.

	Electrode			
	Au	**Au-MPA-PAMAM-AuNPs**	**Au-MPS-PAMAM-AuNPs**	**Au-ATP-PAMAM-AuNPs**
E^A (mV)	239.2 ± 2.6	233.2 ± 2.2	227.5 ± 1.7	228.1 ± 0.7
i^A (μA)	10.3 ± 0.1	8.4 ± 0.2	8.9 ± 0.3	9.5 ± 0.0
E^C (mV)	170.2 ± 2.2	162.4 ± 3.1	158.2 ± 2.9	159.3 ± 1.8
i^C (μA)	-9.4 ± 0.1	-7.0 ± 0.1	-7.8 ± 0.2	-9.1 ± 0.1
$E_{1/2}$ (mV)	204.7 ± 2.2	197.8 ± 1.9	192.9 ± 1.7	193.7 ± 1.2
R_{CT} (ohms)	557.1 ± 48.2	1333.6 ± 53.3	1214.6 ± 80.5	1548.5 ± 78.9

Table 11. Current and potentials of anodic and cathodic peaks, half-wave potentials and charge-transfer resistance. (GC) bare, (GC-MPA-PAMAM-AuNPs) gold and PAMAM-MPA-modified, (GC-MPS-PAMAM-AuNPs) gold and PAMAM-MPS-modified, (GC-ATP-PAMAM-AuNPs) gold and PAMAM-ATP-modified glassy carbon electrode. Modification of PAMAM and MPA, MPS and ATP-modified electrodes with gold nanoparticles was made with citrate-stabilized gold nanoparticles. v: 50 mV s^{-1}. Values are mean ± SD.

	Electrode			
	GC	**GC-MPA-PAMAM-AuNPs**	**GC-MPS-PAMAM-AuNPs**	**GC-ATP-PAMAM-AuNPs**
E^A (mV)	260.8 ± 3.9	230.7 ± 1.5	229.5 ± 2.2	227.7 ± 2.2
i^A (μA)	57.5 ± 0.5	63.0 ± 0.4	63.0 ± 1.4	65.6 ± 0.6
E^C (mV)	148.0 ± 0.8	154.6 ± 4.6	159.7 ± 3.3	154.6 ± 2.3
i^C (μA)	-53.0 ± 1.1	-60.3 ± 1.3	-59.8 ± 0.6	-61.4 ± 1.6
$E_{1/2}$ (mV)	204.4 ± 1.9	192.6 ± 2.6	194.6 ± 2.2	191.2 ± 1.2
R_{CT} (ohms)	378.2 ± 1.2	178.8 ± 13.1	18.7 ± 1.2	74.2 ± 2.4

3.5 4-Nitrophenol reduction

Nitrophenols and derivatives are by-products of synthetic dyes, pesticides, insecticides and herbicides production. These compounds are highly pollutant and represent a great threat to ecosystems even at low concentrations, thus, its presence in wastewaters is undesired and research is made in an effort so that these pollutants are removed or even attenuated from the waste released. Nanomaterials are directly employed in the formulation of agents responsible for the conversion of nitrophenols into less harmful molecules.[55,71-73] Xia *et al.* modified a glassy carbon electrode with graphite nanoflakes and applied it to the reduction of 4-nitrophenol, process which was assessed by cyclic voltammetry.[74] 4-nitrophenol detection was performed in 0.2 M phosphate buffer (pH 7), with potential scans between -1.4 and 0 V (*vs*. SMSE). The built sensor had detection and quantification limits of 0.7 μM and 2.3 μM, respectively. Cheng *et al.* modified glassy carbon with reduced graphene oxide and iron oxide nanoparticles and detected and quantified 4-nitrophenol by differential pulse voltammetry (DPV) and square-wave voltammetry (SWV) in 0.067 M phosphate buffer (pH 6).[75] The potential scan was made between -0.6 and 0.7 V (*vs*. Ag/AgCl, 3 M KCl). This sensor had detection and quantification limits of 0.26 μM and 0.86 μM, respectively. Umesh *et al.* modified glassy carbon with silver nanodendrites and detected 4-nitrophenol in 0.05 M phosphate buffer (pH 5), with potential scan between -0.6 and 0 V (*vs*. Ag/AgCl, saturated KCl) for linear sweep voltammetry (LSV) and -0.8 and 0 V for cyclic voltammetry experiments.[66] The sensor had a limit of detection of 1.76 μM.

4-nitrophenol detection by the bare electrodes was carried on 0.05 M PBS (pH 7.4) and 4-nitrophenol at 0.5 mM (Figure 29). In the first negative scan, from 0.4 V to -1.2 V, large and small cathodic peaks occur at around -0.8 V, for vitreous carbon and gold electrodes, respectively; as for the reverse scan, a small peak around 0.1 V is formed for both electrodes. A novel peak near 0 V appears during the second cycle, forming a redox couple with the peak at 0.1 V, moreover, the reduction peak below -0.8 V decreases in intensity, contrary to the peak at 0.1 V. According to the literature, 4-nitrophenol is irreversibly reduced to 4-(hydroxyamino)phenol, which in turn is oxidized to form 4-nitrosophenol, which can be reduced back to 4-(hydroxyamino)phenol (Figure 30).[76] The first forward scan reduces the 4-nitrophenol at the electrode surface to 4-(hydroxyamino)phenol, which is oxidized to 4-nitrosophenol on the reverse scan. On the second forward scan, just-formed 4-nitrosophenol is reduced back to 4-(hydroxyamino)phenol and a smaller amount of 4-nitrophenol is able to reach the electrode surface and be reduced. The peak associated to the oxidation of 4-(hydroxyamino)phenol increases in the second cycle due to a higher concentration of this compound, product of the reduction of both 4-nitrosophenol and 4-nitrophenol.

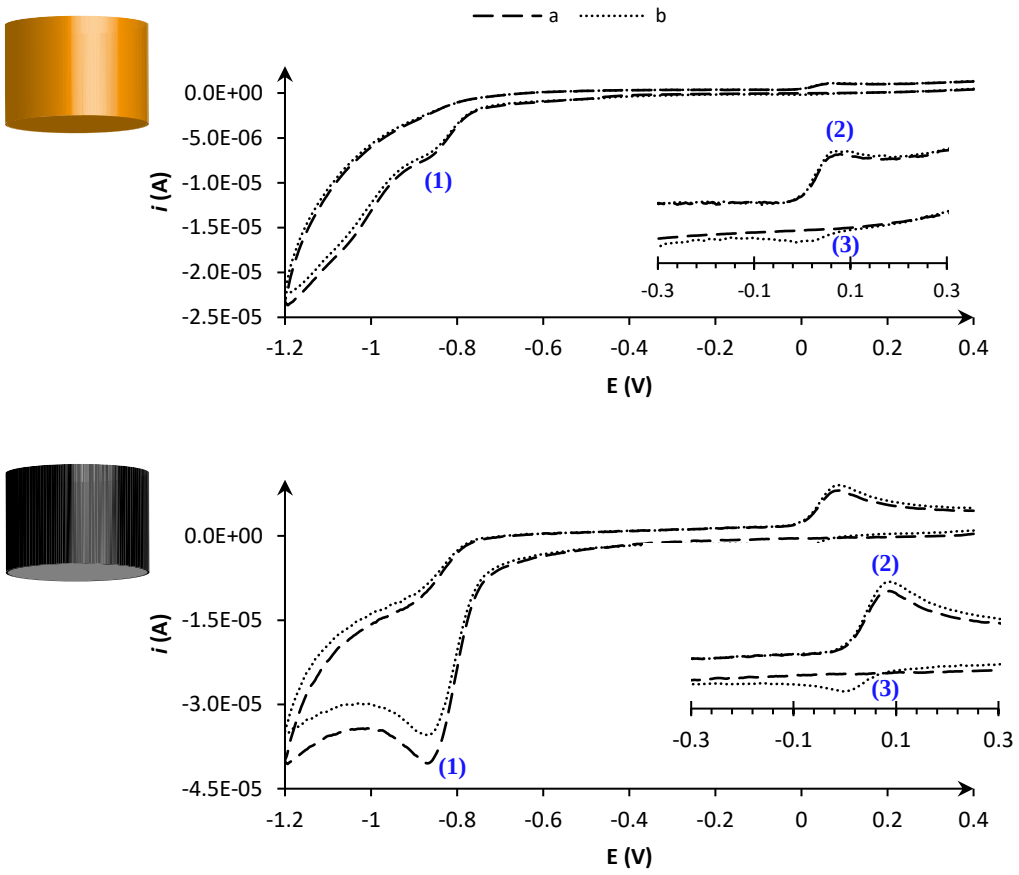

Figure 29. Cyclic voltammogram of gold (top) and glassy carbon (bottom) electrodes in 0.05 M PBS (pH 7.4) and 4-nitrophenol at 0.5 mM (*vs*. SCE), v: 50 mV s^{-1}. (a) first cycle, (b) second cycle.

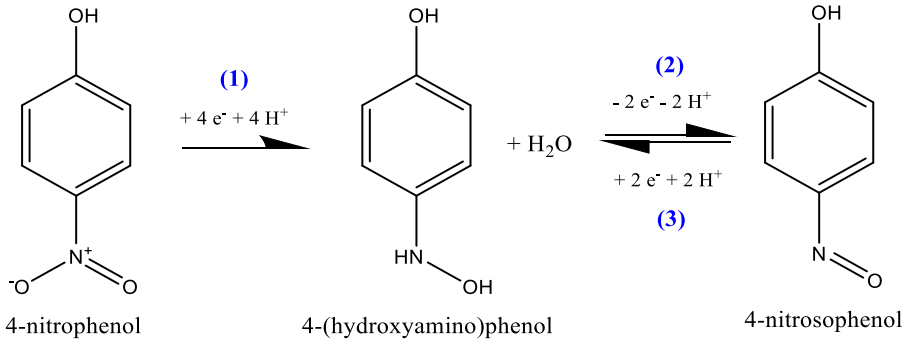

Figure 30. Electrochemical reduction mechanism of 4-nitrophenol.[76]

3.5.1 *Oxygen reduction*

Acidic environments favour the conversion of 4-nitrophenol to 4-(hydroxyamino)phenol, therefore, the following measurements were made in phosphate buffer solution at pH 5.3. Similarly to p-nitrophenol, oxygen is reduced at low potentials, thus, oxygen reduction was assessed in the potential window used, with potential scan between 0.4 and -1.2 V (Figure 31). Bare electrodes were tested in 0.05 M PBS (pH 5) solutions in the presence and absence of 4-nitrophenol, with and without nitrogen purge. Results demonstrate that cycling bare electrodes in nitrogen unpurged phosphate buffer solution below potentials of –0.4 and –0.3 V gives rise to cathodic currents, in gold and glassy carbon electrodes, correspondingly. The aforementioned cathodic currents are diminished after a nitrogen purge is performed, beginning at potentials below -0.8 V and -0.9 V, respectively.

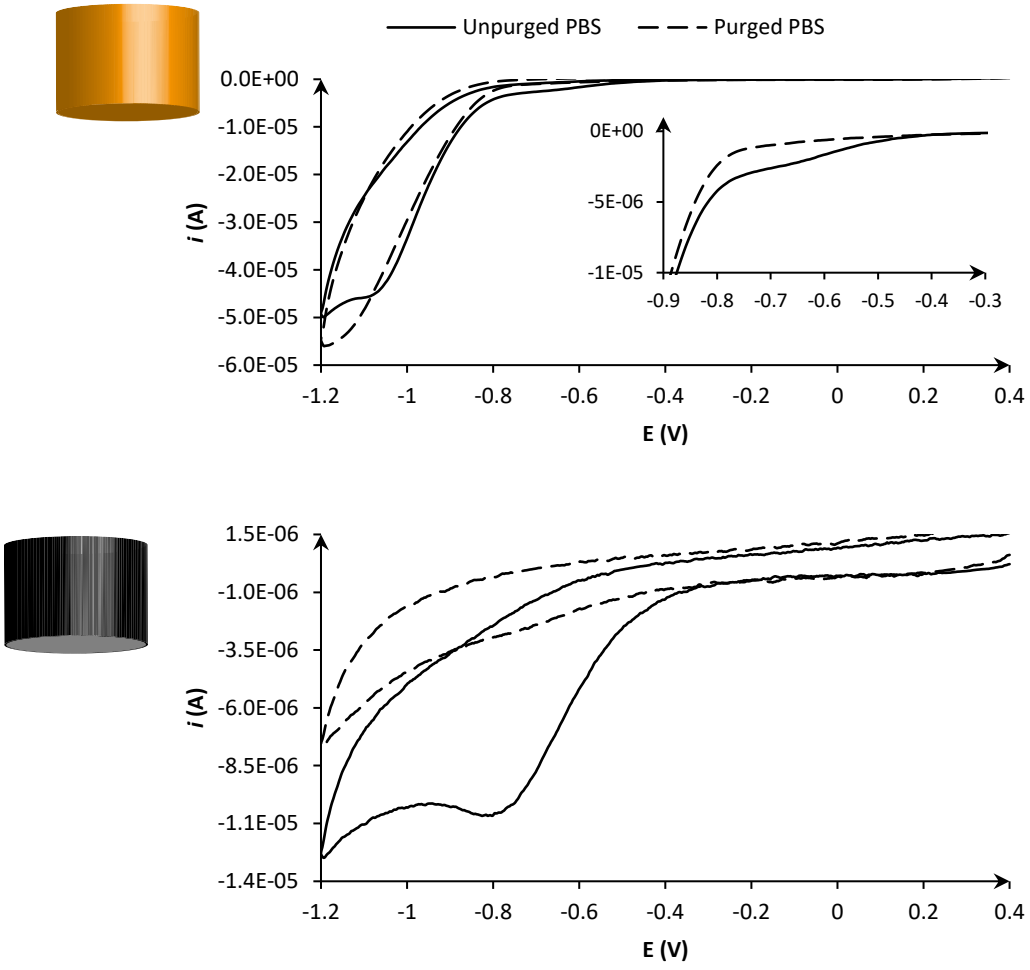

Figure 31. Cyclic voltammogram of gold and glassy carbon electrodes in 0.05 M PBS (pH 5) (*vs*. SCE), v: 50 mV s^{-1}.

The next step comprised cycling bare electrodes in both nitrogen unpurged and purged phosphate buffer solutions, whilst in the presence of p-nitrophenol at 500 μM (Figures 32-33). Cathodic currents are formed at more negative potentials than -0.8 and -0.9 V on nitrogen purged phosphate buffer, indicating that currents formed at -0.8 V on 4-nitrophenol-containing solutions are strictly due to the reduction of 4-nitrophenol and not oxygen. In the cyclic voltammogram of gold on PBS and 4-nitrophenol, a cathodic peak past -0.9 V is present, suggesting a redox reaction taking place at the electrode surface besides the expected reduction of 4-nitrophenol.

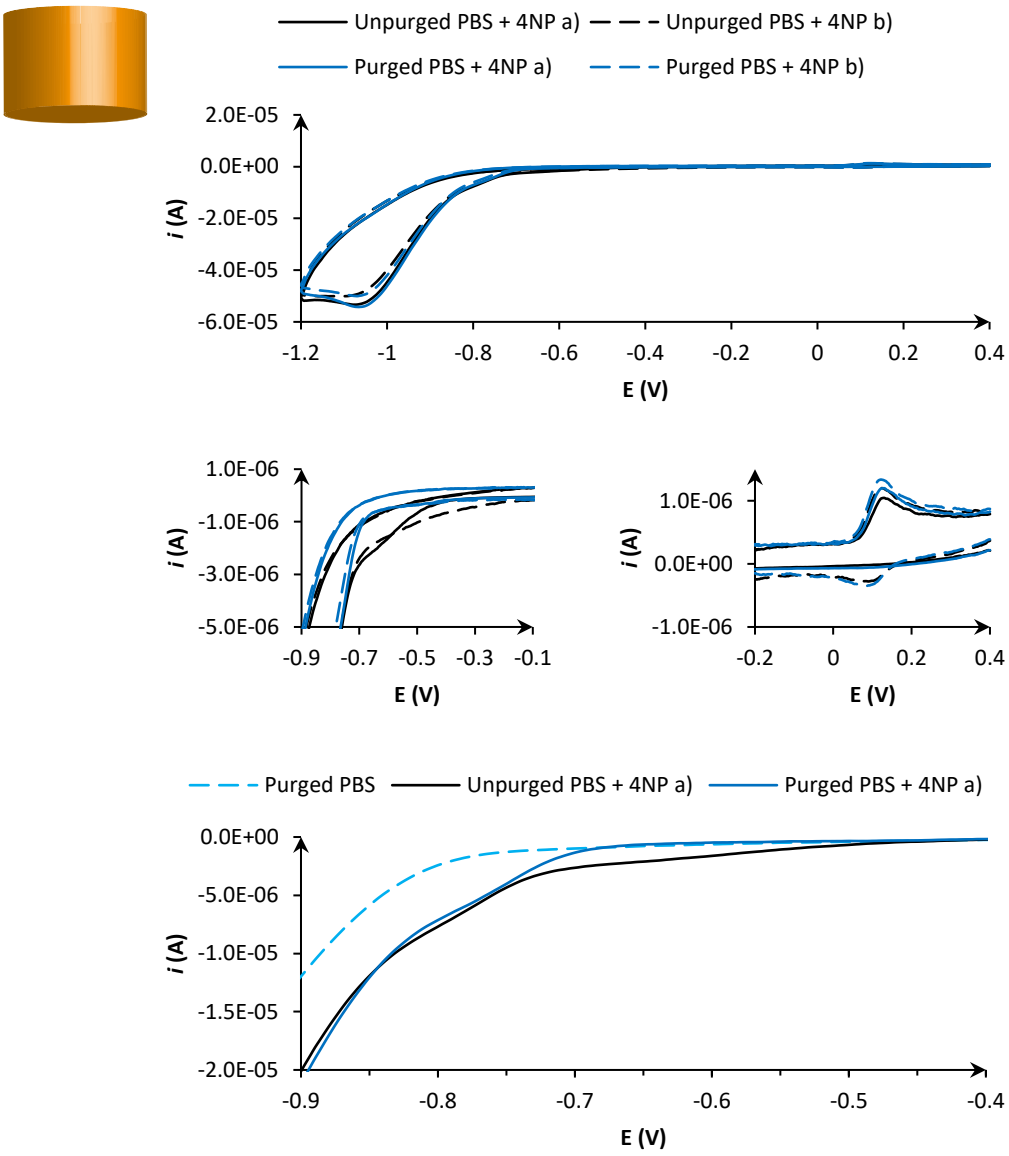

Figure 32. Cyclic voltammogram of gold electrode in the absence and presence of 4-nitrophenol at 0.5 mM in nitrogen unpurged and purged 0.05 M PBS (pH 5) (*vs*. SCE), v: 50 mV s^{-1}. (a) first cycle, (b) second cycle.

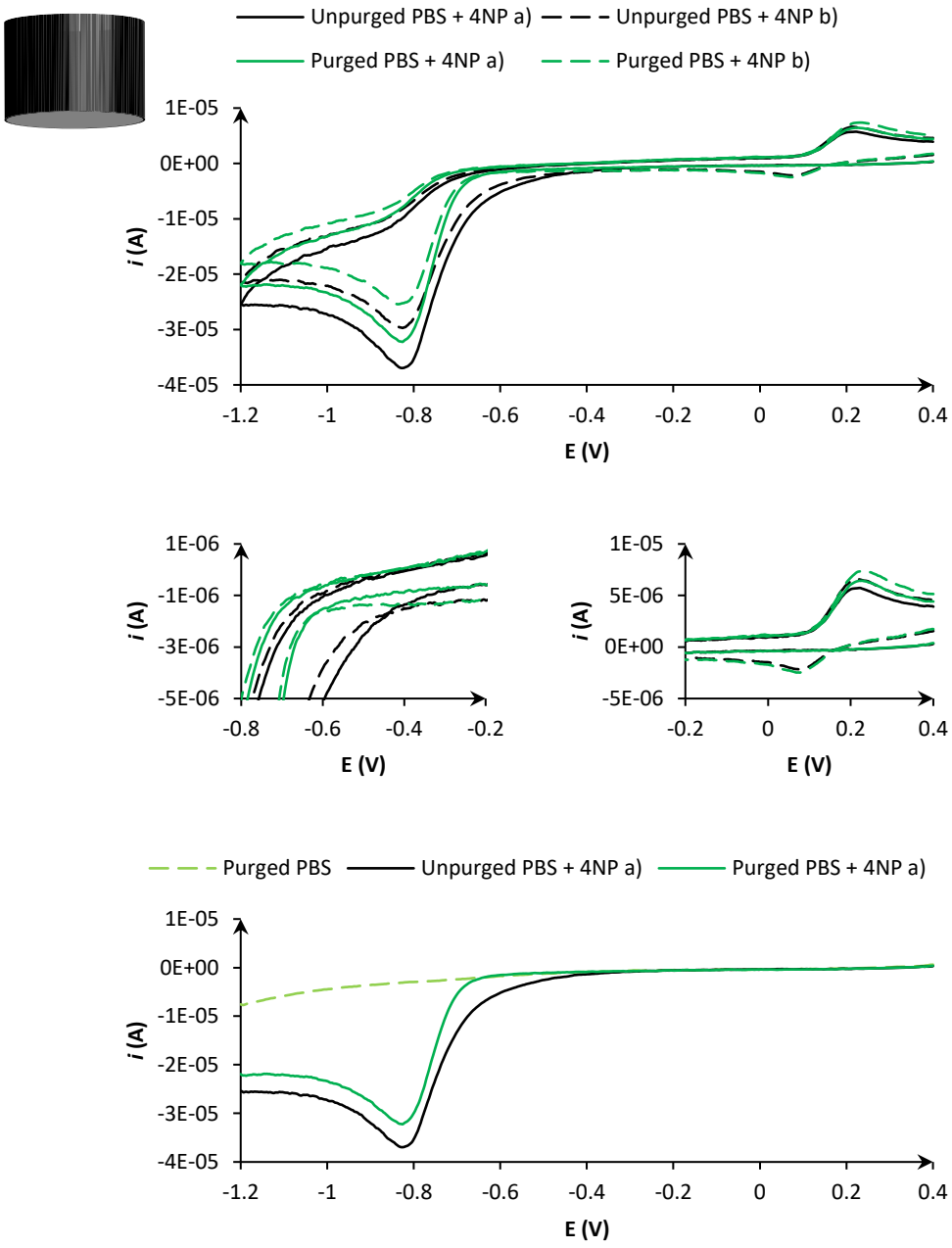

Figure 33. Cyclic voltammogram of vitreous carbon electrode in the absence and presence of 4-nitrophenol at 0.5 mM in nitrogen unpurged and purged 0.05 M PBS (pH 5) (*vs*. SCE), v: 50 mV s^{-1}. (a) first cycle, (b) second cycle.

To limit the variety of molecules and aiming strictly for the reduction of 4-nitrophenol, the potential window was restricted to between -0.2 V and -1.2 V, and several concentrations were tested. Herein, concentration of 0 μM represents the absence of p-nitrophenol, meaning the measurement is made in phosphate buffer solution, also termed the blank. Different p-nitrophenol concentrations gave rise to different responses, relation which follows the tendency depicted in the current *vs.* 4-nitrophenol concentration plots. Cyclic voltammetry studies of the bare electrodes in the presence of 4-nitrophenol were made in PBS (pH 5.3), with 4-nitrophenol at a concentration range of 600 – 12 μM (Figures 34-35). A cathodic peak near -0.8 V indicates the reduction of p-nitrophenol to 4-(hydroxyamino)phenol. An additional cathodic peak past -0.9 V is present in the cyclic voltammogram of gold electrode, hinting a redox reaction taking place at the electrode surface in addition to the expected reduction of p-nitrophenol, namely the reduction of solution components at the electrode surface.

A great volume of 4-nitrophenol reduction research is directed to nanocomposite architectures built over glassy carbon electrodes, which is understandable, once p-nitrophenol reduction takes place at an inert potential for vitreous carbon electrode in phosphate buffer medium. Gold is a known catalyst for the reduction of oxygen, which might explain the low volume and even lack of research regarding 4-nitrophenol reduction using gold-based electrodes.[75,77,78] As previously stated, the interference of oxygen is nullified with nitrogen purge, making the usable potential window stretch to -0.8 V. The current values taken into consideration for the concentration-dependent plot were measured at the potential value -0.8 V, potential at which the currents are formed by the reduction of 4-nitrophenol, without oxygen interference.

The reduction of p-nitrophenol at bare electrodes revealed linear range between 600 – 12 μM, translating into limits of detection of 179 and 33 μM for gold and glassy carbon electrodes, respectively. Limit of detection, LOD[79], represents the minimum amount of analyte that can be detected by the sensor and discerned from the medium, and was calculated as:

$$LOD = 3 \times SD/a$$

Where *SD* is the standard deviation of the y-intercept and *a* is the slope of the calibration curve. As the concentration of the analyte decreases and leans to zero, the electrochemical response will approach that of the analyte-free medium (blank). Estimated limit of detection for gold electrode is higher than for glassy carbon electrode due to the inherent cathodic current resultant from the electroreduction of the electrode itself. In other words, 4-nitrophenol reduction is hindered by the electroreduction of the solution on gold surfaces, which do not occur in vitreous carbon electrodes.

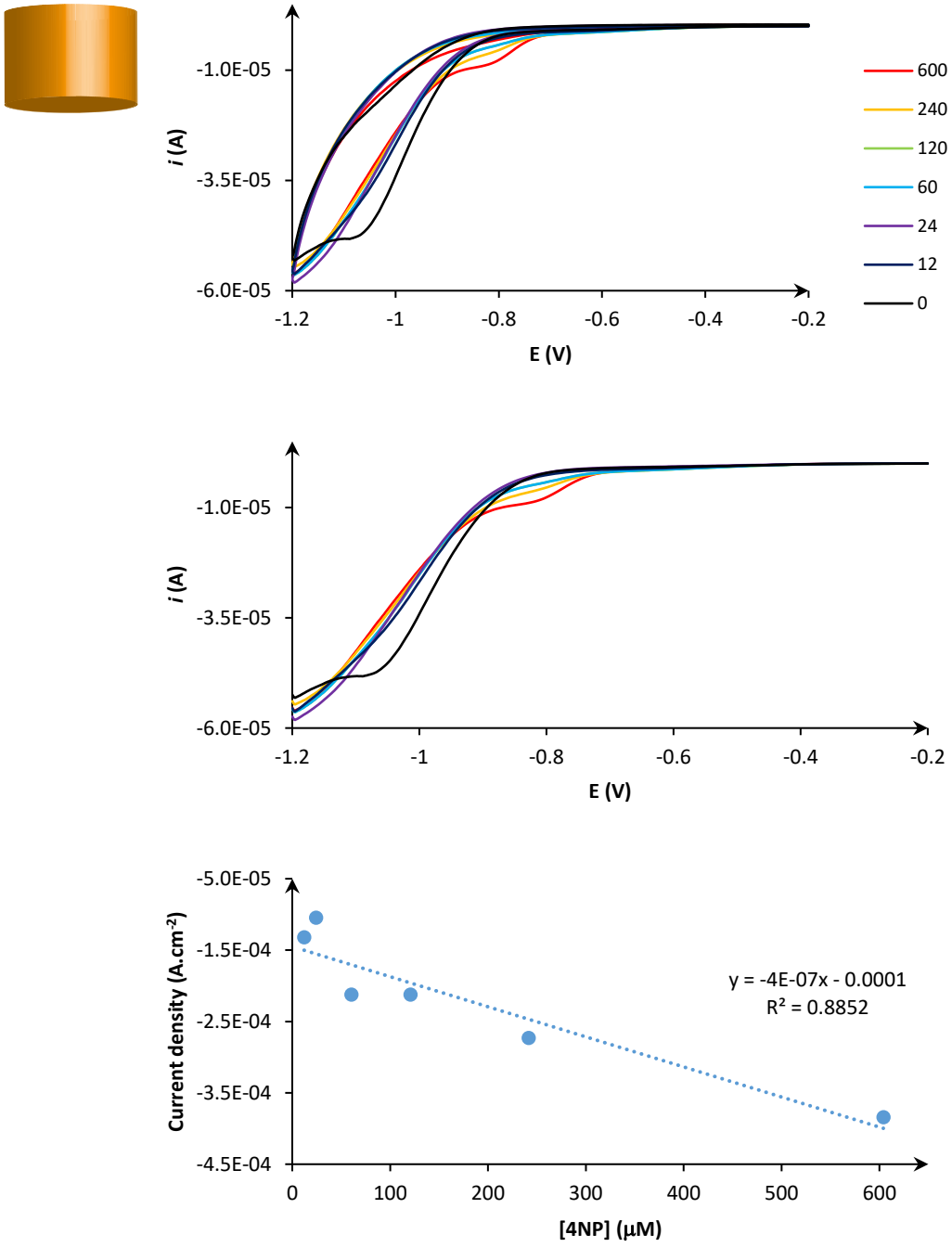

Figure 34. Cyclic voltammogram of gold electrode in 0.05 M PBS (pH 5.3) and 4-nitrophenol at different concentrations, ranging from 600 µM to 12 µM (*vs*. SCE), v: 50 mV s^{-1}. Current-concentration dependence plot.

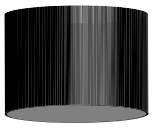

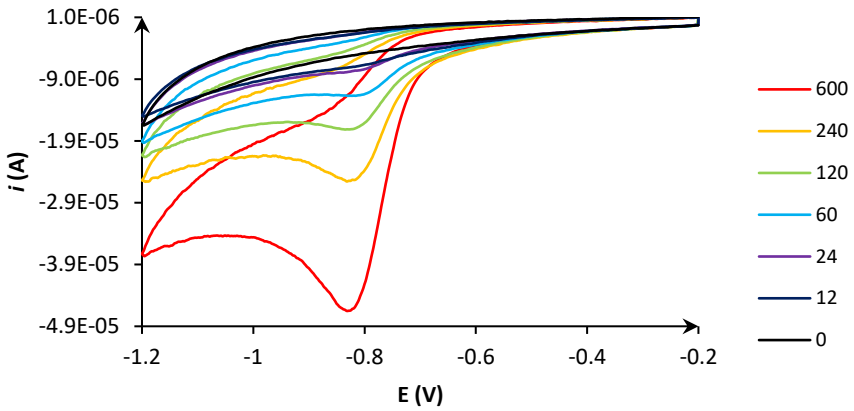

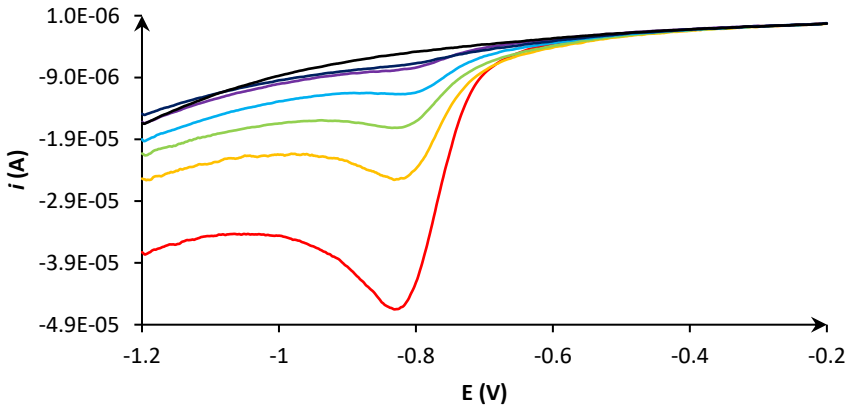

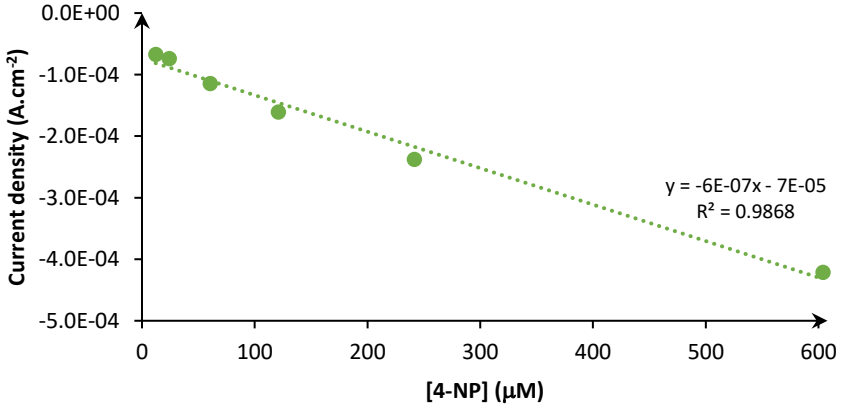

Figure 35. Cyclic voltammogram of glassy carbon electrode in 0.05 M PBS (pH 5.3) and 4-nitrophenol at different concentrations, ranging from 600 µM to 12 µM (*vs*. SCE), v: 50 mV s^{-1}. Current-concentration dependence plot.

3.5.2 *PAMAM-NH_2 dendrimer-modified electrodes*

Cyclic voltammetry studies of PAMAM-modified electrodes in 4-nitrophenol were made in PBS (pH 5.3) at a concentration range of 1200 - 35 μM (Figures 36-41).

3-mercaptopropionic acid-based electrodes were tested on PBS with p-nitrophenol concentration varying between 690 – 35 μM (Figures 36-37). A linear response is observed in both electrochemical profiles, between the current produced when the potential is -0.8 V and p-nitrophenol concentration. Limits of detection of 219 and 17 μM were estimated for gold and glassy carbon electrodes modified with PAMAM and MPA. PAMAM assembly over MPA-modified electrode resulted in a shift of the electroreduction of the electrode towards less negative potentials. PAMAM and MPA-modified glassy carbon electrode is more sensitive to p-nitrophenol detection than its bare counterpart, as suggested by a smaller limit of detection.

Mercaptopropionic sulfonic acid-based electrodes were tested in PBS (pH 5.3) with 4-nitrophenol concentration ranging from 1200 to 60 μM (Figures 38-39). Limits of detection of 319 and 22 μM were estimated for gold and glassy carbon electrodes modified with PAMAM and MPS. Similar to the effect of PAMAM assembly over Au-MPA, Au-MPS-PAMAM electrochemical behaviour revealed an electroreduction peak shifted to more positive potentials (-1.1 V), suggesting PAMAM assembly onto the electrode improves the electrocatalytic activity of the electrode. Regarding 4-nitrophenol detection, PAMAM dendrimer and mercaptopropionic sulfonic acid assembly over glassy carbon electrode represents an improvement sensitivity-wise, as supported by a smaller limit of detection for GC-MPS-PAMAM.

4-aminothiophenol-based electrodes were tested in PBS (pH 5.3) with 4-nitrophenol concentration ranging from 575 to 60 μM (Figures 40-41). Limits of detection of 296 and 38 μM were estimated for gold and glassy carbon electrodes modified with PAMAM and ATP. Contrary to MPA and MPS-based electrodes, where a shoulder near -0.8 V indicated the reduction of p-nitrophenol to 4-(hydroxyamino)phenol, PAMAM and ATP-modified gold electrode electrochemical behaviour was characterized by a sole peak, corresponding to the reduction of solution components on gold electrode. The shoulder near -0.8 V may be less accentuated because 4-nitrophenol concentration is lower. PAMAM and 4-aminothiophenol-modified glassy carbon electrode cyclic voltammogram is characterized by a peak near -0.8 V, in similarity with bare, PAMAM and 3-mercaptopropionic acid, PAMAM and mercaptopropionic sulfonic acid-modified electrode.

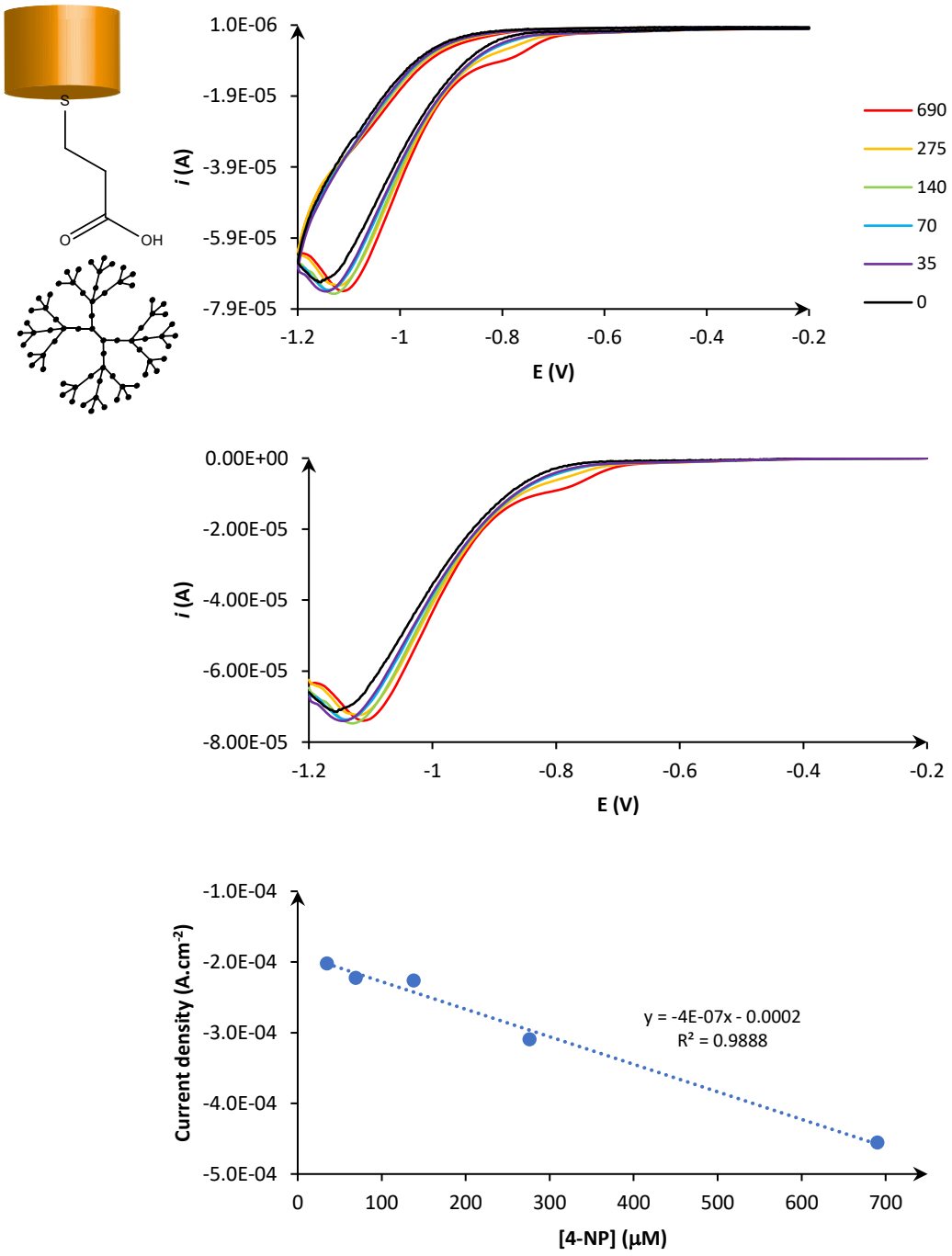

Figure 36. Cyclic voltammogram of gold electrode modified with MPA and G5-NH_2 PAMAM dendrimer in 0.05 M PBS (pH 5.3) and 4-nitrophenol at different concentrations, ranging from 690 µM to 35 µM (*vs*. SCE), v: 50 mV s^{-1}.

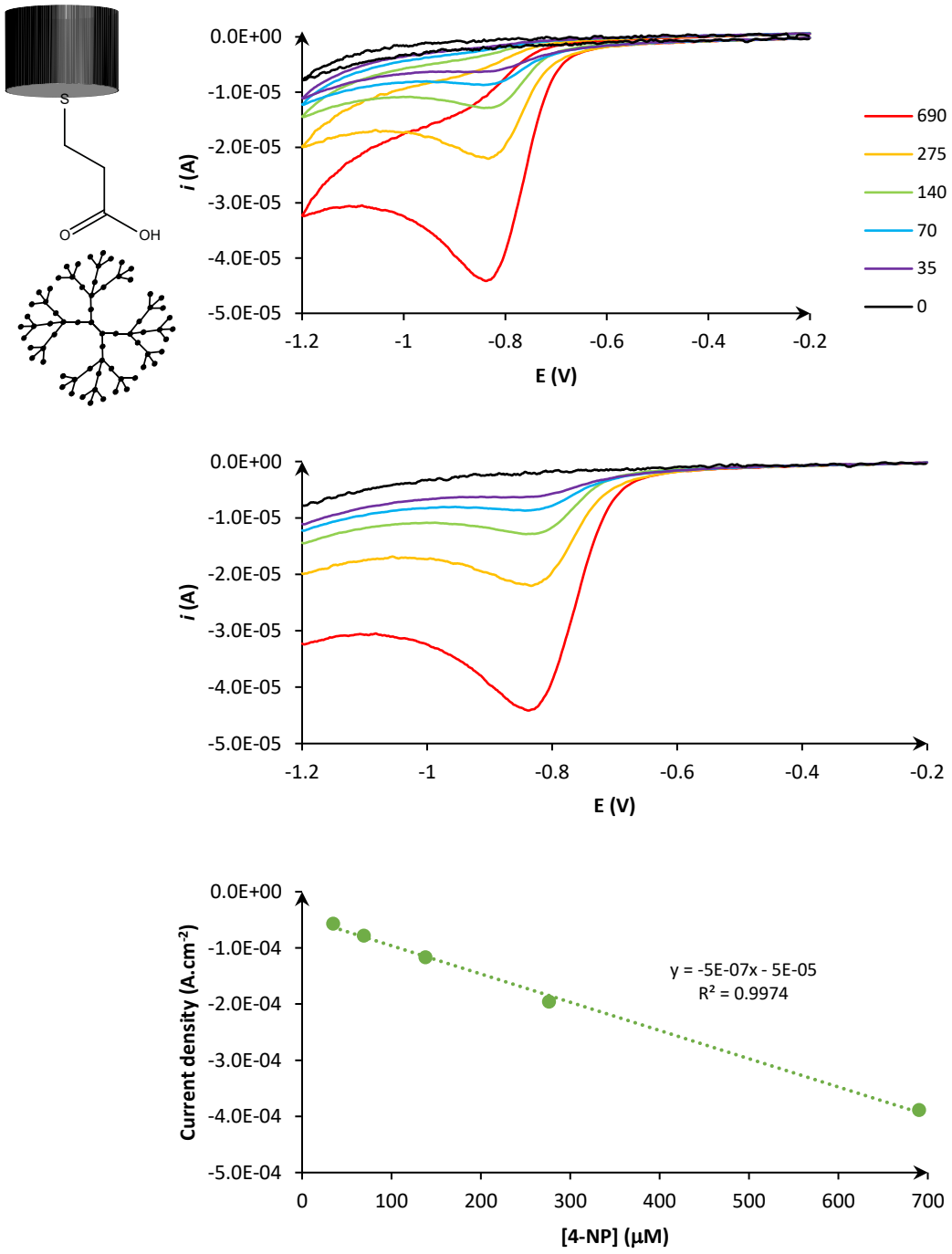

Figure 37. Cyclic voltammogram of glassy carbon electrode modified with MPA and G5-NH_2 PAMAM dendrimer in 0.05 M PBS (pH 5.3) and 4-nitrophenol at different concentrations, ranging from 690 µM to 35 µM (*vs*. SCE), v: 50 mV s^{-1}.

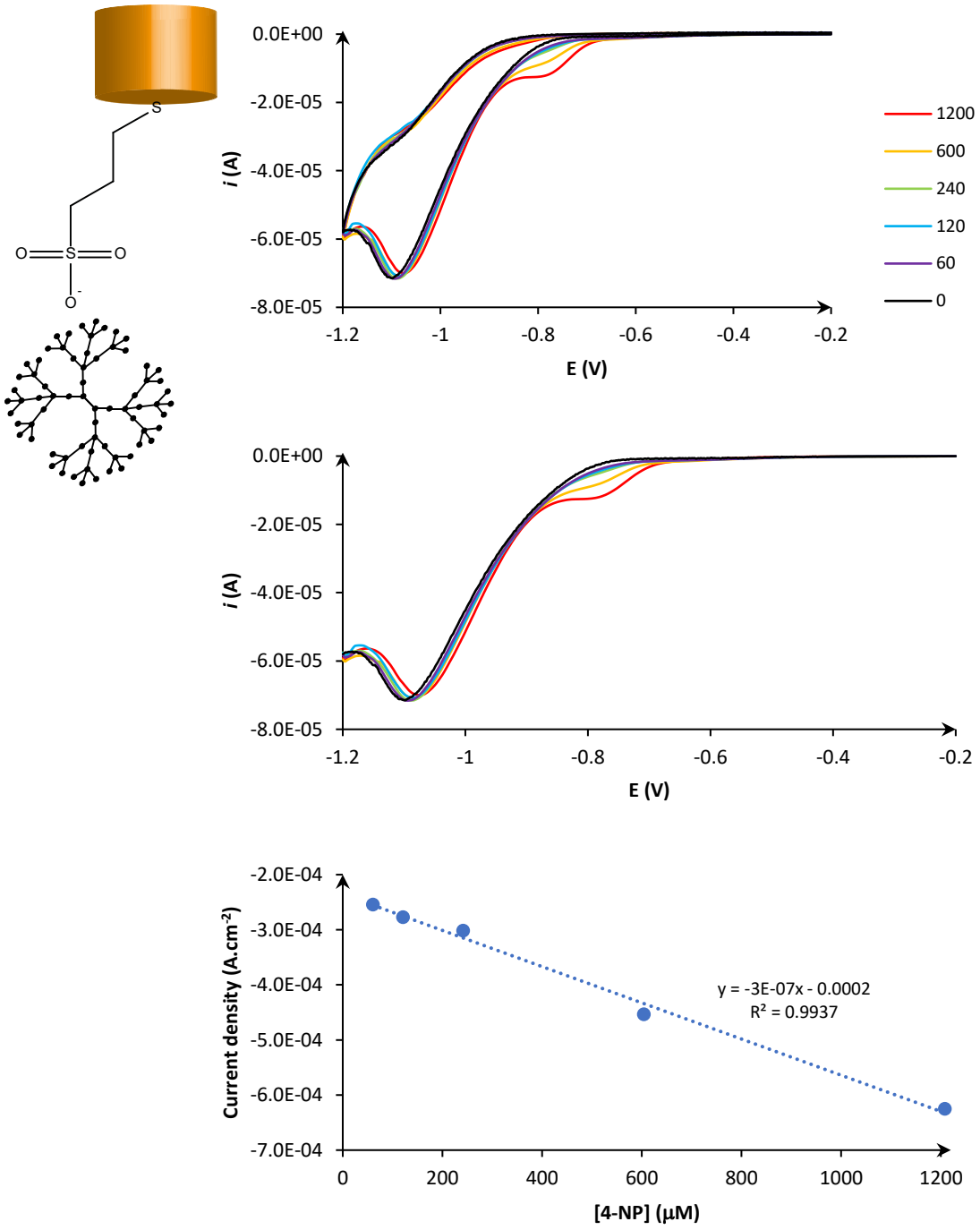

Figure 38. Cyclic voltammogram of gold electrode modified with MPS and G5-NH_2 PAMAM dendrimer in 0.05 M PBS (pH 5.3) and 4-nitrophenol at different concentrations, ranging from 1200 µM to 60 µM (*vs*. SCE), v: 50 mV s^{-1}.

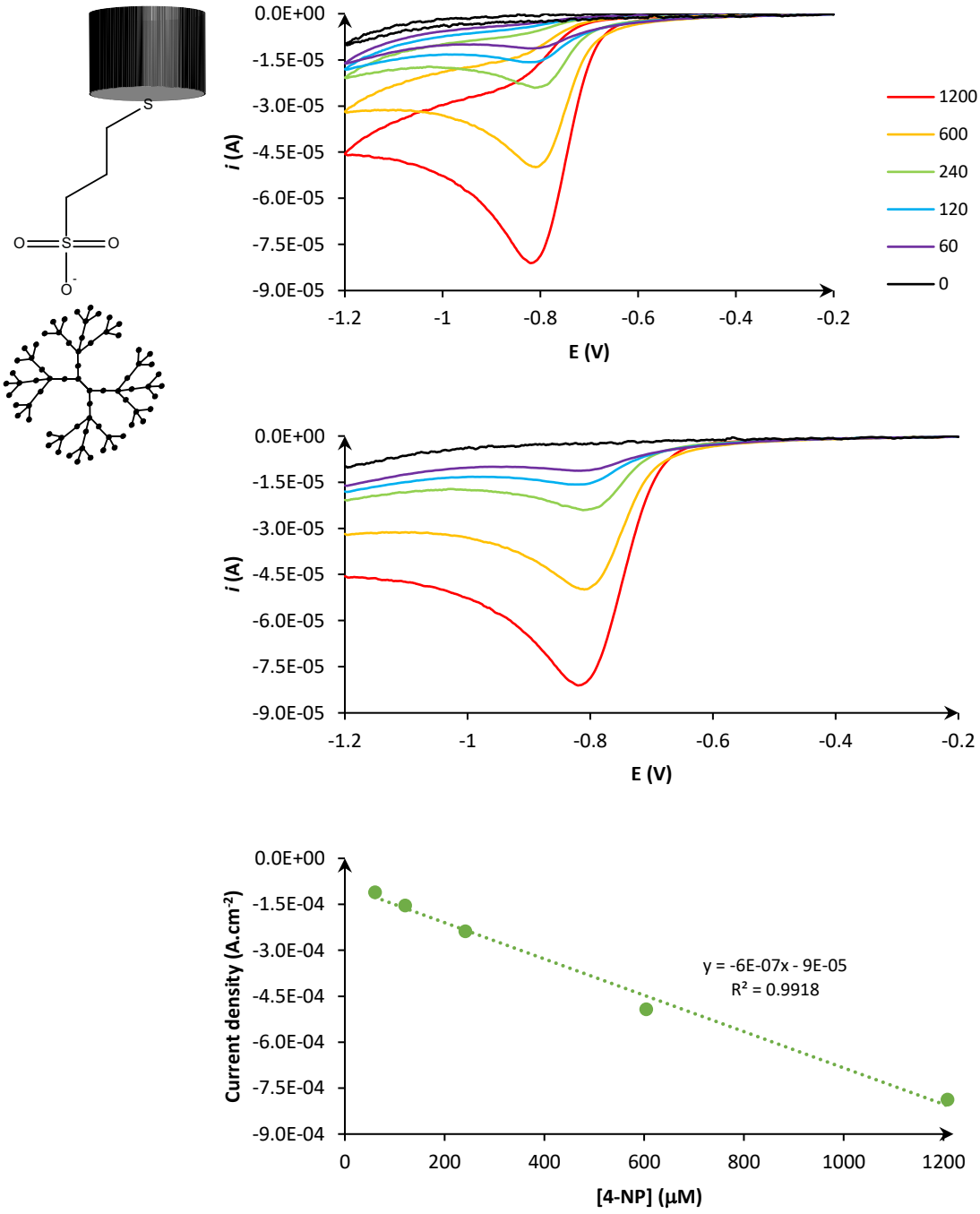

Figure 39. Cyclic voltammogram of glassy carbon electrode modified with MPS and G5-NH_2 PAMAM dendrimer in 0.05 M PBS (pH 5.3) and 4-nitrophenol at different concentrations, ranging from 1200 µM to 60 µM (*vs*. SCE), v: 50 mV s^{-1}.

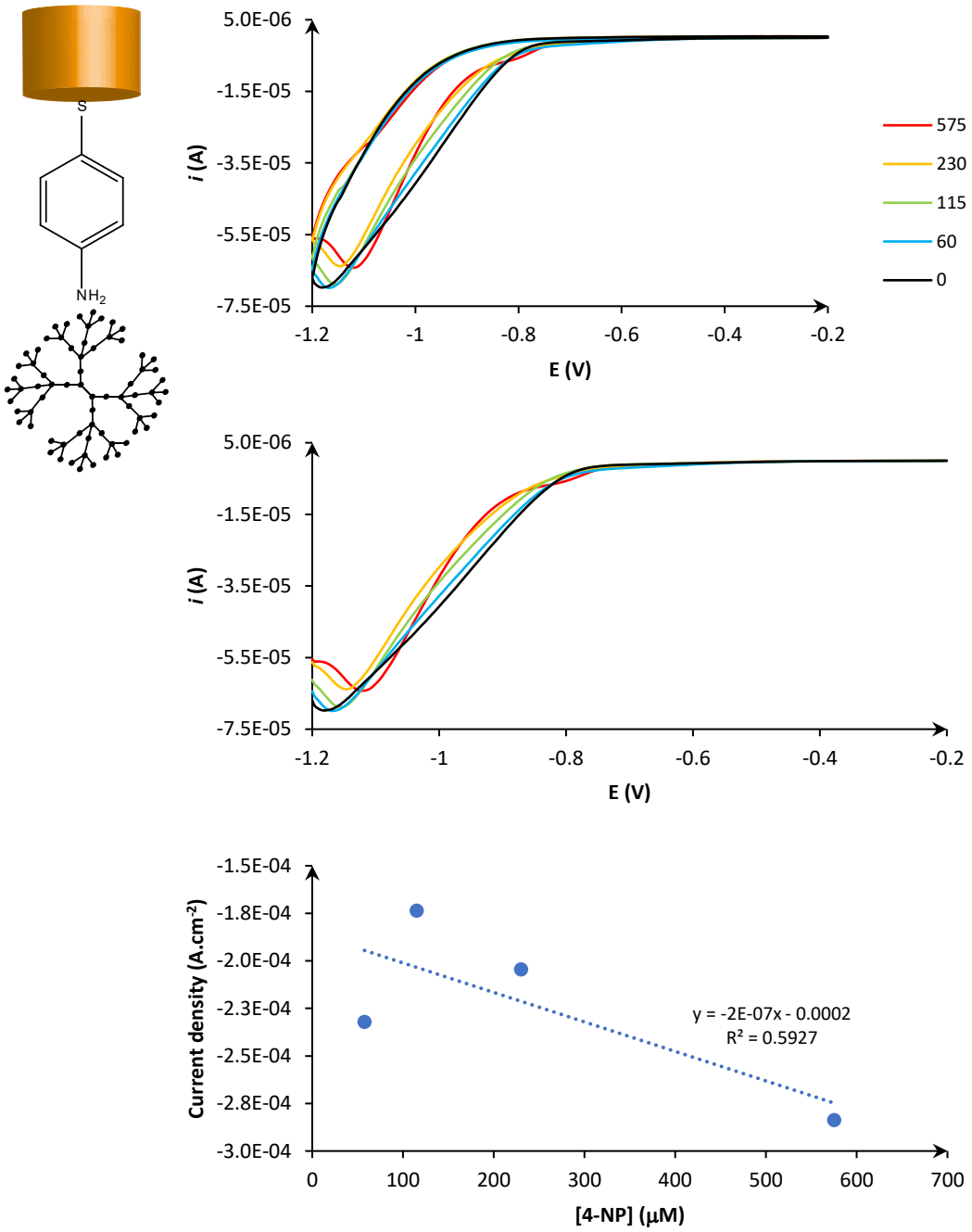

Figure 40. Cyclic voltammogram of gold electrode modified with ATP and G5-NH_2 PAMAM dendrimer in 0.05 M PBS (pH 5.3) and 4-nitrophenol at different concentrations, ranging from 575 µM to 60 µM (*vs*. SCE), v: 50 mV s^{-1}.

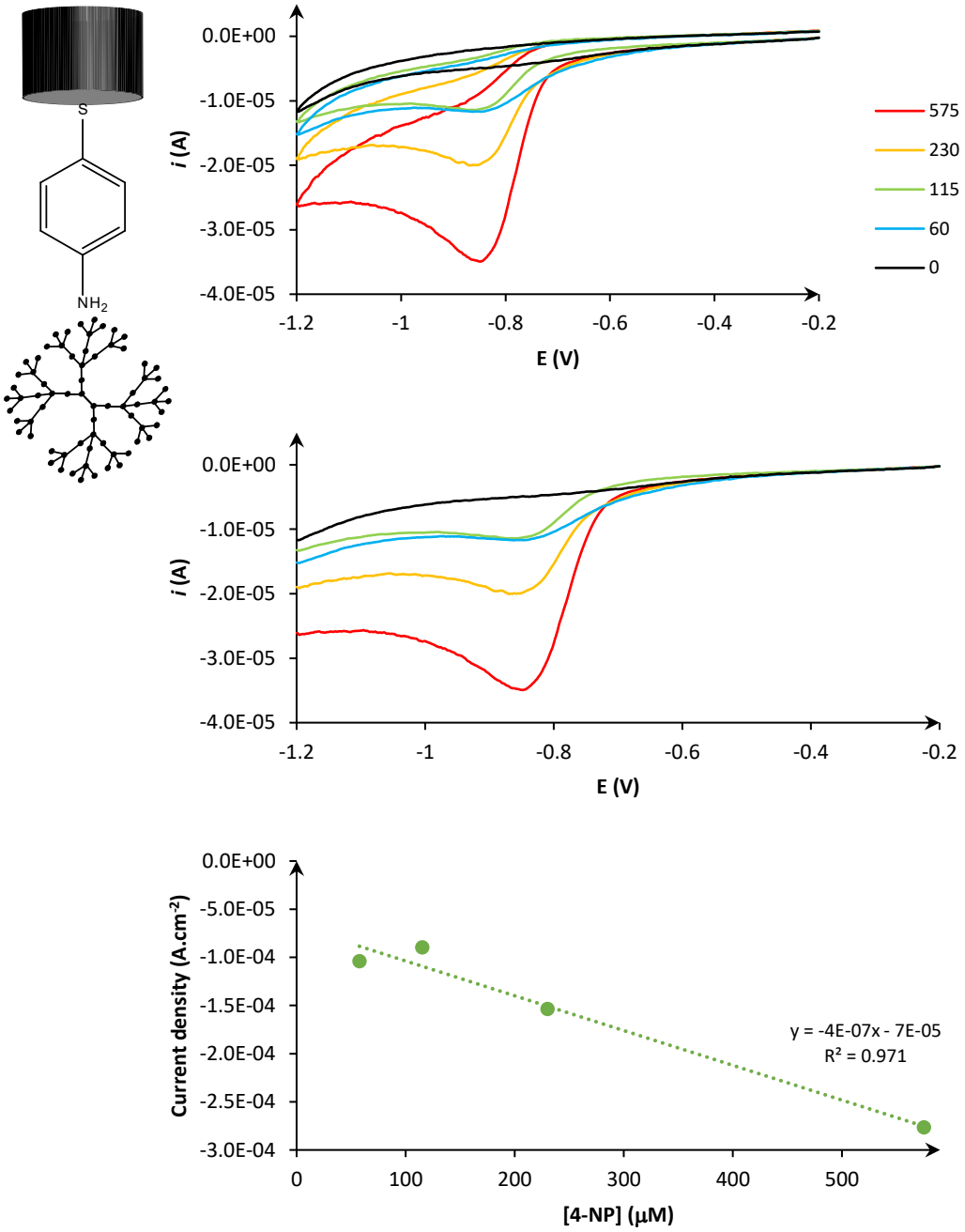

Figure 41. Cyclic voltammogram of glassy carbon electrode modified with ATP and G5-NH_2 PAMAM dendrimer in 0.05 M PBS (pH 5.3) and 4-nitrophenol at different concentrations, ranging from 575 µM to 60 µM (*vs*. SCE), v: 50 mV s^{-1}.

3.5.3 *Gold-modified electrodes*

3.5.3.1 Modification with gold layer

Cyclic voltammetry studies of gold layer-modified electrodes in 4-nitrophenol were made in PBS (pH 5.3) at a concentration range of 1090 - 20 μM (Figures 42-47).

3-mercaptopropionic acid-based electrodes were tested on PBS with p-nitrophenol concentration varying between 1090 – 110 μM (Figures 42-43). Limits of detection of 463 and 68 μM were estimated for gold and glassy carbon electrodes modified with gold layer and 3-mercaptopropionic acid. The defined shoulder associated to 4-nitrophenol reduction was absent in the cyclic voltammogram of gold electrode modified with 3-mercaptopropionic acid and gold layer, even at high concentrations such as 1090 μM. Electroreduction of gold over thiol-modified glassy carbon electrode resulted in an electrode that exhibits similar features to gold electrode regarding 4-nitrophenol detection, namely a shoulder around -0.8 V and a cathodic current rise at lower potentials, both attributed to p-nitrophenol and solution reduction. These results confirm that gold is indeed present in glassy carbon electrodes modified with gold layer. Gold layer and MPA-modified glassy carbon electrode is less sensitive to 4-nitrophenol detection than its bare counterpart, as suggested by a larger limit of detection, owing to the presence of gold.

Mercaptopropionic sulfonic acid-based electrodes were tested on PBS with p-nitrophenol concentration varying between 520 – 20 μM (Figures 44-45). Limits of detection of 426 and 74 μM were estimated for gold and glassy carbon electrodes modified with gold layer and mercaptopropionic sulfonic acid. Both electrodes based on gold and vitreous carbon substrates exhibited similar electrochemical behaviour, shoulder near -0.8 V and a peak at more negative potentials, representing 4-nitrophenol and solution reduction, respectively.

4-aminothiophenol-based electrodes were tested on PBS with p-nitrophenol concentration ranging between 630 – 60 μM (Figures 46-47). Limits of detection of 281 and 81 μM were estimated for gold and glassy carbon electrodes modified with gold layer and 4-aminothiophenol. The shoulder attributed to 4-nitrophenol reduction was absent in the cyclic voltammogram of gold electrode modified with 4-aminothiophenol and gold layer. However, electrochemical characterization of gold layer over 3-mercaptopropionic acid and 4-aminothiophenol-modified gold electrode revealed that although a defined shoulder was inexistent, a cathodic current was formed near -0.8 V, which could be correlated to 4-nitrophenol concentration.

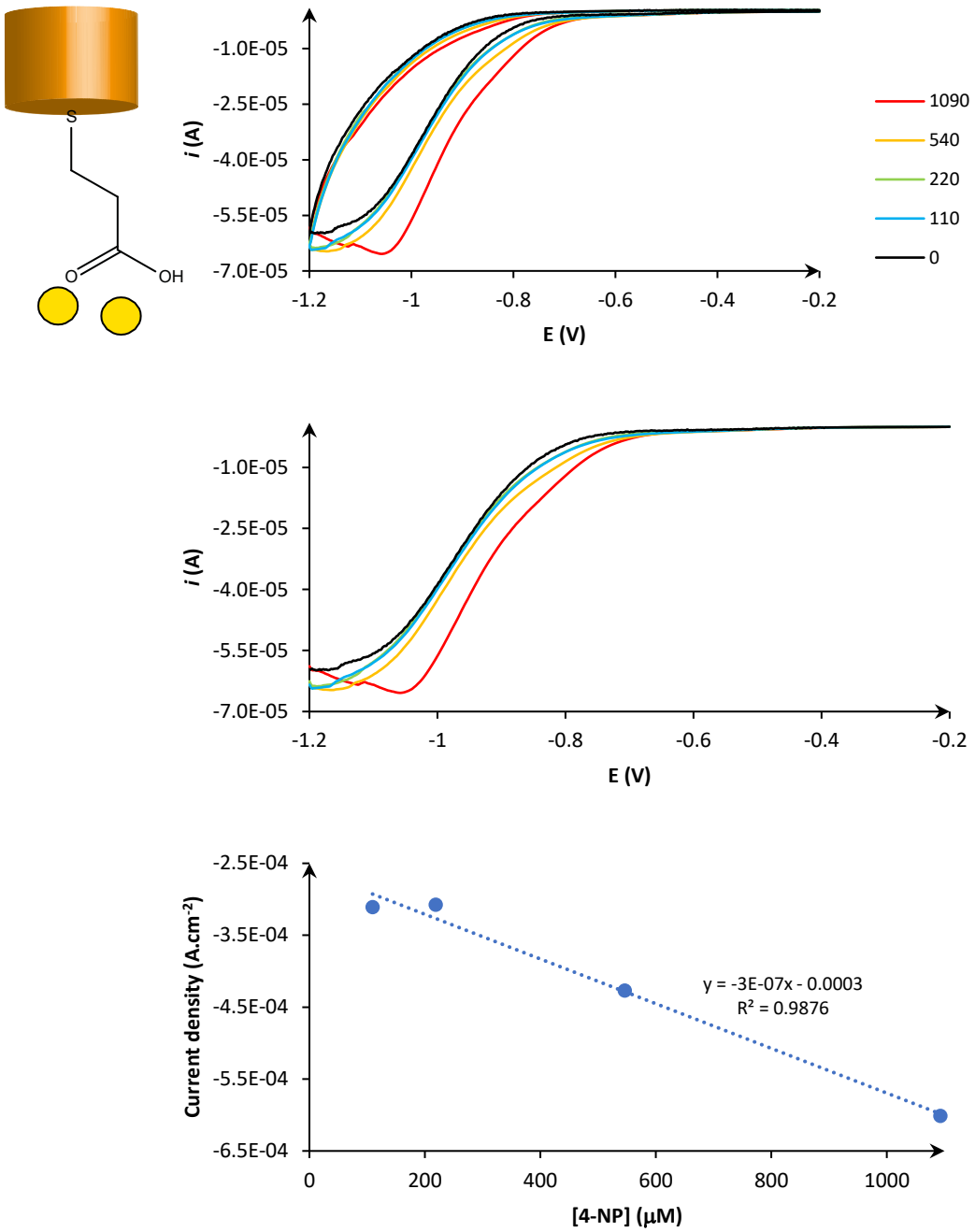

Figure 42. Cyclic voltammogram of gold electrode modified with MPA and gold layer in 0.05 M PBS (pH 5.3) and 4-nitrophenol at different concentrations, ranging from 1090 µM to 110 µM (*vs*. SCE), v: 50 mV s^{-1}.

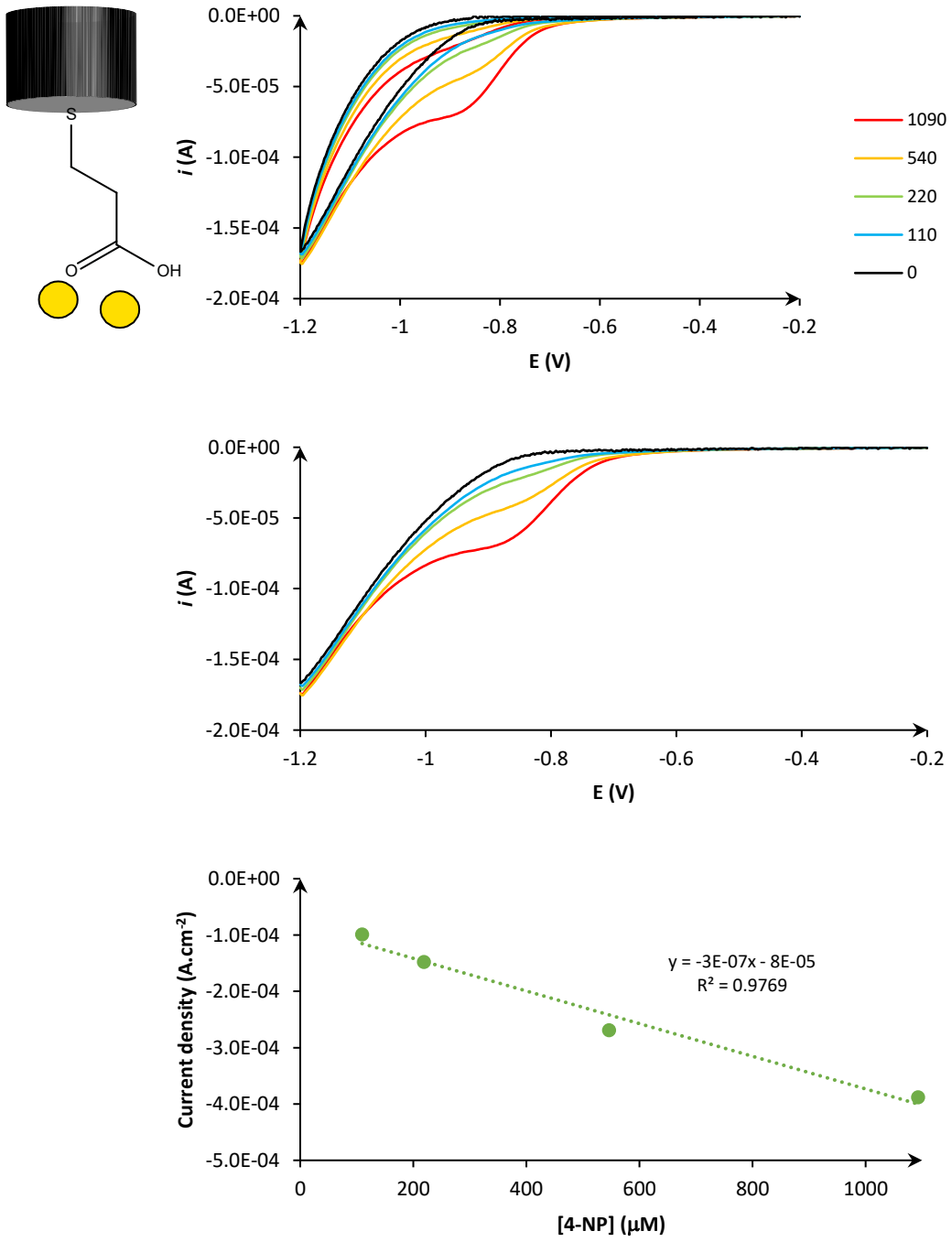

Figure 43. Cyclic voltammogram of glassy carbon electrode modified with MPA and gold layer in 0.05 M PBS (pH 5.3) and 4-nitrophenol at different concentrations, ranging from 1090 µM to 110 µM (*vs*. SCE), v: 50 mV s^{-1}.

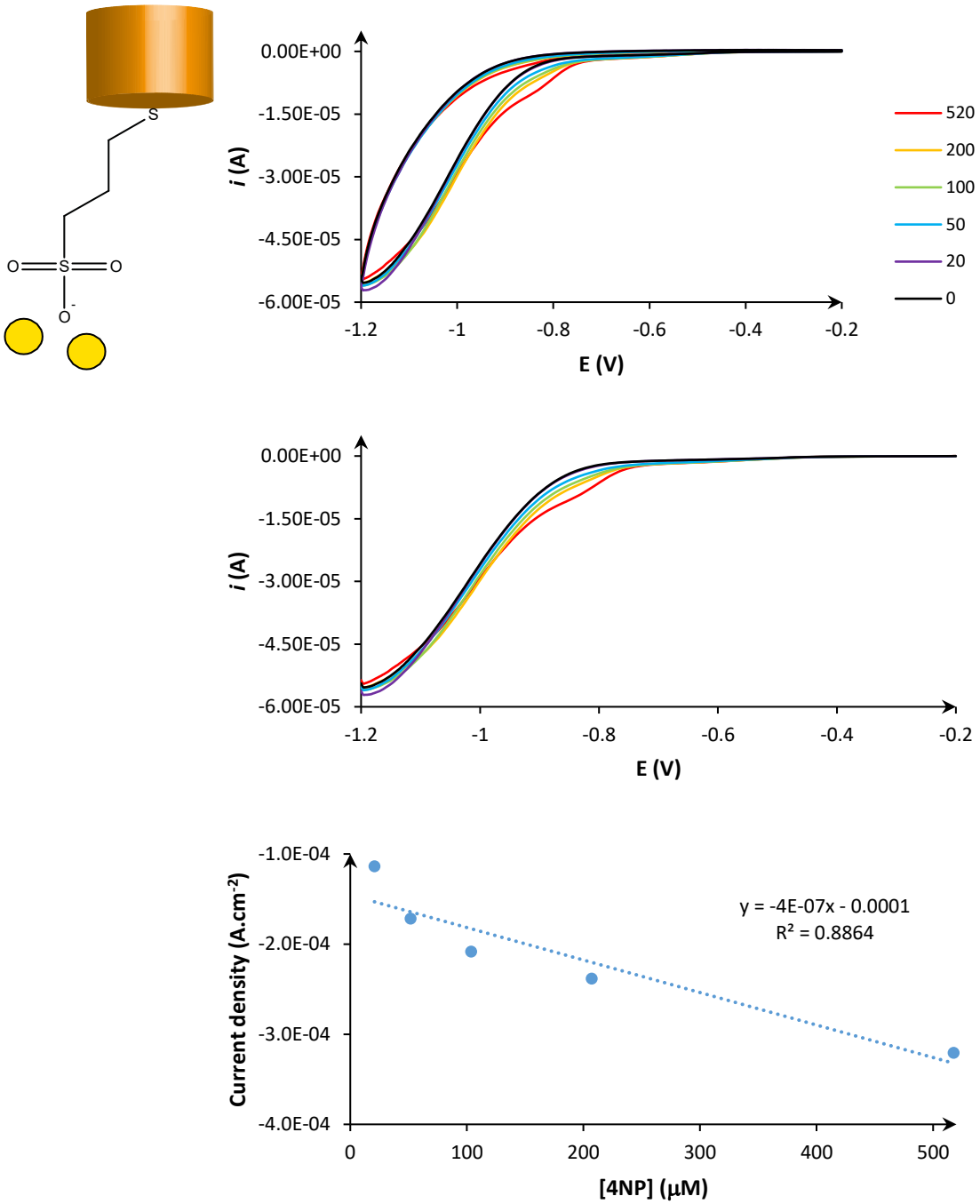

Figure 44. Cyclic voltammogram of gold electrode modified with MPS and gold layer in 0.05 M PBS (pH 5.3) and 4-nitrophenol at different concentrations, ranging from 520 µM to 20 µM (*vs*. SCE), v: 50 mV s^{-1}.

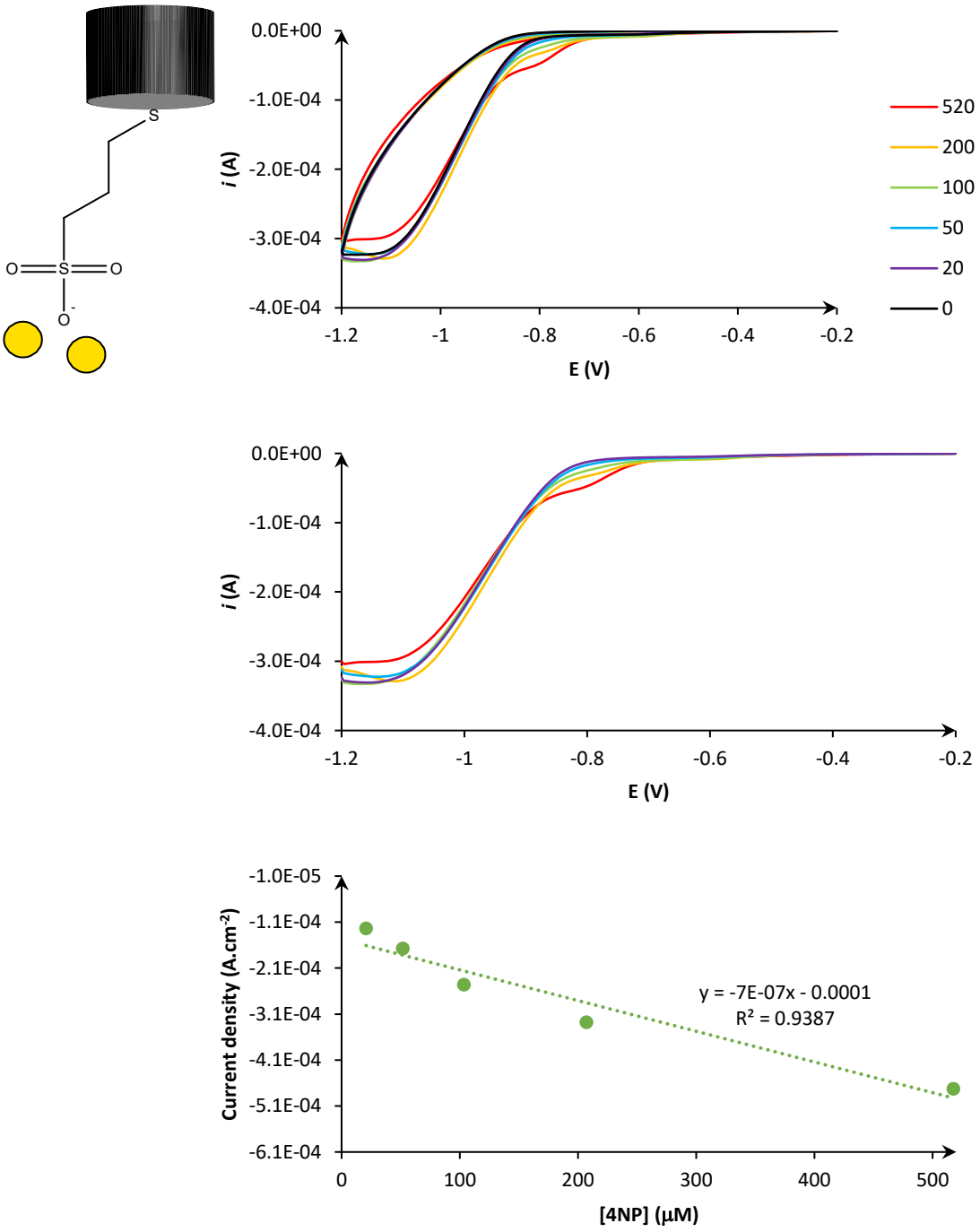

Figure 45. Cyclic voltammogram of glassy carbon electrode modified with MPS and gold layer in 0.05 M PBS (pH 5.3) and 4-nitrophenol at different concentrations, ranging from 520 µM to 20 µM (*vs*. SCE), v: 50 mV s^{-1}.

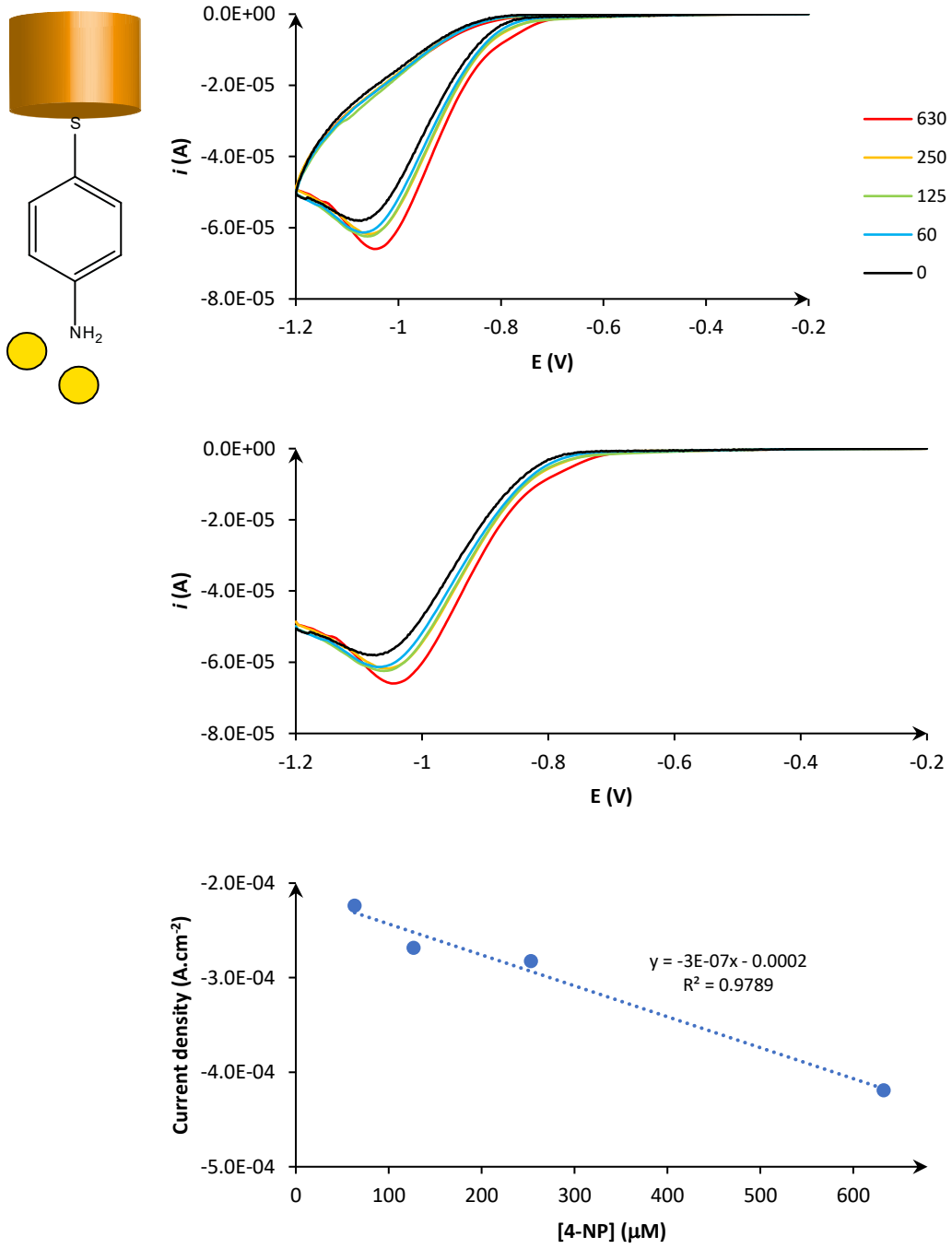

Figure 46. Cyclic voltammogram of gold electrode modified with ATP and gold layer in 0.05 M PBS (pH 5.3) and 4-nitrophenol at different concentrations, ranging from 630 µM to 60 µM (*vs*. SCE), v: 50 mV s^{-1}.

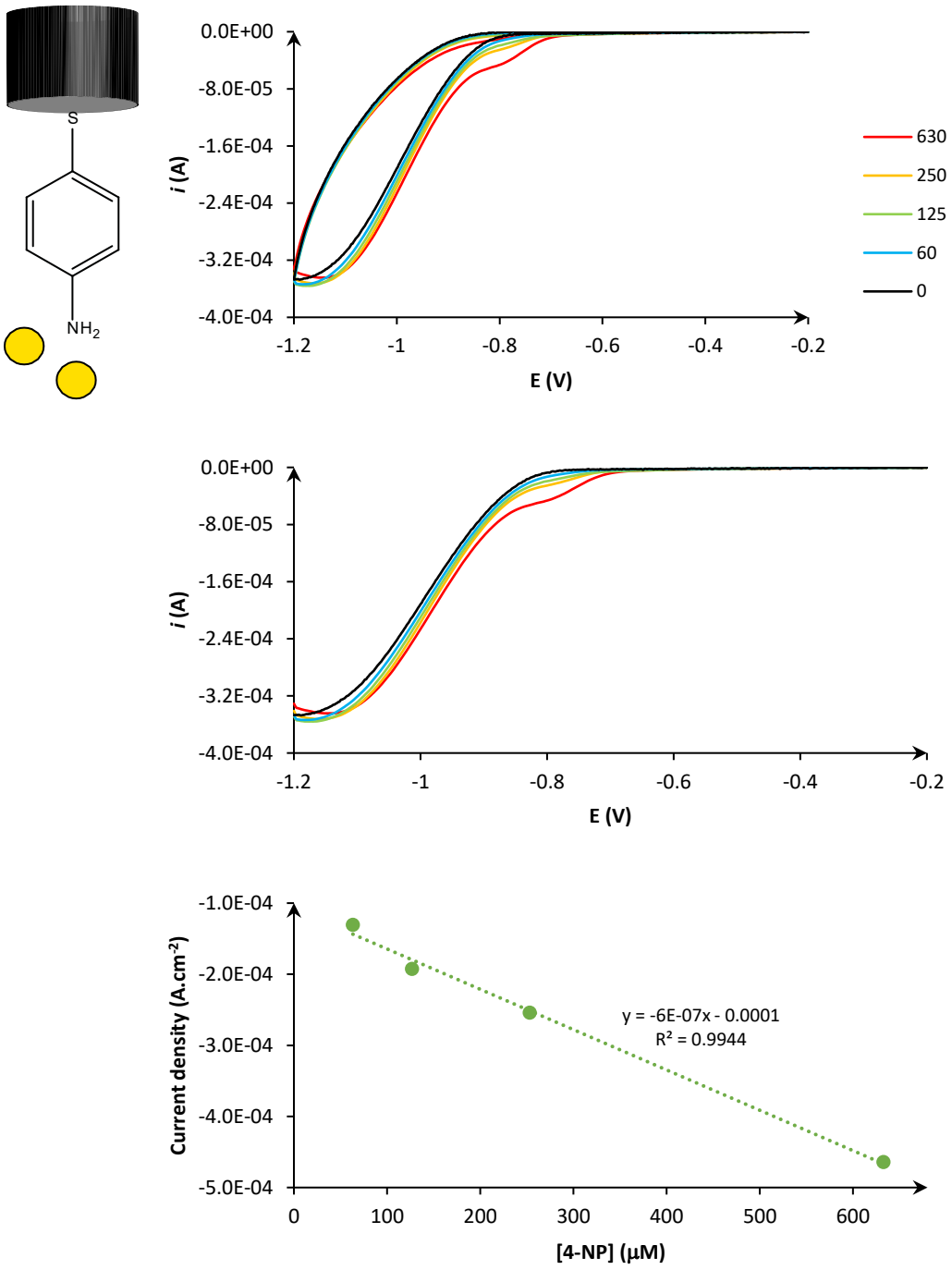

Figure 47. Cyclic voltammogram of glassy carbon electrode modified with ATP and gold layer in 0.05 M PBS (pH 5.3) and 4-nitrophenol at different concentrations, ranging from 630 µM to 60 µM (*vs*. SCE), v: 50 mV s^{-1}.

3.5.3.2 Modification with citrate-stabilized gold nanoparticles

Cyclic voltammetry studies of electrodes modified with citrate-stabilized gold nanoparticles in 4-nitrophenol were made in PBS (pH 5.3) at a concentration range of 800 - 40 μM (Figures 48-53).

3-mercaptopropionic acid-based electrodes were tested on PBS with p-nitrophenol concentration varying between 520 – 50 μM (Figures 48-49). Limits of detection of 186 and 52 μM were estimated for gold and glassy carbon electrodes modified with citrate-stabilized gold nanoparticles, PAMAM and 3-mercaptopropionic acid. Both exhibited similar electrochemical behaviour, shoulder near -0.8 V and a peak at more negative potentials, representing 4-nitrophenol and solution reduction, correspondingly.

Mercaptopropionic sulfonic acid-based electrodes were tested on PBS with p-nitrophenol concentration varying between 800 – 40 μM (Figures 50-51). Limits of detection of 226 and 20 μM were determined for gold and glassy carbon electrodes modified with citrate-stabilized gold nanoparticles, PAMAM and mercaptopropionic sulfonic acid. Assembly of gold nanoparticles over PAMAM and MPS-modified gold electrode resulted in a shifted cathodic peak towards more negative potentials. Both gold nanoparticles, PAMAM and MPS-modified gold and vitreous carbon electrodes exhibit similar electrochemical behaviour to PAMAM and MPS-modified electrodes, suggesting that gold nanoparticles were not present in the electrode architecture.

4-aminothiophenol-based electrodes were tested on PBS with p-nitrophenol concentration ranging between 490 – 50 μM (Figures 52-53). Limits of detection of 298 and 29 μM were estimated for gold and glassy carbon electrodes modified with citrate-stabilized gold nanoparticles, PAMAM and 4-aminothiophenol. Like every variant of 4-aminothiophenol-modified gold electrode, the shoulder attributed to 4-nitrophenol reduction was absent in the cyclic voltammogram of gold electrode modified with 4-aminothiophenol, PAMAM and gold nanoparticles. Furthermore, a shoulder near -0.8 V and a peak at lower potential values suggest that gold nanoparticles are present in its vitreous carbon-based counterpart.

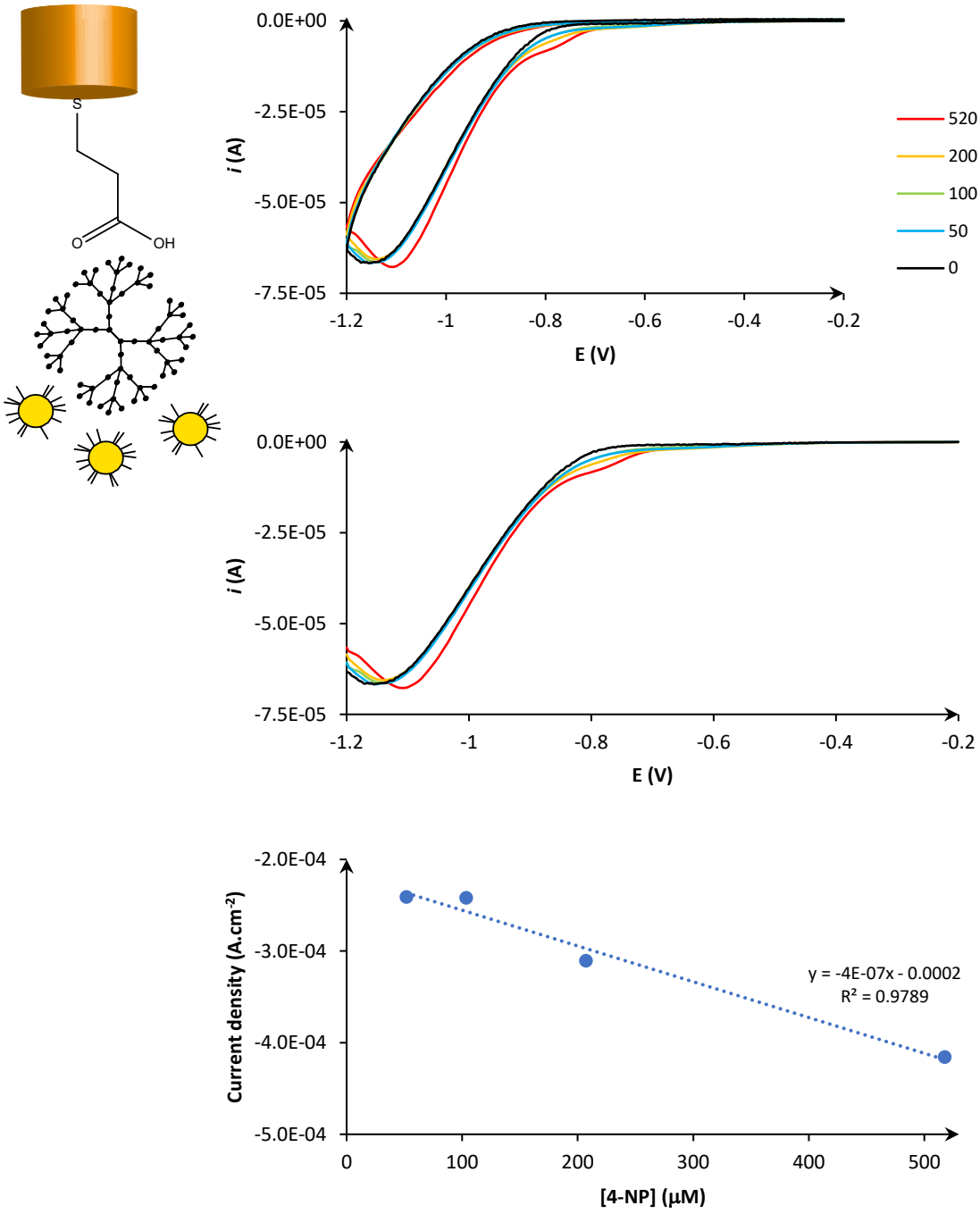

Figure 48. Cyclic voltammogram of gold electrode modified with MPA, PAMAM and citrate-stabilized gold nanoparticles in 0.05 M PBS (pH 5.3) and 4-nitrophenol at different concentrations, ranging from 520 µM to 50 µM (vs. SCE), v: 50 mV s^{-1}.

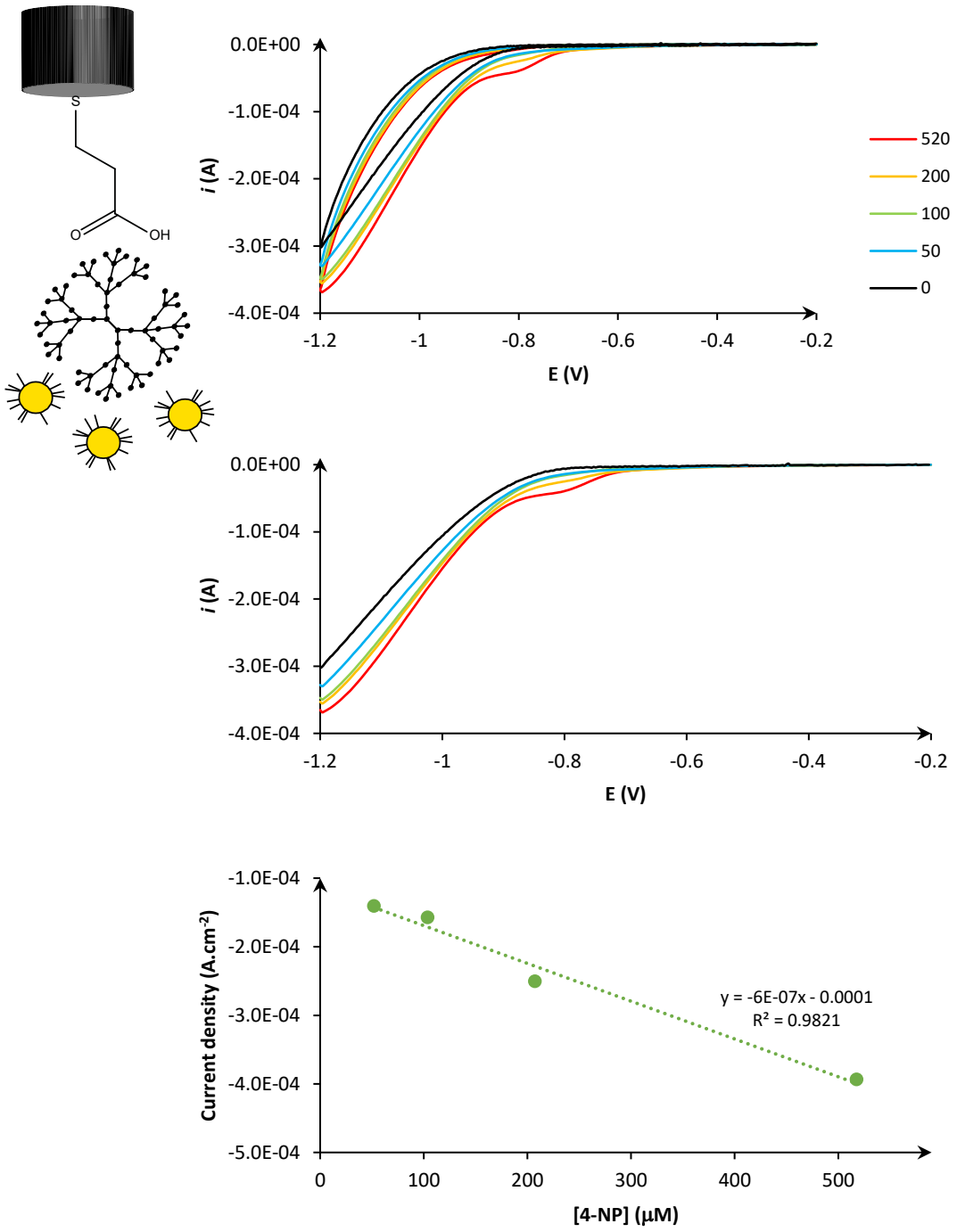

Figure 49. Cyclic voltammogram of glassy carbon electrode modified with MPA, PAMAM and citrate-stabilized gold nanoparticles in 0.05 M PBS (pH 5.3) and 4-nitrophenol at different concentrations, ranging from 520 µM to 50 µM (*vs*. SCE), v: 50 mV s^{-1}.

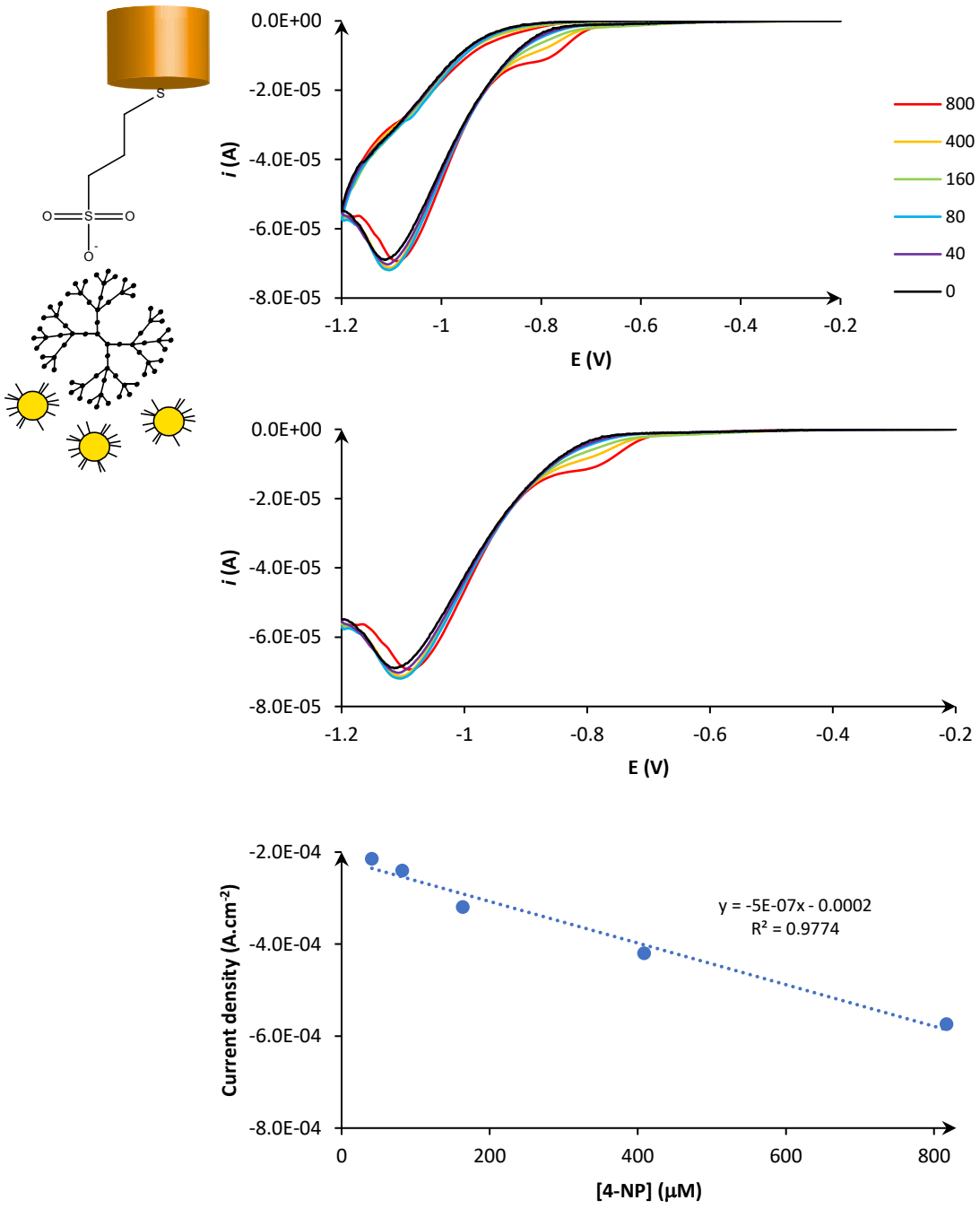

Figure 50. Cyclic voltammogram of gold electrode modified with MPS, PAMAM and citrate-stabilized gold nanoparticles in 0.05 M PBS (pH 5.3) and 4-nitrophenol at different concentrations, ranging from 800 µM to 40 µM (*vs*. SCE), v: 50 mV s^{-1}.

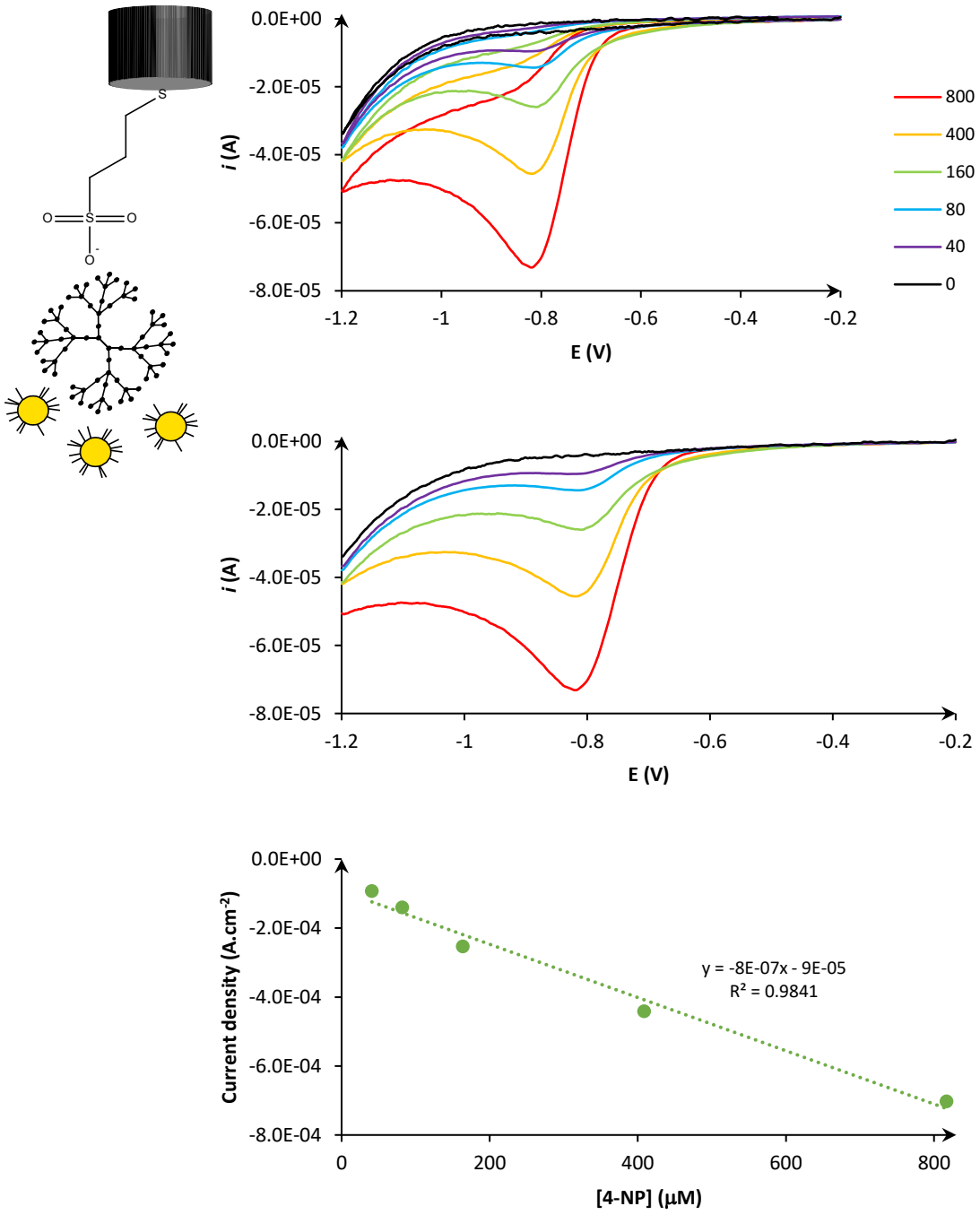

Figure 51. Cyclic voltammogram of glassy carbon electrode modified with MPS, PAMAM and citrate-stabilized gold nanoparticles in 0.05 M PBS (pH 5.3) and 4-nitrophenol at different concentrations, ranging from 800 µM to 40 µM (*vs.* SCE), v: 50 mV s^{-1}.

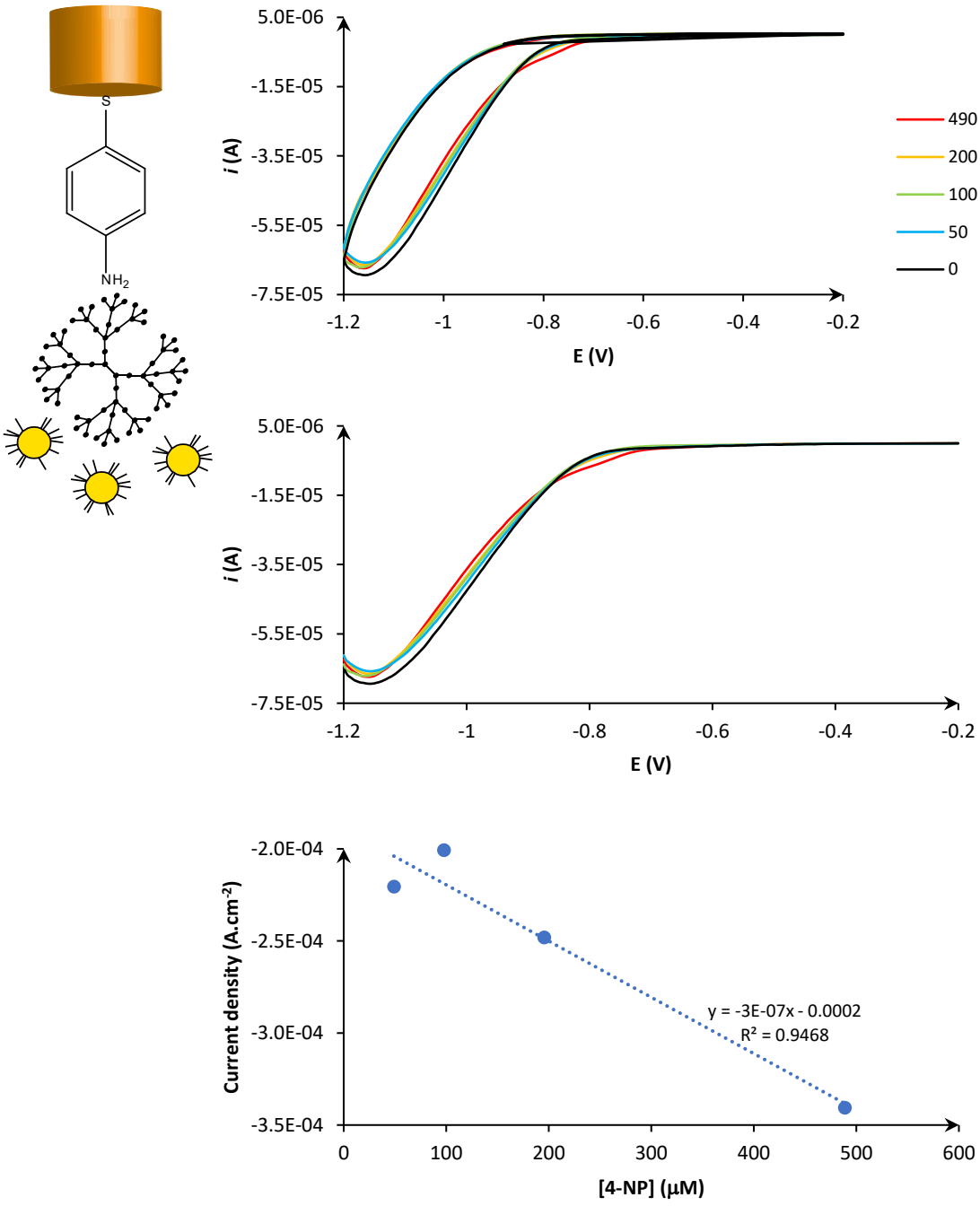

Figure 52. Cyclic voltammogram of gold electrode modified with ATP, PAMAM and citrate-stabilized gold nanoparticles in 0.05 M PBS (pH 5.3) and 4-nitrophenol at different concentrations, ranging from 490 µM to 50 µM (*vs*. SCE), v: 50 mV s^{-1}.

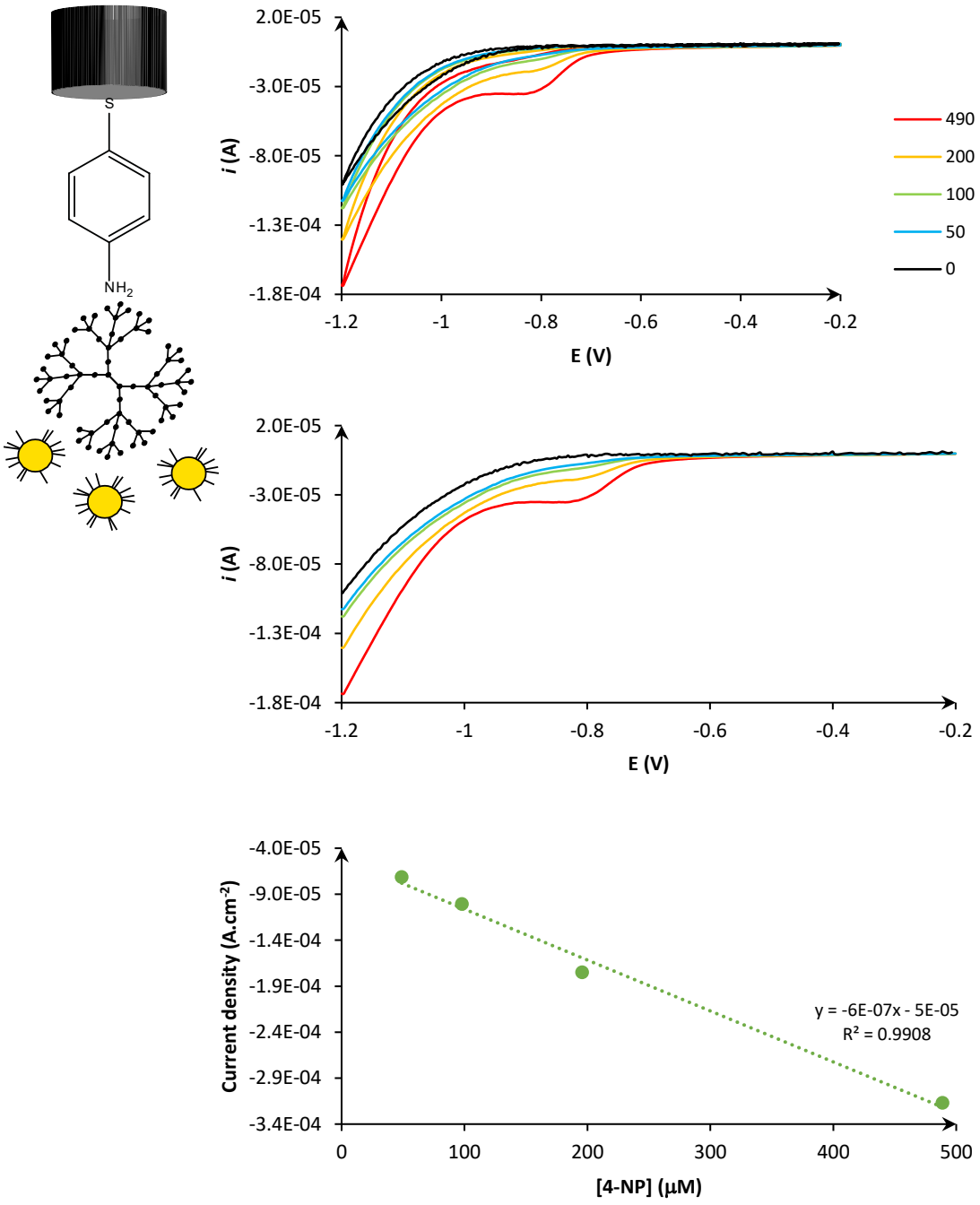

Figure 53. Cyclic voltammogram of glassy carbon electrode modified with ATP, PAMAM and citrate-stabilized gold nanoparticles in 0.05 M PBS (pH 5.3) and 4-nitrophenol at different concentrations, ranging from 490 µM to 50 µM (*vs*. SCE), v: 50 mV s^{-1}.

3.5.4 *Detection limits*

Detection limits of the tested electrodes are summarized in Table 12. Despite all modifications made to gold electrode, bare gold electrode had the lowest limit of detection towards 4-nitrophenol, 179 μM, while all other variations exhibited a higher limit of detection. Concerning the last self-assembled monolayer, no tendency was evident, thus, modification of gold electrode with PAMAM, citrate-stabilized gold nanoparticles and gold layer diminished the electrode surface sensibility towards the detection of 4-nitrophenol.

Detection limit calculations indicate an improvement in both PAMAM dendrimer, and 3-mercaptopropionic acid and mercaptopropionic sulfonic acid-modified glassy carbon electrode; as well as citrate-stabilized gold nanoparticles, and mercaptopropionic sulfonic acid and 4-aminothiophenol-modified vitreous carbon electrode. Overall, PAMAM dendrimer assembly onto thiol-modified glassy carbon translated to lower limits of detection, whereas gold layer-modified electrodes displayed the highest limits of detection, therefore constituting the less sensitive electrodes. Unchanged limit of detection further suggests an unsuccessful assembly of gold nanoparticles over PAMAM and mercaptopropionic sulfonic acid-modified vitreous carbon electrode. Generally, electrodes modified with gold layer were less sensitive than electrodes modified with citrate-stabilized gold nanoparticles, owing to the different underlying architecture. The surface area onto which citrate-stabilized gold nanoparticles are to assemble is larger than the surface area available for gold to be reduced onto, because G5 PAMAM dendrimers possess high surface area.

Table 12. 4-nitrophenol concentration range used for each electrode and estimated limit of detection (LOD).

Electrode	4-nitrophenol range (μM)	LOD (μM)
Au	600 – 12	179
Au-MPA-PAMAM	690 – 35	219
Au-MPS-PAMAM	1200 – 60	319
Au-ATP-PAMAM	575 – 60	296
Au-MPA-Au	1090 – 110	463
Au-MPS-Au	520 - 20	426
Au-ATP-Au	630 – 60	281
Au-MPA-PAMAM-AuNPs	520 – 50	186
Au-MPS-PAMAM-AuNPs	800 – 40	226
Au-ATP-PAMAM-AuNPs	490 – 50	298
GC	600 – 12	33
GC-MPA-PAMAM	690 – 35	17
GC-MPS-PAMAM	1200 – 60	22
GC-ATP-PAMAM	575 – 60	38
GC-MPA-Au	1090 – 110	68
GC-MPS-Au	520 – 20	74
GC-ATP-Au	630 – 60	81
GC-MPA-PAMAM-AuNPs	520 - 50	52
GC-MPS-PAMAM-AuNPs	800 – 40	20
Au-ATP-PAMAM-AuNPs	490 – 50	298
GC-ATP-PAMAM-AuNPs	490 - 50	29

3.5.5 *Scanning electron microscopy*

To replicate the surface of glassy carbon electrode, a portion of glassy carbon was polished in alumina slurries of 0.3 and 0.05 μm, with distilled water rinse in between, followed by sonication in distilled water; this treatment was made prior every modification made. Scanning electron microscopy images of bare, citrate-stabilized gold nanoparticles, PAMAM dendrimer and mercaptopropionic sulfonic acid, and citrate-stabilized gold nanoparticles, PAMAM dendrimer and 4-aminothiophenol-modified glassy carbon were obtained (Figure 54). The surface of the bare and modified glassy carbon is mostly flat and uniform, with minimal roughness.

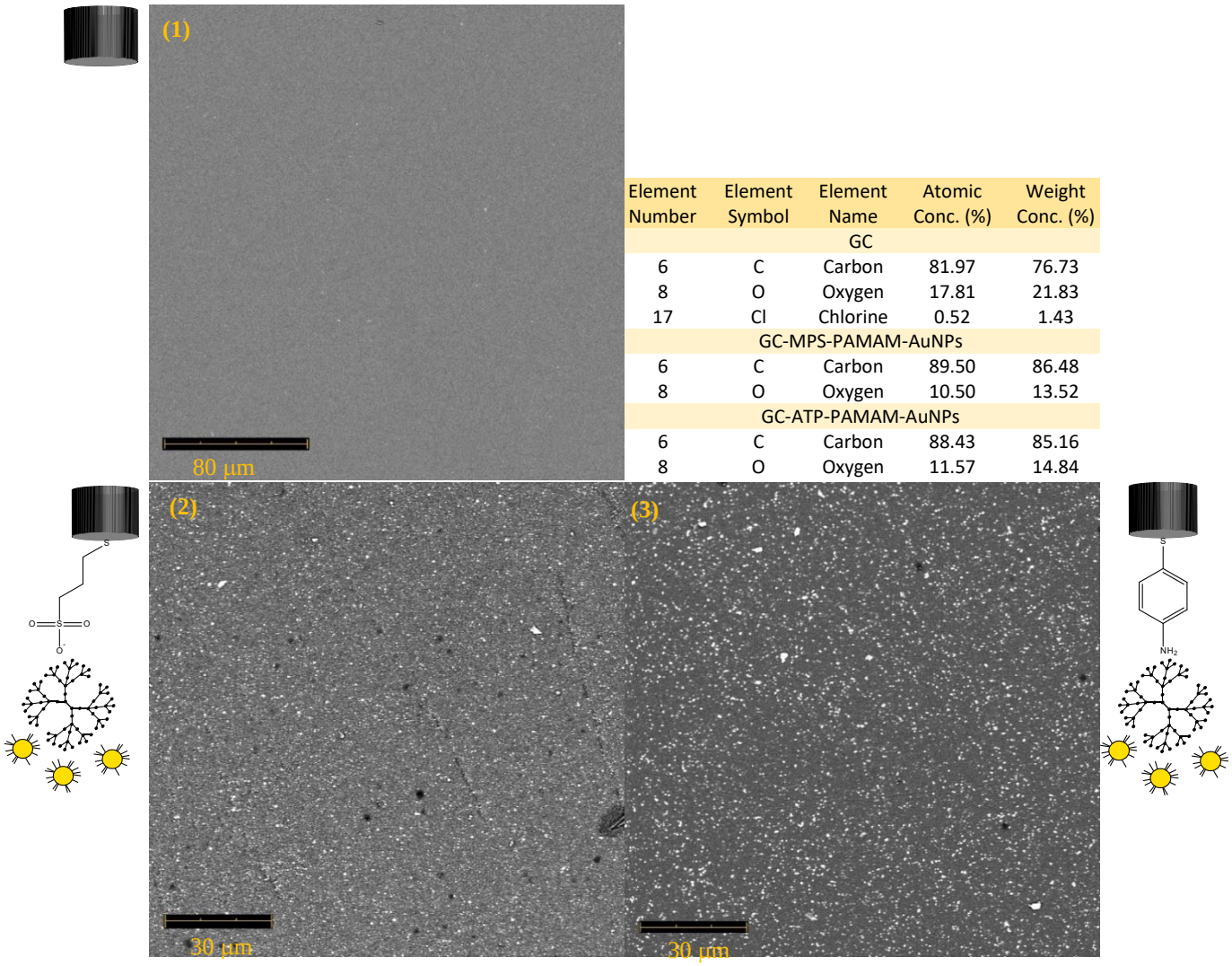

Element Number	Element Symbol	Element Name	Atomic Conc. (%)	Weight Conc. (%)
		GC		
6	C	Carbon	81.97	76.73
8	O	Oxygen	17.81	21.83
17	Cl	Chlorine	0.52	1.43
		GC-MPS-PAMAM-AuNPs		
6	C	Carbon	89.50	86.48
8	O	Oxygen	10.50	13.52
		GC-ATP-PAMAM-AuNPs		
6	C	Carbon	88.43	85.16
8	O	Oxygen	11.57	14.84

Figure 54. SEM images of (1) bare, (2) citrate-stabilized gold nanoparticles, PAMAM dendrimer and mercaptopropionic sulfonic acid-modified, and (3) citrate-stabilized gold nanoparticles, PAMAM dendrimer and 4-aminothiophenol-modified vitreous carbon electrodes; and corresponding elemental composition.

Surface elemental composition was mainly carbon, followed by oxygen, and trace amounts of chlorine were detected in bare vitreous surface. Once both modified electrodes were exposed to PAMAM dendrimers and gold nanoparticles, elements such as nitrogen and gold were expected; however, neither was detected. Electrochemical characterization indicated a successful modification of glassy carbon with 4-aminothiophenol, PAMAM dendrimer and citrate-stabilized gold nanoparticles. Nonetheless, nitrogen and gold are absent from the elemental analysis. EDX measurements are made with an acceleration voltage of 15 kV, which is powerful enough to deeply penetrate the sample and reach both nanoparticles and dendrimer. Bustos *et. al* modified a glassy carbon electrode with PAMAM-OH dendrimers, whose composition includes nitrogen, and nitrogen was equally undetected in EDX analysis.[80]

Modifications made throughout this project and resultant electrodes are resumed in Figure 55. Cyclic voltammetry and impedance spectroscopy studies indicate the presence of PAMAM dendrimers on all PAMAM-modified electrodes, while gold nanoparticle assembly appears to be successful over all electrodes apart from glassy carbon electrode previously modified with mercaptopropionic sulfonic acid and G5 PAMAM-NH_2 dendrimer.

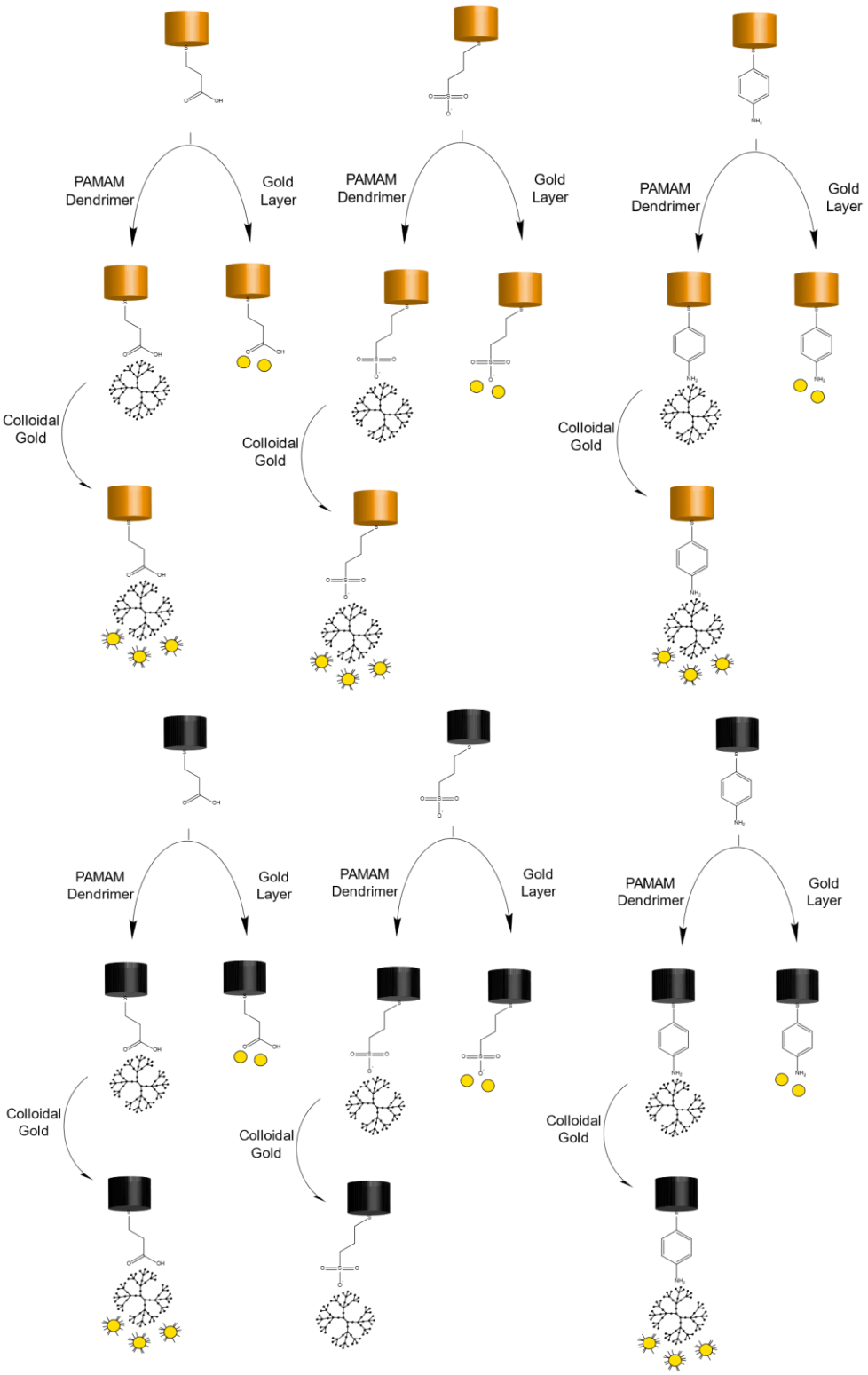

Figure 55. Modification steps and obtained electrodes, in accordance with the performed electrochemical characterization.

Chapter 4

4. Conclusions

In this work, we aim the consequent modification of electrodes with PAMAM dendrimers and gold nanoparticles through self-assembly at room temperature for sensing purposes. PAMAM dendrimers and gold nanoparticles are nanomaterials that have been explored for their innocuous and biocompatible properties, also, gold nanoparticles have conductive properties, which make them ideal for the building of electrochemical biosensors. This work focused on electrode modification with these two nanomaterials in the absence of the biological entity, therefore, an electrochemical sensor.

Gold and vitreous carbon electrodes were sequentially modified in a first phase. Modification assessment was made by cyclic voltammetry and impedance spectroscopy in a hexacyanoferrate (II)/(III) redox couple system. Cyclic voltammetry and impedance studies suggest that 3-mercaptopropionic acid, mercaptopropionic sulfonic acid, and 4-aminothiophenol self-assembled onto the electrodes surface, inducing different electrochemical properties, as probed by hexacyanoferrate (II)/(III) redox pair. G5 PAMAM-NH_2 dendrimer assembly over the thiol monolayers was successfully made at room temperature, translating to electrodes with similar electrochemical properties, independently of the monolayer it was assembled over. Overall, an increased electrocatalytic activity towards hexacyanoferrate (II) oxidation was observed on PAMAM-modified electrodes; in parallel with an element of stability offered by the modification with the dendrimer.

A gold layer of reduced gold was formed at low potentials over 3-mercaptopropionic acid, mercaptopropionic sulfonic acid, and 4-aminothiophenol-modified gold and glassy carbon electrodes. Electrochemical characterization suggests that a modification indeed took place, for electrochemical properties were distinct from the bare electrode and previous modifications. Citrate-stabilized gold nanoparticles were synthesized and used to further modify G5 PAMAM-NH_2 dendrimer-modified electrodes through self-assembly at room temperature. Cyclic voltammetry and impedance analysis suggest that colloidal gold assembled successfully over PAMAM and 3-mercaptopropionic acid, PAMAM and 4-aminothiophenol-modified gold and glassy carbon electrodes, in addition to PAMAM and mercaptopropionic sulfonic acid-modified gold electrode. However, both electrochemical characterization and SEM/EDX analysis imply that gold nanoparticles did not assemble onto PAMAM and mercaptopropionic sulfonic acid-modified vitreous carbon electrode.

The second phase consisted on the assessment of 4-nitrophenol reduction on the electrodes modified with G5 PAMAM-NH_2 dendrimers, gold layer and citrate-stabilized gold nanoparticles. Electrocatalytic activity of the modified electrodes towards 4-nitrophenol reduction was assessed in phosphate buffer solution (pH 5.3). Linear correlations were obtained in the majority of the measurements. Limits of detection of 33 and 179 mM

were calculated for bare glassy carbon and gold electrodes, which was altered with every modification. The highest decrease and therefore better catalytic activity towards 4-nitrophenol reduction was obtained with G5 PAMAM-NH_2 dendrimer and 3-mercaptopropionic acid-modified vitreous carbon electrode (detection limit of 17 μM). Apart from 4-aminothiophenol-based electrodes, vitreous carbon surface modification with PAMAM dendrimers resulted in improved detection of 4-nitrophenol. Regarding modification with gold, either gold layer or citrate-stabilized gold nanoparticles, with the exception of GC-MPS-PAMAM-AuNPs, cyclic voltammetry in hexacyanoferrate (II) and 4-nitrophenol infers all modifications were successful. G5 PAMAM-NH_2 dendrimer-modified electrodes were the most sensitive, as implied by smaller charge-transfer resistances and lower limits of detection.

In conclusion, PAMAM dendrimers and citrate-stabilized gold nanoparticles assemble at room temperature onto the substrates used, constituting a barrier between the substrate and the external environment, and changing the electrochemical properties of the whole substrate.

References

5. References

1. Ionic solids. https://goo.gl/wWxz48. (accessed February 12, 2019)
2. Hamann, Carl H.; Hamnett, Andrew; Vielstich, Wolf. *Electrochemistry*; Wiley: Weinheim, 1998.
3. Bagotsky, V. S. *Fundamentals of Electrochemistry;* Wiley-Interscience: Hoboken, N.J., 2005.
4. Brett, Christopher M. A.; Brett, Ana M. O. *Electrochemistry: Principles, Methods, and Applications*; Oxford University Press: New York, USA, 1993.
5. Wang, Joseph. *Analytical electrochemistry*; Wiley-VCH: New York, 2000.
6. Sawyer, Donald T.; Sobkowiak, Andrzej; Roberts, Julian L. *Electrochemistry for chemists*; Wiley, 1995.
7. Brownson, Dale A. C; Kampouris, Dimitrios K.; Banks, Craig E. Graphene electrochemistry: fundamental concepts through to prominent applications. *Chem. Soc. Rev.* **2012**, *41*, 6944-6976.
8. Lvovich, Vadim F. *Impedance spectroscopy – Applications to Electrochemical and Dielectric Phenomena*; Wiley, 2012.
9. Brosel-Oliu, Sergi; Uria, Naroa; Abramova, Natalia; Bratov, Andrey. Impedimetric Sensors for Bacteria Detection. In *Biosensors - Micro and Nanoscale Applications*; Rinken, Toonika, Ed.; 2015; 257-288.
10. Mendes, Renata K.; Freire, Renato S.; Fonseca, Carla P.; Neves, Silmara; Kubota, Lauro T. Characterization of self-assembled thiols monolayers on gold surface by electrochemical impedance spectroscopy. *J. Braz. Chem. Soc.*, **2004**, *15*, 849-855.
11. Stradiotto, Nelson R.; Yamanaka, Hideko; Zanoni, Maria Valnice B. Electrochemical sensors: A powerful tool in analytical chemistry. *J. Braz. Chem. Soc.*, **2003**, *14*, 159-173.
12. Shaw, Lynsey; Dennany, Lynn. Applications of electrochemical sensors: Forensic drug analysis. *Curr. Opin. Electrochem.* **2017**, *3*, 23-28.
13. Privett, Benjamin J.; Shin, Jae Ho; Schoenfisch, Mark H. Electrochemical Sensors. *Anal. Chem.,* **2008**, *80,* 4499-4517.
14. Yin, Tanji; Qin, Wei. Applications of nanomaterials in potentiometric sensors. *Trends Anal. Chem.*, **2013**, *51*, 79-86.
15. Gopalan, Anantha Iyengar; Lee, Kwang-Pill; Manesh, Kalayil Manian; Santhosh, Padmanabhan; Kim, Jun Heon; Kang, Jae Soo. Electrochemical determination of dopamine and ascorbic acid at a novel gold nanoparticles distributed poly(4-aminothiophenol) modified electrode. *Talanta*. **2007**, *71*, 1774-1781.
16. Cheng, Hui-Wen; Thiagarajan, Soundappan; Chen, Shen-Ming. Fabrication of self adsorbed 3-mercapto-1-propane sulfonic acid- Nano Ag particles modified electrode and electroanalytical applications. *Int. J. Electrochem. Sci.* **2011**, *6*, 4150-4163.
17. Arévalo, Fernando Javier; Osuna-Sánchez, Yolanda; Sandoval-Cortés, José; Tocco, Aylen Di; Granero, Adrián Marcelo; Robledo, Sebastián Noel; Zon, María Alicia; Vettorazzi, Nelio Roberto; Martinéz, José Luis; Segura, Elda PAtricia; Iliná, Anna; Fernández, Héctor. Development of an electrochemical sensor for the determination of

glycerol based on glassy carbon electrodes modified with a copper oxide nanoparticles/multiwalled carbon nanotubes/pectin composite. *Sens. Actuators, B*. **2017**, *244*, 949-957.

18. Jaffrezic-Renault, Nicole; Dzyadevych, Sergei V. Conductometric Microbiosensors for Environmental Monitoring. *Sensors.* **2008**, *8*, 2569-2588.
19. Braiek, Mohamed; Djebbi, Mohamed Amine; Chateaux, Jean-François. A conductometric sensor for potassium detection in whole blood. *Sens. Actuators, B.* **2016**, *235*, 27-32.
20. Panzarini, Elisa; Inguscio, Valentina; Tenzzo, Bernardetta Anna; Carata, Elisabetta; Dini Luciana. Nanomaterials and Autophagy: New Insights in Cancer Treatment. *Cancers*, **2013**, *5*, 296-319.
21. Nanomaterials. http://ec.europa.eu/environment/chemicals/nanotech/index_en.htm (Accessed April 20, 2017)
22. Eustis, Susie; El-Sayed, Mostafa A. Why gold nanoparticles are more precious than pretty gold: Noble metal surface plasmon resonance and its enhancement of the radiative and nonradiative properties of nanocrystals of different shapes. *Chem. Soc. Rev.*, **2006**, *35*, 209-217.
23. Peters, Ruud J. B.; Bouwmeester, Hans; Gottardo, Stefania; Amenta, Valeria; Arena, Maria; Brandhoff, Puck; Marvin, Hans J. P.; Mech, Agnieszka; Moniz, Filipa Botelho; Pesudo, Laia Quiros; Rauscher, Hubert; Schoonjans, Reinhilde; Undas, Anna K.; Vettori, Maria Vittoria; Weigel, Stefan; Aschberger, Karin. Nanomaterials for products and application in agriculture, feed and food. *Trends Food Sci. Technol.* **2016**, *54*, 155-164.
24. Liu, Nian; Li, Weiyang; Pasta, Mauro; Cui, Yi. Nanomaterials for electrochemical energy storage. *Front. Phys.* **2014**, *9*, 323-350.
25. Salata, O. V. Applications of nanoparticles in biology and medicine. *J. Nanobiotechnol.* **2004**, *2*.
26. Edmundson, Matthew C.; Capeness, Michael; Horsfall, Louise. Exploring the potential of metallic nanoparticles within synthetic biology. *New Biotechnol.*, **2014**, *31*, 572-578.
27. Das, Minakshi; Shim, Kyu Hwan; An, Seong Soo A.; Yi, Dong Kee. Review on gold nanoparticles and their applications. *Toxicol. Environ. Health. Sci.*, **2011**, *3*, 193-205.
28. Algar, W. Russ; Tavares, Anthony J.; Krull, Ulrich J. Beyond labels: A review of the application of quantum dots as integrated components of assays, bioprobes, and biosensors utilizing optical transduction. *Anal. Chim. Acta*, **2010**, *673*, 1-25.
29. Kagan, Cherie R.; Murray, Christopher B. Charge transport in strongly coupled quantum dot solids. *Nat. Nanotechnol.*, **2015**, *10*, 1013-1026.
30. Nasir, Amara; Kausar, Ayesha; Younus, Ayesha. A Review on Preparation, Properties and Applications of Polymeric Nanoparticle-Based Materials. *Polym.-Plast. Technol. Eng.*, **2015**, *54*, 325-341.
31. Mody, Vicky V.; Siwale, Rodney; Singh, Ajay; Mody, Hardik R. Introduction to metallic nanoparticles. *J. Pharm Bioallied Sci.* **2010**, *2*, 282-289.
32. Tiwari, Jitendra N.; Tiwari, Rajanish N.; Kim, Kwang S. Zero-dimensional, one.dimensional, two-dimensional and three-dimensional nanostructured materials for advanced electrochemical energy devices. *Prog. Mater. Sci.*, **2012**, *57*, 724-803.

33. Chen, Ying; Li, Chi Pui; Chen, Hua; Chen, Yongjun. One-dimensional nanomaterials synthesized using high-energy ball milling and annealing process. *Sci. Technol. Adv. Mater.*, **2006**, *7*, 839-846.
34. Wang, Xudong; Li, Zhaodng; Shi, Jian; Yu, Yanhao. One-Dimensional Titanium Dioxide Nanomaterials: Nanowires, Nanorods, and Nanobelts. *Chem. Rev.* **2014**, *114*, 9346-3954.
35. Love, J. Christopher; Estroff, Lara A.; Kriebel, Jennah K.; Nuzzo, Ralph G.; Whitesides, George M. Self-Assembled Monolayers of Thiolates on Metals as a Form of Nanotechnology. *Chem. Rev.*, **2005**, *105,* 1103-1169.
36. Sumi, Takayoshi; Uosaki, Kohei. Electrochemical Oxidative Formation and Reductive desorption of a Self-Assembled Monoayer of Decanethiol on a Au(111) Surface in KOH Ethanol Solution. *J. Phys. Chem.* **2004**, *108*, 6422-6428.
37. Brett, Christopher M. A.; Kresak, Slavoj; Hianik, Tibor; Brett, Ana Maria Oliveira. Studies on Self-Assembled Alkanethiol Monolayers Formed at Applied Potential on Polycrystalline Gold Electrodes. *Electroanalysis*, **2003**, *15*, 557-565.
38. Bahadir, Elif Burcu; Sezgintürk, Mustafa Kemal. Poly(amidoamine) (PAMAM): An emerging material for electrochemical bio(sensing) applications. *Talanta*, **2016**, *148*, 427-438.
39. Mignani, Serge; Rodrigues, João; Tomás, Helena; Roy, René; Shi, Xiangyang; Majoral, Jean-Pierre. Bench-to-bedside translation of dendrimers: Reality or utopia? A concise analysis. *Adv. Drug Delivery Rev.* **2018**, *136-137*, 73-81.
40. Mignani, Serge; Rodrigues, João; Tomás, Helena; Zablocka, Maria; Shi, Xiangyang; Caminade, Anne-Marie; Majoral, Jean-Pierre. Dendrimers in combination with natural products and analogues as anti-cancer agents. *Chem. Soc. Rev.* **2018**, *47*, 514-532.
41. Mignani, Serge; Rodrigues, João; Tomás, Helena; Caminade, Anne-Marie; Laurent, Régis; Shi, Xiangyang; Majoral, Jean-Pierre. Recent therapeutic applications of the theranostic principle with dendrimers in oncology. *Sci. China Mater.* **2018**, *61*, 1367-1386.
42. Xie, Jingjing; Wang, Jichuang; Chen, Hongning; Shen, Weiyu; Sinko, Patrick J.; Dong, Haiyan; Zhao, Ronghi; Lu, Yusheng; Zhu, Yewei; Jia, Lee. Multivalent Conjugation of Antibody to Dendrimers for the Enhanced Capture and Regulation on Colon Cancer Cells. *Sci. Rep.* **2015**, *5*, 1-10.
43. Astruc, Didier; Boisselier, Elodie; Ornelas, Cátia. Dendrimers Designed for Functions: From Physical, Photophysical, and Supramolecular Properties to Applications in Sensing, Catalysis, Molecular Electronics, Photonics, and Nanomedicine. *Chem. Rev.* **2010**, *110*, 1857-1959.
44. PAMAM Dendrimers. http://www.dendritech.com/pamam.html. (accessed February 5, 2019)
45. Faraday, Michael. The Bakerian lecture – Experimental relations of gold (and other metals) to light. *Philos. Trans. R. Soc. London.* **1857**, *147*.
46. Tweney, Ryan. Discovering Discovery: How Faraday Found the First Metallic Colloid. *Perspectives on Science*. **2006**, *14*, 97-121.
47. Aqueous Gold Spheres. https://nanocomposix.eu/collections/gold-spheres. (accessed January 30, 2019)

48. 100 nm Standard Gold Nanoparticles. http://www.cytodiagnostics.com/store/pc/100nm-Standard-Gold-Nanoparticles-100ml-p1027.htm. (accessed January 30, 2019)
49. Standard Gold Nanoparticles. http://www.cytodiagnostics.com/store/pc/Standard-Gold-Nanoparticles-c140.htm, (accessed January 30, 2019)
50. Ojea-Jiménez, Isaac; Campanera, Josp M. Molecular Modeling of the Reduction Mechanis, in the Citrate-Mediated Synthesis of Gold Nanoparticles. *J. Phys. Chem.* **2012**, *116*, 23682-23691.
51. Cao, Xiaodong; Ye, Yongkang; Liu, Songqin. Gold nanoparticle-based signal amplification for biosensing. *Anal. Biochem.* **2011**, *417*, 1-16.
52. Plasmonic & Surface Plasmon Resonance. https://nanohybrids.net/pages/plasmonics. (Accessed December 13, 2017)
53. Karadag, Murat; Geyik, Caner; Demirkol, Dilek Odaci; Ertas, F. Nil; Timur, Suna. Modified gold surfaces by 6-(ferrocenyl)hexanethiol/dendrimer/gold nanoparticles as a platform for the mediated biosensing applications. *Mater. Sci. Eng.* **2013**, *33*, 634-640.
54. Luo, Xiliang; Morrin, Aoife; Killard, Anthony J.; Smyth, Malcolm R. Application of Nanoparticles in Electrochemical Sensors and Biosensors. *Electroanalysis*. **2006**, *18*, 319-326.
55. Tang, Ying-Yao; Chen, Po-Yu. Gold Nanoparticle-electrodeposited Electrodes Used for p-Nitrophenol Detection in Acidic Media: Effect of Electrodeposition Parameters on Particle Density, Size distribution, and Electrode Performance. *J. Chin. Chem. Soc.* **2011**, *58*, 723-731.
56. Maduraiveeran, Govindhan; Jin, Wei. Nanomaterials based electrochemical sensor and biosensor platforms for environmental applications. *Trends Environ. Anal. Chem.* **2017**, *13*, 10-23.
57. Pingarrón, José M.; Yáñez-Sedeño, Paloma; González-Cortés, Araceli. Gold nanoparticle-based electrochemical biosensors. *Electrochim. Acta.* **2008**, *53*, 5848-5866.
58. Akella, Sridevi; Mitra, Chanchal K. Electrochemical studies of glucose oxidase immobilized on glutathione coated gold nanoparticles. *Indian J. Biochem. Biophys.* **2007**, *44*, 82-87.
59. Crespilho, Frank N.; Ghica, M. Emilia; Florescu, Monica; Nart, Francisco C.; Oliveira Jr., Osvaldo N.; Brett, Christopher M.A. A strategy for enzyme immobilization on layer-by-layer dendrimer-gold nanoparticle electrocatalytic membrane incorporating redox mediator. *Electrochem. Commun.* **2006**, *8*, 1665-1670.
60. Liu, Guozhen; Luais, Erwann; Gooding, J. Justin. The Fabrication of Stable Gold Nanoparticle-Modified Interfaces for Electrochemistry. *Langmuir*. **2011**, *27*, 4176-4183.
61. Li, Nian Bing; Kwak, Juhyoun. A Penicillamine Biosensor Based in Tyrosinase Immobilized on Nano-Au/PAMAM Dendrimer Modified Gold Electrode. *Electroanalysis*. **2007**, *19*, 2428-2436.
62. Médard, Christelle; Morin, Mario. Chemisorption of aromatic thiols onto glassy carbon surface. *J. Electroanal. Chem.* **2009**, *632*, 120-126.

63. Segura, Rodrigo; Pizarro, Jaime; Díaz, Karina; Placencio, Alan; Godoy, Fernando. Development of electrochemical sensors for the determination of selenium using gold nanoparticles modified electrodes. *Sens. Actuators, B.* **2015**, *220*, 263-269.
64. Benvidi, Ali; Dehghani-Firouzabadi, Afsaneh; Mazloum-Ardakani, Mohammad; Mirjalili, Bi-Bi Fatemeh; Zare, Reza. Electrochemical deposition of gold nanoparticles on reduced graphene oxide modified glassy carbon electrode for simultaneous determination of levodopa, uric acid and folic acid. *J. Electroanal. Chem.* **2015**, *736*, 22-29.
65. McFarland, Adam D.; Haynes, Christy L.; Mirkin, Chad A.; Duyne, Richard P. Van; Godwyn, Hilary A. Color My Nanoworld. *J. Chem. Educ.* **2004**, *81*, 544.
66. Umesh, Narasimha Murthy; Chen, Tse-Wei; Chen, Shen-Ming; Rani, Karuppasamy Kohila; Devasenathipathy, Rajkumar; Wang, Sea-Fue. Phosphate-mediated Silver Nanodentrites Modified Glassy Carbon Electrode for the Determination of Nitrophenol. *Int. J. Electrochem. Sci.* **2018**, *13*, 4946-4955.
67. Moldenhauer, Jonathan; Meier, Madeline; Paul, David W. Rapid and Direct Determination Coefficients Using Microelectrode Arrays. *J. Electrochem. Soc.*, **2016**, *163*, 672-678.
68. Bürgi, Thomas. Properties of gold-sulphur interface: from self-assembled monolayers to clusters. *Nanoscale*, **2015**, *7*, 15553-15567.
69. Cannes, Céline; Kanouf, Frédéric; Bard, Allen J. Cyclic Voltammetric and Scanning Electrochemical Microscopic Study of Menadione Permeability through a Self-Assembled Monolayer on a Gold Electrode. *Langmuir*, **2002**, *18*, 8134-8141.
70. Jiang, Cuijie; Elliott, Joanne M.; Cardin, David J.; Tsang, Shik Chi. An Electrochemical Study of 4-Aminothiophenol/Pt Nanoparticle Multilayers on Gold Electrodes. *Langmuir*, **2008**, *25*, 534-541.
71. Parida, Kulamani; Das, Dipti Prakasini. Photo-oxidation of 4-nitrophenol in aqueous suspensions, catalysed by titania intercalated zirconium phosphate (ZrP) and titanium phosphate (TiP). *J. Photochem. Photobiol., A.* **2004**, *163*, 561-567.
72. Lu, Wenbo; Ning, Rui; Qin, Xiaoyun; Zhang, Yingwei; Chang, Guohui; Liu, Sen; Luo, Yonglan; Sun, Xuping. Synthesis of Au nanoparticles decorated graphene oxide nanosheets: Nanocovalent functionalization by TWEEN 20 in situ reduction of aqueous chloroaurate ions for hydrazine detection and catalytic reduction of 4-nitrophenol. *J. Hazard. Mater.* **2011**, *197*, 320-326.
73. Ragu, Sasikumar; Chen, Shen-Ming; Ranganathan, Palraj; Rwei, Syang-Peng. Fabrication of a Novel Nickel-Curcumin/Graphene Oxide Nanocomposites for Superior Electrocatalytic Activity toward the Detection of Toxic p-nitrophenol. *Int. J. Elecrochem. Sci.* **2016**, *11*, 9133-9144.
74. Wang, Pengshu; Xiao, Jiayang; Guo, Manman; Xia, Yue; Li, Zelin; Jiang, Xiaochun; Huang, Wei. Voltammetric Determination of 4-Nitrophenol at Graphite Nanoflakes Modified Glassy Carbon Electrode. *J. Electrochem. Soc.* **2015**, *162*, 72-78.

75. Cheng, Yongqiang; Li, Yaohua; Li, Dan; Zhang, Bo; Hao, Runfang; Sang, Shengbo. A Sensor for Detection of 4-nitrophenol Based on a Glassy Carbon Electrode Modified with a Reduced Graphene Oxide/Fe_3O_4 Nanoparticle Composite. *Int. J. Electrochem. Sci.* **2017**, *12*, 7754-7764.
76. Liu, Zhaona; Du, Junguo; Qiu, Cuicui; Huang, Lihui; Ma, Houyi; Shen, Dazhong; Ding, Yi. Electrochemical sensor for detection of p-nitrophenol based on nanoporous gold. *Electrochem. Commun.* **2009**, *11*, 1365-1368.
77. Kim, Jongwon; Gewirth, Andrew A. Mechanism of Oxygen Electroreduction on Gold Surfaces in Basic Media. *J. Phys. Chem. B.* **2006**, *110*, 2565-2571.
78. Li, Xiao; Gewirth, Andrew A. Oxygen Electroreduction through a Superoxide Intermediate on Bi-Modified Au Surfaces. *J. Am. Chem. Soc.* **2005**, *127*, 5252-5260.
79. Shrivastava, Alankar; Gupta, Vipin B. Methods of the determination of limit of detection and limit of quantification of the analytical methods. *Chron. Young Sci.* **2011**, *2*, 21-25.
80. Bustos, Erika Bustos; Jiménez, Ma. Guadalupe García; Díaz-Sánchez, Blanca R.; Juaristi, Eusebio; Chapman, Thomas W.; Godínez, Luis A. Glassy carbon electrodes modified with composites of starbust-PAMAM dendrimers containing metal nanoparticles for amperometric detection of dopamine in urine. *Talanta*, **2007**, *72*, 1586-1592.

Appendix

Impedance data

Charge-transfer resistance values were obtained through the analysis of the semicircle obtained at high frequencies depicted in the Nyquist plot. The software gave the best fit to the data, circle diameter and center coordinates were retrieved and R_{CT} was estimated through the following process. A circumference of center (a,b) is represented by the equation:

$$(x-a)^2 + (y-b)^2 = r^2$$

$$x^2 + y^2 - 2ax - 2by + a^2 + b^2 - r^2 = 0$$

To know the two points at which the circumference intersects with the x axis (y=0):

$$x^2 - 2ax + a^2 + b^2 - r^2 = 0$$

Equation roots were calculated, and the difference represents the charge-transfer resistance associated to the electrode itself ($x_1 < x_2$, $x_2 - x_1 = R_{CT}$).

Phosphate buffer solution preparation

Phosphate buffer solutions were prepared with KH_2PO_4 and K_2HPO_4, whose concentrations were estimated through the Henderson-Hasselbalch equation:

$$pH = pKa + \log\frac{[Base]}{[Acid]}$$

Respecting a molarity of 0.05 M, the calculations took the acidic constant of the chosen acid-base pair to be 6.23×10^{-8}, translating to a pKa value of 7.21. Lastly, the pH was adjusted to the desired value.

Characterization of modified electrodes

Organized by the thiol monolayer over which the successive modifications were made, Figures 56-61 depict cyclic voltammograms and impedance results of modified electrodes obtained throughout this project. Tables 13-18 reunite information regarding current and potentials of anodic and cathodic peaks, half-wave potentials and charge-transfer resistance, for every modified electrode. Figure 62 shows the cyclic voltammogram of GC-MPS-PAMAM and GC-MPS-PAMAM-AuNPs in PBS and 4-nitrophenolat different concentrations, both electrodes behave similarly.

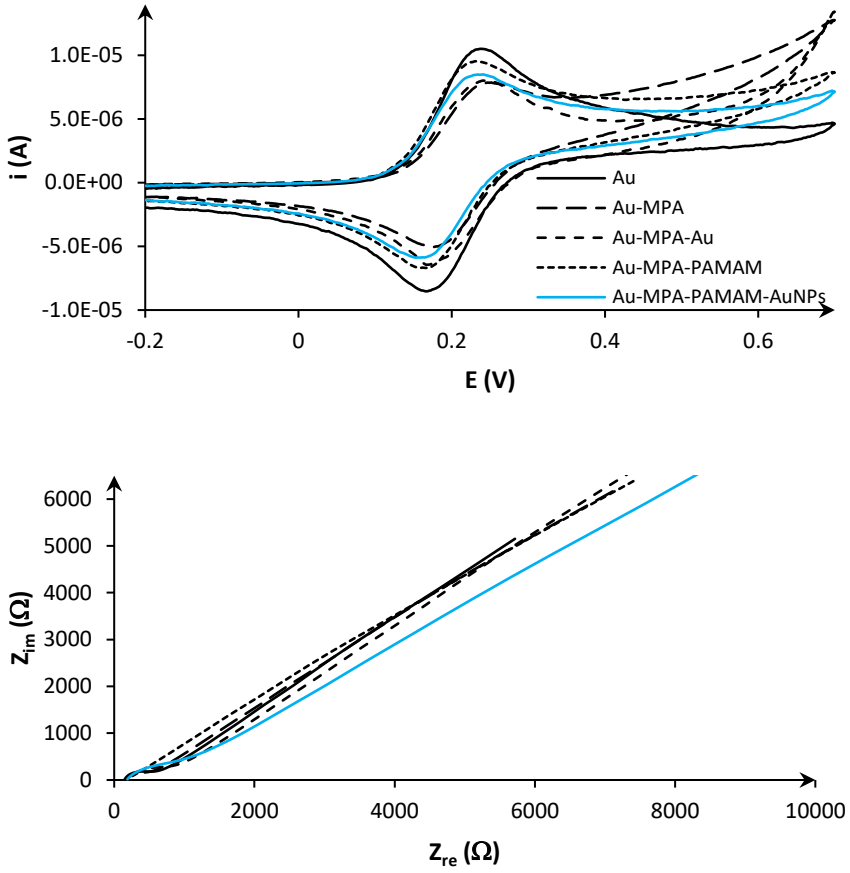

Figure 56. Cyclic voltammogram of gold electrode in 5mM hexacyanoferrate (II) and 0.2 M potassium chloride aqueous solution (*vs*. SCE), v: 50 mV s^{-1}. Complex impedance plot of the gold electrode in equimolar 2.5 mM solution of hexacyanoferrate (II) and (III) in 0.2 M potassium chloride (*vs*. Pt). The frequency range is 2×10^5 – 0.1 Hz, AC amplitude of 10 mV rms. Modification with MPA.

Table 13. Current and potentials of anodic and cathodic peaks, half-wave potentials and charge-transfer resistance. v: 50 mV s^{-1}. Values are mean ± SD. Modification with MPA.

	Electrode				
	Au	**Au-MPA**	**Au-MPA-Au**	**Au-MPA-PAMAM**	**Au-MPA-PAMAM-AuNPs**
E^A (mV)	239.2 ± 2.6	252.5 ± 1.4	245.8 ± 3.1	231.6 ± 1.8	233.2 ± 2.2
i^A (μA)	10.3 ± 0.1	7.9 ± 0.2	7.7 ± 0.1	9.6 ± 0.3	8.4 ± 0.2
E^C (mV)	170.2 ± 2.2	176.6 ± 0.7	168.4 ± 0.8	166.5 ± 2.2	162.4 ± 3.1
i^C (μA)	-9.4 ± 0.1	-4.9 ± 0.1	-6.1 ± 0.3	-7.5 ± 0.2	-7.0 ± 0.1
$E_{1/2}$ (mV)	204.7 ± 2.2	214.5 ± 0.7	207.1 ± 1.1	199.1 ± 1.1	197.8 ± 1.9
R_{CT} (ohms)	557.1 ± 48.2	507.6 ± 39.3	836.2 ± 52.9	82.1 ± 6.3	1333.6 ± 53.3

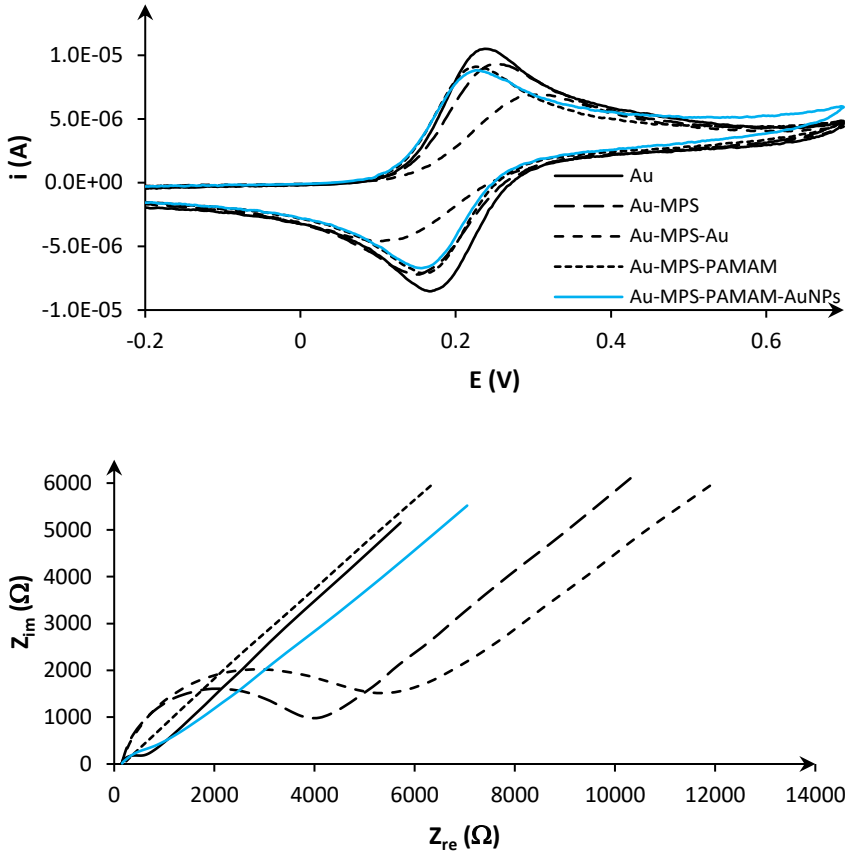

Figure 57. Cyclic voltammogram of gold electrode in 5mM hexacyanoferrate (II) and 0.2 M potassium chloride aqueous solution (*vs*. SCE), v: 50 mV s^{-1}. Complex impedance plot of the gold electrode in equimolar 2.5 mM solution of hexacyanoferrate (II) and (III) in 0.2 M potassium chloride (*vs*. Pt). The frequency range is 2×10^5 – 0.1 Hz, AC amplitude of 10 mV rms. Modification with MPS.

Table 14. Current and potentials of anodic and cathodic peaks, half-wave potentials and charge-transfer resistance. v: 50 mV s^{-1}. Values are mean ± SD. Modification with MPS.

	Electrode				
	Au	**Au-MPS**	**Au-MPS-Au**	**Au-MPS-PAMAM**	**Au-MPS-PAMAM-AuNPs**
E^A (mV)	239.2 ± 2.6	252.4 ± 1.7	308.0 ± 5.6	226.6 ± 1.3	227.5 ± 1.7
i^A (μA)	10.3 ± 0.1	9.3 ± 0.0	6.7 ± 0.1	9.0 ± 0.1	8.9 ± 0.3
E^C (mV)	170.2 ± 2.2	154.6 ± 1.5	106.5 ± 2.0	160.9 ± 2.0	158.2 ± 2.9
i^C (μA)	-9.4 ± 0.1	-8.4 ± 0.1	-4.7 ± 0.1	-8.3 ± 0.1	-7.8 ± 0.2
$E_{1/2}$ (mV)	204.7 ± 2.2	203.5 ± 1.1	207.3 ± 2.0	193.8 ± 1.0	192.9 ± 1.7
R_{CT} (ohms)	557.1 ± 48.2	3856.5 ± 36.6	5313.3 ± 371.5	86.3 ± 8.0	1214.6 ± 80.5

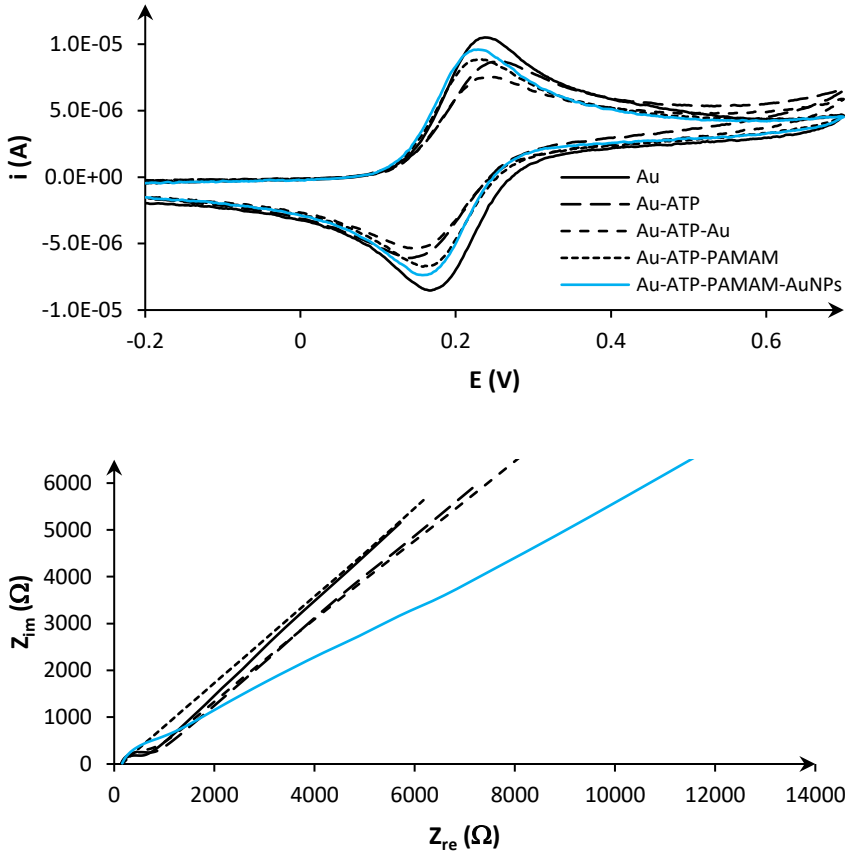

Figure 58. Cyclic voltammogram of gold electrode in 5mM hexacyanoferrate (II) and 0.2 M potassium chloride aqueous solution (*vs*. SCE), v: 50 mV s^{-1}. Complex impedance plot of the gold electrode in equimolar 2.5 mM solution of hexacyanoferrate (II) and (III) in 0.2 M potassium chloride (*vs*. Pt). The frequency range is 2×10^5 – 0.1 Hz, AC amplitude of 10 mV rms. Modification with ATP.

Table 15. Current and potentials of anodic and cathodic peaks, half-wave potentials and charge-transfer resistance. v: 50 mV s^{-1}. Values are mean ± SD. Modification with ATP.

	Electrode				
	Au	**Au-ATP**	**Au-ATP-Au**	**Au-ATP-PAMAM**	**Au-ATP-PAMAM-AuNPs**
E^A (mV)	239.2 ± 2.6	250.7 ± 4.2	237.0 ± 6.6	229.1 ± 2.7	228.1 ± 0.7
i^A (μA)	10.3 ± 0.1	8.9 ± 0.3	7.9 ± 0.4	8.9 ± 0.2	9.5 ± 0.0
E^C (mV)	170.2 ± 2.2	147.8 ± 4.2	153.2 ± 4.3	161.5 ± 2.6	159.3 ±1.8
i^C (μA)	-9.4 ± 0.1	-7.7 ± 0.2	-6.6 ± 0.2	-7.8 ± 0.2	-9.1 ± 0.1
$E_{1/2}$ (mV)	204.7 ± 2.2	199.3 ± 1.9	195.1 ± 3.6	195.3 ± 1.3	193.7 ± 1.2
R_{CT} (ohms)	557.1 ± 48.2	696.6 ± 42.0	982.8 ± 27.1	58.2 ± 2.3	1548.5 ± 78.9

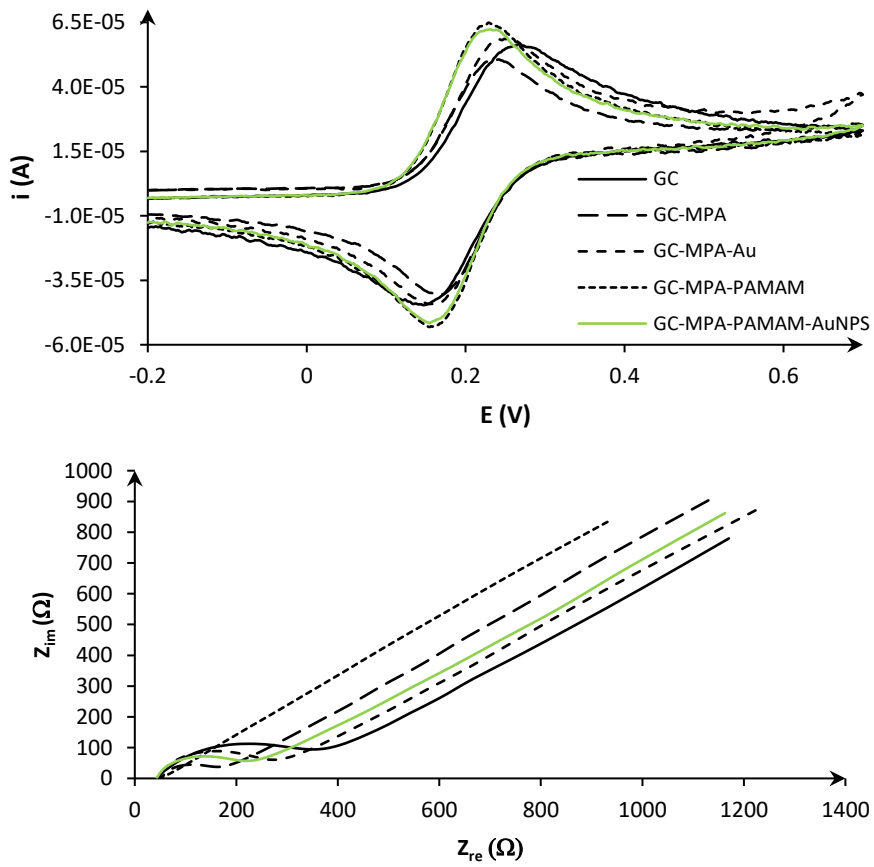

Figure 59. Cyclic voltammogram of vitreous carbon electrode in 5mM hexacyanoferrate (II) and 0.2 M potassium chloride aqueous solution (*vs*. SCE), v: 50 mV s^{-1}. Complex impedance plot of the gold electrode in equimolar 2.5 mM solution of hexacyanoferrate (II) and (III) in 0.2 M potassium chloride (*vs*. Pt). The frequency range is 2×10^5 – 0.1 Hz, AC amplitude of 10 mV rms. Modification with MPA.

Table 16. Current and potentials of anodic and cathodic peaks, half-wave potentials and charge-transfer resistance. v: 50 mV s^{-1}. Values are mean ± SD. Modification with MPA.

	Electrode				
	GC	**GC-MPA**	**GC-MPA-Au**	**GC-MPA-PAMAM**	**GC-MPA-PAMAM-AuNPs**
E^A (mV)	260.8 ± 3.9	240.6 ± 1.5	248.2 ± 1.3	230.2 ± 2.2	230.7 ± 1.5
i^A (μA)	57.5 ± 0.5	56.0 ± 4.7	58.0 ± 2.4	65.2 ± 0.8	63.0 ± 0.4
E^C (mV)	148.0 ± 0.8	166.3 ± 2.7	158.2 ± 3.4	158.7 ± 3.2	154.6 ± 4.6
i^C (μA)	-53.0 ± 1.1	-54.8 ± 3.3	-54.5 ± 1.7	-62.6 ± 1.0	-60.3 ± 1.3
$E_{1/2}$ (mV)	204.4 ± 1.9	203.4 ± 1.7	203.2 ± 1.6	194.4 ± 2.3	192.6 ± 2.6
R_{CT} (ohms)	378.2 ± 1.2	120.1 ± 5.7	259.7 ± 15.7	17.7 ± 1.0	178.8 ± 13.1

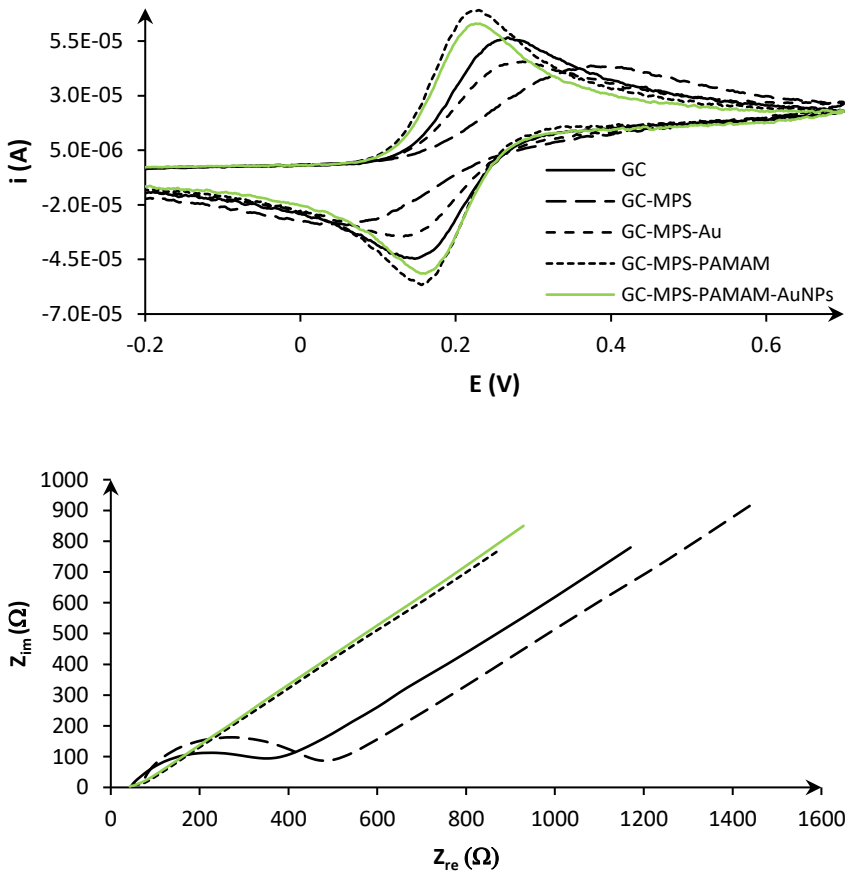

Figure 60. Cyclic voltammogram of vitreous carbon electrode in 5mM hexacyanoferrate (II) and 0.2 M potassium chloride aqueous solution (*vs*. SCE), v: 50 mV s^{-1}. Complex impedance plot of the gold electrode in equimolar 2.5 mM solution of hexacyanoferrate (II) and (III) in 0.2 M potassium chloride (*vs*. Pt). The frequency range is 2×10^5 – 0.1 Hz, AC amplitude of 10 mV rms. Modification with MPS.

Table 17. Current and potentials of anodic and cathodic peaks, half-wave potentials and charge-transfer resistance. v: 50 mV s^{-1}. Values are mean ± SD. Modification with MPS.

	Electrode				
	GC	**GC-MPS**	**GC-MPS-AuNPs**	**GC-MPS-PAMAM**	**GC-MPS-PAMAM-AuNPs**
E^A (mV)	260.8 ± 3.9	377.8 ± 3.6	282.8 ± 4.1	224.8 ± 3.9	229.5 ± 2.2
i^A (μA)	57.5 ± 0.5	41.8 ± 0.1	44.5 ± 0.8	70.0 ± 0.2	63.0 ± 1.4
E^C (mV)	148.0 ± 0.8	56.6 ± 2.7	132.6 ± 3.5	154.6 ± 2.5	159.7 ± 3.3
i^C (μA)	-53.0 ± 1.1	-27.1 ± 0.2	-36.0 ± 0.9	-64.9 ± 1.9	-59.8 ± 0.6
$E_{1/2}$ (mV)	204.4 ± 1.9	217.2 ± 0.4	207.7 ± 3.2	189.7 ± 2.6	194.6 ± 2.2
R_{CT} (ohms)	378.2 ± 1.2	399.3 ± 24.8	753.9 ± 9.3	20.4 ± 2.1	18.7 ± 1.2

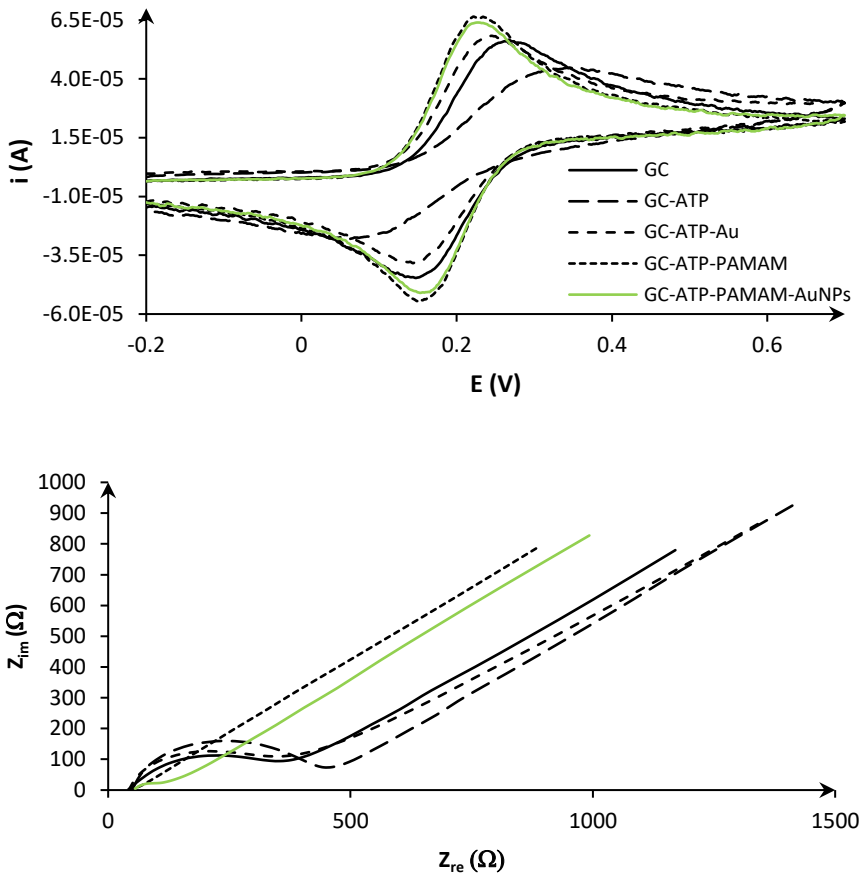

Figure 61. Cyclic voltammogram of vitreous carbon electrode in 5mM hexacyanoferrate (II) and 0.2 M potassium chloride aqueous solution (*vs*. SCE), v: 50 mV s^{-1}. Complex impedance plot of the gold electrode in equimolar 2.5 mM solution of hexacyanoferrate (II) and (III) in 0.2 M potassium chloride (*vs*. Pt). The frequency range is 2×10^5 – 0.1 Hz, AC amplitude of 10 mV rms. Modification with ATP.

Table 18. Current and potentials of anodic and cathodic peaks, half-wave potentials and charge-transfer resistance. v: 50 mV s^{-1}. Values are mean ± SD. Modification with ATP.

	Electrode				
	GC	**GC-ATP**	**GC-ATP-AuNPs**	**GC-ATP-PAMAM**	**GC-ATP-PAMAM-AuNPs**
E^A (mV)	260.8 ± 3.9	273.4 ± 8.3	257.6 ± 8.6	227.0 ± 3.5	227.7 ± 2.2
i^A (μA)	57.5 ± 0.5	47.1 ± 3.3	53.8 ± 1.8	68.1 ± 0.7	65.6 ± 0.6
E^C (mV)	148.0 ± 0.8	122.2 ± 5.2	129.4 ± 9.4	153.9 ± 3.7	154.6 ± 2.3
i^C (μA)	-53.0 ± 1.1	-41.8 ± 4.0	-44.2 ± 2.3	-63.8 ± 0.5	-61.4 ± 1.6
$E_{1/2}$ (mV)	204.4 ± 1.9	196.9 ± 4.9	193.5 ± 3.4	190.4 ± 3.3	191.2 ± 1.2
R_{CT} (ohms)	378.2 ± 1.2	408.7 ± 37.1	434.6 ± 51.8	18.3 ± 0.8	74.2 ± 2.4

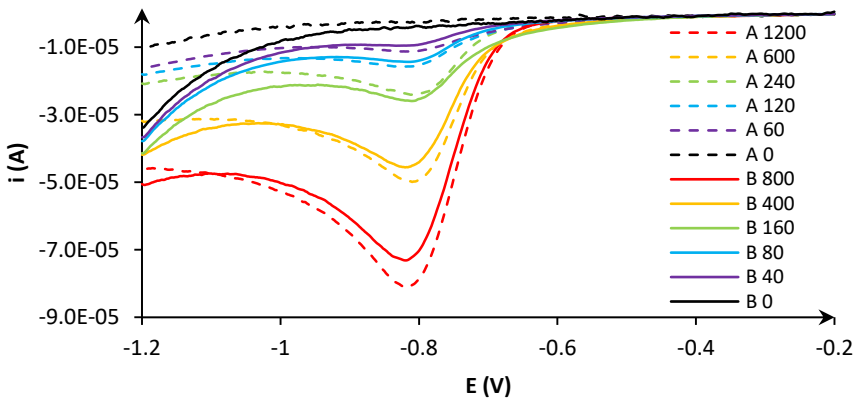

Figure 62. Cyclic voltammogram of modified glassy carbon electrode in 0.05 M PBS (pH 5.3) and 4-nitrophenol at different concentrations (*vs*. SCE), v: 50 mV s^{-1}. (A) GC-MPS-PAMAM, and (B) GC-MPS-PAMAM-AuNPs.

PEst-OE/QUI/UI0674/2013

M1420-01-0145-FEDER-000005

Centro de Química da Madeira - CQM^{+} (Madeira 14-20)

Cofinanciado por: